IN THIS JOURNAL

Great Britain Journals Press

journalspress.com

London Journal of Research in Science: Natural & Formal

Print ISSN: 2631-8490
Online ISSN: 2631-8504
DOI: 10.17472/LJRS

Volume 24 | Issue 13 | Compilation 1.0

COMPILED IN UNITED KINGDOM

ENGLISH

London Journal of Research in Science: Natural and Formal

Volume 24 | Issue 13 | Compilation 1.0

PUBLISHER

Great Britain Journals Press
1210th, Waterside Dr, Opposite Arlington Building, Theale, Reading
Phone:+444 0118 965 4033 Pin: RG7-4TY United Kingdom

SUBSCRIPTION

Frequency: Quarterly

Print subscription
$280USD for 1 year
$500USD for 2 year
(*color copies including taxes and international shipping with TSA approved)*
Find more details at https://journalspress.com/journals/subscription

ENVIRONMENT

Great Britain Journals Press is intended about Protecting the environment. This journal is printed using led free environmental friendly ink and acid–free papers that are 100% recyclable.

Great Britain Journals Press Headquaters

1210th, Waterside Dr,
Opposite Arlington
Building, Theale, Reading
Phone:+444 0118 965 4033
Pin: RG7-4TY
United Kingdom

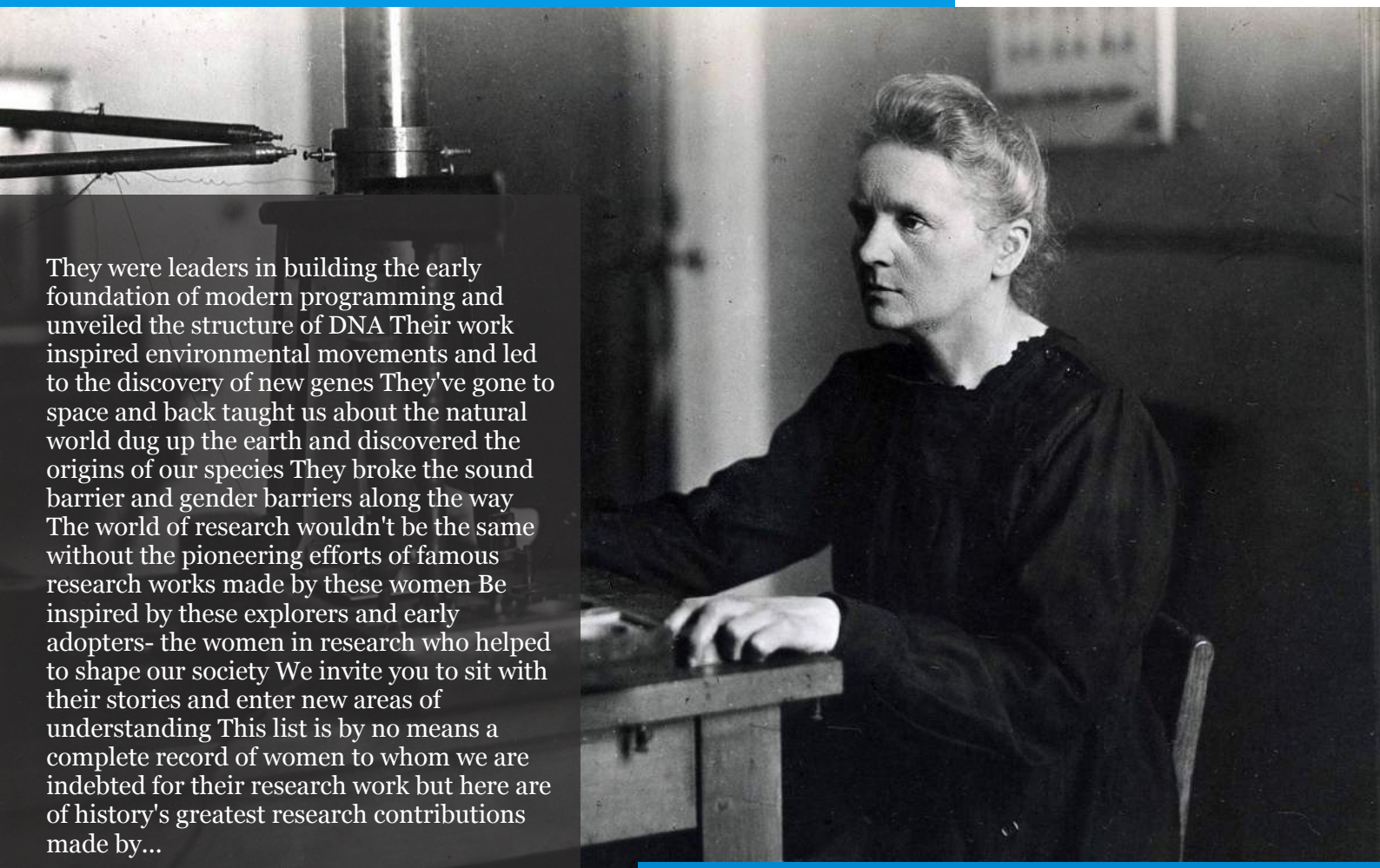

They were leaders in building the early foundation of modern programming and unveiled the structure of DNA Their work inspired environmental movements and led to the discovery of new genes They've gone to space and back taught us about the natural world dug up the earth and discovered the origins of our species They broke the sound barrier and gender barriers along the way The world of research wouldn't be the same without the pioneering efforts of famous research works made by these women Be inspired by these explorers and early adopters- the women in research who helped to shape our society We invite you to sit with their stories and enter new areas of understanding This list is by no means a complete record of women to whom we are indebted for their research work but here are of history's greatest research contributions made by...

Read complete here:
https://goo.gl/1vQ3lS

Women In Research

Computing in the cloud!

Cloud Computing is computing as a Service and not just as a Product Under Cloud Computing...

Read complete here:
https://goo.gl/VvHC72

Writing great research...

Prepare yourself before you start Before you start writing your paper or you start reading other...

Read complete here:
https://goo.gl/np73jP

Journal Content
In this Issue

Great Britain Journals Press

Editorial Board

Curated board members

Nicola Mastronardi

Consiglio Nazionaledelle Ricerche,
Ph.D. Applied Mathematics Katholieke
Universiteit Leuven
Belgium

Dr. Indranil Sen Gupta

Ph.D., Mathematics
Texas A & M University
Department of Mathematics
North Dakota State University
North Dakota, USA

Dr. Arvind Chhabra

University of Connecticut Health Center
USA Ph.D., Biotechnology Central
Drug Research Institute

Dr. Vladimir Burtman

Research Scientist
The University of Utah
Geophysics
Frederick Albert Sutton Building
115 S 1460 E Room 383
Salt Lake City, UT 84112, US

Dr. Xianghong Qi

University of Tennessee
Oak Ridge National Laboratory
Center for Molecular Biophysics
Oak Ridge National Laboratory
Knoxville, TN 37922
United States

Dr. Arshak Poghossian

Ph.D. Solid-State Physics
Leningrad Electrotechnical Institute, Russia
Institute of Nano and Biotechnologies
Aachen University of Applied Sciences, Germany

Dr. Bingyun Li

Ph.D. Fellow, IAES
Guest Researcher, NIOSH, CDC, Morgantown, WV
Institute of Nano and Biotechnologies
West Virginia University, US

Dr. Maria Gullo

Ph.D., Food Science, and Technology
University of Catania
Department of Agricultural and Food Sciences
University of Modena and Reggio Emilia, Italy

Dr. A. Heidari

Ph.D., D.Sc
Faculty of Chemistry
California South University (CSU), United States

Dr. Alicia Esther Ares

Ph.D. in Science and Technology,
University of General San Martin, Argentina
State University of Misiones, US

Research papers and articles

Volume 24 | Issue 13 | Compilation 1.0

The Origin of Life on Earth: An Economic Interpretation

Jong Soue You

Algoma University

ABSTRACT

Economists believe that most theories in economics, if not all, can be formulated in terms of minimization or maximization of a suitable economic quantity. Recent studies in geophysics and biophysics have found convincing evidence that the principle driving the origin of life is energy-dissipation-driven adaptation of matter. In this view, life is a result of maximizing entropy production through a maximum dissipation of sunlight energy efficiently transforming it into heat. This suggests a possible analogy between economic principles and the physical processes underlying life's origin, with an implication that in a fundamental sense it is the economic forces that are responsible for the creation of life on Earth. To be more accurate, it is the physical forces based on the second law of thermodynamics driven by the fundamental economic forces of maximizing entropy along the evolutionary path of the universe that are responsible for the origin of life on Earth. This is not surprising considering the fact that the behaviors of most animal and plant species including their genome itself can be explained in terms of constrained dynamic optimization producing efficient outcomes through decentralized decision making.

Keywords: origin of life, energy dissipation, entropy production, constrained dynamic optimization, efficient decentralized decision making, second law of thermodynamics., economic principles in biology, self-organization, abiogenesis, thermodynamic adaptation.

Classification: LCC Code: QH 540

Language: English

Great Britain Journals Press

LJP Copyright ID: 925671
Print ISSN: 2631-8490
Online ISSN: 2631-8504

London Journal of Research in Science: Natural & Formal

Volume 24 | Issue 13 | Compilation 1.0

The Origin of Life on Earth: An Economic Interpretation

Jong Soue You

ABSTRACT

Economists believe that most theories in economics, if not all, can be formulated in terms of minimization or maximization of a suitable economic quantity. Recent studies in geophysics and biophysics have found convincing evidence that the principle driving the origin of life is energy-dissipation-driven adaptation of matter. In this view, life is a result of maximizing entropy production through a maximum dissipation of sunlight energy efficiently transforming it into heat. This suggests a possible analogy between economic principles and the physical processes underlying life's origin, with an implication that in a fundamental sense it is the economic forces that are responsible for the creation of life on Earth. To be more accurate, it is the physical forces based on the second law of thermodynamics driven by the fundamental economic forces of maximizing entropy along the evolutionary path of the universe that are responsible for the origin of life on Earth. This is not surprising considering the fact that the behaviors of most animal and plant species including their genome itself can be explained in terms of constrained dynamic optimization producing efficient outcomes through decentralized decision making. Colonies of ants and bees and trees in the forest are the good examples of this studied widely elsewhere in the literature. It is highly unlikely that the similarities between the efficient biological system and the efficient economic system, both with efficient decentralized signaling and responses, are merely coincidental. After all, evidence suggests that the origin of life was a result of economically efficient maximizing of entropy production through a maximum dissipation of sunlight energy driven by the fundamental economic forces.

Keywords: origin of life, energy dissipation, entropy production, constrained dynamic optimization, efficient decentralized decision making, second law of thermodynamics., economic principles in biology, self-organization, abiogenesis, thermodynamic adaptation.

Author: Professor Emeritus of Economics, Algoma University, Canada.

London Journal of Research in Science: Natural & Formal

I. INTRODUCTION

Joseph-Louis Lagrange believed that most theories in physics, if not all, can be formulated in terms of minimization or maximization of a suitable quantity.[1] Economists believe that most theories in economics, if not all, can be formulated in terms of minimization or maximization of a suitable economic quantity.[2] In his 2013 paper Jeremy England proposed an idea that the principle driving the origin of life is energy-dissipation-driven adaptation of matter.[3] In this view, life is a result of maximizing entropy production through a maximum dissipation of sunlight energy efficiently transforming it into heat. This suggests a possible analogy between economic principles and the physical processes underlying life's origin. This implies that in a fundamental sense it is the economic forces that are responsible for the creation of life on Earth. To be more accurate, it is the physical forces based on the second law of thermodynamics driven by the fundamental economic forces of maximizing

[1] Clerke, AM. *Lagrange, Joseph-Louis*. Encyclopedia Britanica, 16 (11th ed.) 1911: 75-78.
[2] Samuelson, P. *Foundations of Economic Analysis*, Harvard University Press, 1947.
[3] England, JL. (2013)

entropy along the evolutionary path of the universe that are responsible for the origin of life on Earth. This is not surprising considering the fact that the behaviors of most animal and plant species including their genome itself can be explained in terms of constrained dynamic optimization producing efficient outcomes through decentralized decision making as can the human behaviors in the market economies.[4] Colonies of ants and bees and the trees in the forest are the good examples of this studied widely elsewhere in the literature. It is highly unlikely that the similarities between the efficient biological system and the efficient economic system, both with efficient decentralized signaling and responses, are merely coincidental.

The paper is organized as follows. This introduction is followed by a brief literature review in Ch. II. Chapter III discusses a wide variety of natural phenomena, both biological and physical, that can be explained by the economic principle of minimization or maximization of a suitable economic quantity which strongly suggests that the origin of life on Earth can also be explained by this principle. Chapter IV presents the conclusion of the paper.

II. LITERATURE REVIEW

The Bible describes the birth of the universe and the earth; "In the beginning God created the heavens and the earth. The earth was without form and void and darkness was over the face of the deep. And the spirit of God was hovering over the face of the waters. And God said: 'Let there be light,' and there was light."[5] Scientists believe that around 13.8 billion years ago the universe started with a Big Bang, an explosion with unimaginable force of a very tiny point into which every speck of its energy was jammed into. Immediately after the Big Bang the universe was formless made up of virtually weightless hot gases, surprisingly similar to the conditions described in the Bible. The early universe was too hot for electrons to remain bound to atoms. The first elements, hydrogen and helium, couldn't form until the universe had cooled enough to allow their nuclei to capture electrons, about 380,000 years after the Big Bang. Then as the universe got cooler with continuous expansion, slightly heavier but still very light gases emerged followed by even heavier elements as the universe continued to cool. The universe followed an evolutionary path of increasing entropy based on the second law of thermodynamics. Along the evolutionary path nevertheless, the total energy of the universe would have to remain constant to preserve the first law of thermodynamics. Along this path the lighter atoms combined themselves to form heavier atoms as the universe was getting cooler with continuous expansion. The Earth formed roughly 4.5 billion years ago, still a ball of hot gases. By the time the conditions were ripe for the birth of life on Earth there would have emerged a sufficient variety of atoms to allow the first organic molecule to be formed, for example, RNA (Ribonucleic acid). Scientists estimate that life probably began between 3.5 and 3.9 billion years ago.

There exist a number of hypotheses in the literature on the origin of life on Earth. The Oparin-Haldane hypothesis suggests that life arose gradually from inorganic molecules, with "building blocks" like amino acids forming first and then combining to make complex polymers. The Miller-Urey experiment provided the first evidence that the organic molecules needed for life could be formed from inorganic components.[6] Some scientists support the RNA world hypothesis, which suggests that the

[4] You, JS. (2023a)
[5] Genesis 1:1-3, *Study Bible*, English Standard Version, Crossway: Wheaton, Illinois, 2008
[6] In 1924 a Russian scientist named Alexander Oparin and, in 1929, an English scientist named J. B. S. Haldane, proposed that life arose from inorganic matter mixed with other compounds (known as the *primordial soup*) under an oxygen-deprived (reducing) atmosphere and gradually evolved into more complex organisms over time. This is known as the Oparin-Haldane or heterotrophic theory of the origin of life. They suggested that this inorganic matter may have experienced reactions caused by lightning that resulted in the formation of amino acids and other important building blocks for the formation of life, thus creating the primordial soup. Reactions within this primordial soup could have then allowed for the formation of molecules of greater complexity, such as proteins, and eventually evolution into complex organisms.

first life was self-replicating RNA[7]. Other ideas include the pre-RNA world hypothesis and the metabolism-first hypothesis. Organic compounds could have been delivered to early Earth by meteorites and other celestial objects. The deep-sea vents theory is still another theory on the subject[8] for which empirical evidence is still lacking.

III. THE ECONOMIC PRINCIPLE OF MINIMIZATION OR MAXIMIZATION OBSERVED IN NATURE

Evidence seems to suggest that the driving force behind all activities of animals and plants and indeed all organisms in the organic world including humans is economic in nature. Their behaviors seem to be driven by the objective of constrained dynamic optimization under the environmental constraints they are faced with, i.e., that they behave rationally. The evidence for this proposition is rooted in a wide range of observations on the behaviors of many plants and animals and indeed in how their genome is organized and functions. Behaviors of the colonies of ants and bees are good examples of what may be characterized as constrained dynamic optimization resulting in efficient decentralized decision making as are the trees in the forest (You, 2023a). Recent research seems to suggest that the motive of economic efficiency underlies the origin of life itself as life can be viewed as the *inevitable spontaneous outcome* of *economically efficient* energy-dissipation-driven organization of matters along the evolutionary path of increasing entropy production.

Recently reported research findings in geophysics and biophysics strongly suggest that the origin of life on Earth was an inevitable outcome of the tendency of increasing entropy or the second law of thermodynamics (Michaelian, 2011; England, 2013). According to this view, the principle driving the origin of life on Earth is energy-dissipation-driven adaptation of matter. To borrow Michaelian's words: "Understanding the thermodynamic function of life may shed light on its origin. Life, as are all irreversible processes, is contingent on entropy production. Entropy production is a measure of the rate of the tendency of Nature to explore available microstates. The most important irreversible process generating entropy in the biosphere and, thus, facilitating this exploration, is the absorption and transformation of sunlight into heat. Here we hypothesize that life began, and persists today, as a catalyst for the absorption and dissipation of sunlight on the surface of Archean seas." "RNA and DNA are the most efficient of all known molecules for absorbing the intense ultraviolet light that penetrated the dense early atmosphere and are remarkably rapid in transforming this light into heat in the presence of liquid water. From this perspective, the origin and evolution of life, inseparable from water and the water cycle, can be understood as resulting from the natural thermodynamic imperative of increasing the entropy production of the Earth in its interaction with its solar environment." In this view, life is a result of maximizing entropy production through a maximum dissipation of sunlight energy efficiently transforming it into heat. In other words, the molecules are driven by the fundamental forces of nature to solve the constrained dynamic optimization problems they are faced with. The result is an efficient maximization of entropy production which reflects what may be termed "the economic law of evolution," *economic in the sense of maximizing efficiency*. A similar view is advanced by England. According to England, "when a group of atoms is driven by an external source of energy (like the sun or chemical fuel) and surrounded by a heat bath (like the ocean or atmosphere), it will often gradually restructure itself in order to dissipate increasingly more energy." This could mean that under certain conditions, matter inexorably acquires the key physical attribute associated with life.

[7]The "RNA world" theory states that life may have begun with molecules of RNA (Ribonucleic acid), which are able to perform self-replication and catalyze reactions. Over time, these molecules evolved to become more complex organisms.

[8]The deep-sea vents theory involves deep-sea hydrothermal vents, which are geologic structures that spew molecules that have abundant hydrogen. Billions of years ago, these molecules may have then clumped together and experienced chemical reactions, which may have resulted in the emergence of life. The world's oldest fossils, containing microorganisms and dating to between 3.8 and 4.3 billion years old, were discovered in hydrothermal vents in Quebec in 2017.

From the standpoint of physics, there is one essential difference between living things and inanimate clumps of carbon atoms: The former tend to be much better at capturing energy from their environment and dissipating that energy as heat. A plant, for example, is much better at capturing and routing solar energy through itself than an unstructured heap of carbon atoms. Thus, under certain conditions, matter will spontaneously self-organize. This tendency could account for the internal order of living things and of many inanimate structures as well." England observes: "Snowflakes, sand dunes and turbulent vortices all have in common that they are strikingly patterned structures that emerge in many particle systems driven by some dissipative process."

It is worthwhile remembering the different functions of RNAs and DNAs. The main function of DNA is to store and replicate genetic information, while RNA's main function is to copy DNA's genetic information to build proteins needed for building the organs of the body. This genetic information accumulated and constantly updated throughout the process of economic natural selection is an outcome of the long evolutionary process since the beginning of life (You, 2023b). Contrary to popular understanding, the brain designed by the DNAs does not control the body functions but the body including the brain functions as an integral system of signals and responses without a central control. This is a highly efficient biological system with decentralized signaling and responses – a product of economic natural selection. Any biological system designed to be controlled by a central command would not have the kind of flexibility and adaptability required for survival in the constantly and often unpredictably changing environment. This is akin to a highly efficient economic system:

"The illusion that economies run better if somebody is in charge of them – and decides what gets manufactured where and by whom – has done devastating harm to the wealth and health of peoples all over the world, not just in the former Soviet Union, but in the west as well. From the Roman Empire to the European Union, centralized decisions about what to invest in have been disastrously worse than the decentralized chaos of the market." (Ridley, 1999).

IV. CONCLUSION

Economists believe that most theories in economics, if not all, can be formulated in terms of minimization or maximization of a suitable economic quantity (Samuelson, 1947). Recent researches in geophysics and biophysics have revealed convincing evidence that the principle driving the origin of life on Earth is energy-dissipation-driven adaptation of matter (Michaelian, 2011, and England, 2013). In this view, life is a result of maximizing entropy production through a maximum dissipation of sunlight energy efficiently transforming it into heat. This implies that in a fundamental sense it is the economic forces that are responsible for the creation of life on Earth. To be more accurate, it is the physical forces based on the second law of thermodynamics driven by the fundamental economic forces of maximizing entropy along the evolutionary path of the universe that are responsible for the origin of life on Earth. This is not surprising considering the fact that the behaviors of most animal and plant species including their genome itself can be explained in terms of constrained dynamic optimization producing efficient outcomes through decentralized signaling and responses (You, 2023a). It is highly unlikely that the similarities between the efficient biological system and the efficient economic system, both with efficient decentralized signaling and responses, are merely coincidental. After all, there exists a persuasive thermodynamic imperative that the origin of life was a result of economically efficient maximizing of entropy production through a maximum dissipation of sunlight energy driven by the fundamental economic forces along the evolutionary path of the universe. The strength of the Michaelian-England hypothesis is the spontaneity and inevitability nature of energy-dissipation-driven adaptation of matter as the principle driving the origin of life without having to rely on the possible involvement of an external source such as meteorites or other celestial objects or on the probabilistic nature of the deep-sea vents hypothesis for which empirical evidence is lacking.

ACKNOWLEDGEMENTS

The author wishes to thank the anonymous reviewers for helpful comments on the earlier version of the manuscript.

Conflict of interests:
The author declares no conflict of interest regarding the publication of this paper.
The author received no funding from the public or private sources for this research.

REFERENCES

1. Clerke. AM. .(1911) Lagrange, Joseph-Louis. *Encyclopoedia Britanica*, 16 (11th ed.) 1911: 75-78.
2. England, JL. (2013)"Statistical physics of self-replication," *Journal of Chemical Physics* 139, 121923, Sept. 2013.
3. Haldane, JBS. (born, 1892—died, 1964) was a British geneticist, biometrician and physiologist noted for his studies on the origin of life (*Oparin-Haldane hypothesis*).
4. Michaelian, K. (2011) "Thermodynamic dissipation theory of the origin of life," *Earth System Dynamics* 2, 37–51.
5. Oparin, A. (born, 1894—died, 1980) was a Russian biochemist noted for his studies on the origin of life (*Oparin-Haldane hypothesis*).
6. Ridley, M. (1999) *Genome* (New York: Harper Collins)
7. Samuelson, P. (1947) *Foundations of Economic Analysis*, Harvard University Press, 1947
8. *Study Bible*, English Standard Version, Crossway: Wheaton, Illinois, 2008.
9. You, JS., (2023a) "The Economics of Nature: Constrained Dynamic Optimization and Efficient Decentralized Decision Making in Nature," Theoretical Economics Letters, vol. 13, no. 2, April 2023.
10_____, (2023b) "Economic Natural Selection: Interpretation of Natural Selection as Economic Selection in the Evolutionary Process," Theoretical Economics Letters, vol. 13, no. 5, Oct. 2023.

This page is intentionally left blank

An Alternative for Time Series Models

Jerzy K. Filus

ABSTRACT

Two methods for construction of new stochastic processes with discrete time are presented. One of the methods employs as the defining tool 'triangular (more specifically 'pseudoaffine') transformations' which are extended from the Euclidean Rnto infinite dimension space. They transform any well-known discrete time stochastic process into the constructed one. The other, more flexible, method is the "method of parameter dependence", extended to infinite dimension. Properties of the obtained stochastic processes (by either method) indicate the possibility to apply them for financial analysis, as an alternative for the classical time series models. The advantage of the presented models over the existing ones first of all relies on expected better accuracy. This follows from the fact that the typically held assumption on Markovianity in the existing models can easily be relaxed. The defined processes may incorporate a quite long including, among others, the k-Markovian cases for $k \geq 2$. Regardless of the non-Markovianity of the models they still are tractable in an analytical or numerical way.

Keywords: stochastic dependence, stochastic processes, alternative for time series financial models, parameter dependence method of construction, k-Markovianity.

Classification: LCC Code: QA276.5

Language: English

Great Britain Journals Press

LJP Copyright ID: 925672
Print ISSN: 2631-8490
Online ISSN: 2631-8504

London Journal of Research in Science: Natural & Formal

Volume 24 | Issue 13 | Compilation 1.0

An Alternative for Time Series Models

Jerzy K. Filus

ABSTRACT

Two methods for construction of new stochastic processes with discrete time are presented. One of the methods employs as the defining tool is'triangular (more specifically 'pseudoaffine') transformations' which are extended from the Euclidean $R^n$to infinite dimension space. They transform any well-known discrete time stochastic process into the constructed one. The other, more flexible, method is the "method of parameter dependence", extended to infinite dimension. Properties of the obtained stochastic processes (by either method) indicate the possibility to apply them for financial analysis, as an alternative for the classical time series models. The advantage of the presented models over the existing ones first of all relies on expected better accuracy. This follows from the fact that the typically held assumption on Markovianity in the existing models can easily be relaxed. The defined processes may incorporate a quite long list including, among others, the k-Markovian cases for $k \geq 2$. Regardless of the non-Markovianity of the models they still are tractable in an analytical or numerical way.

*The stochastic processes defined in this paper provide more flexible and more general tools than the existing time series models for modeling financial problems. Among others, they make it possible to incorporate the influence of environmental (explanatory) random variables on the underlying stochastic models' behavior. These additional features turn out to be describable by the method of parameter dependenc*e. Some suggestions for an associated preliminary statistical analysis are included.

Keywords: stochastic dependence, stochastic processes, alternative for time series financial models, parameter dependence method of construction, k-Markovianity.

Author: Department of Mathematics and Computer Science, Oakton Community College Des Plaines, IL 60016, USA.

I. INTRODUCTION

In this work a pattern for construction of new stochastic models is proposed. The models modification and generalization of the classical time series frameworks for financial analysis (Tsay, 2005). As such they are considered a possible alternative to these known ones. They can be obtained by two different methods.

One of the methods employs triangular transformations (Filus & Filus& Arnold, 2010), as the defining tool and may therefore be more useful in a further statistical analysis and possible simulation studies. This method is described in Section 2 and 3. The other, described in Section 4, relies on application of the 'parameter dependence method' (Filus & Filus, 2012), (Filus & Filus, 2013), which is more flexible than the first method in the sense that it produces more models. The models obtained by either of the two methods are stochastic processes whose terms have financial meanings, especially the meaning of log returns for a single asset.

London Journal of Research in Science: Natural & Formal

All the stochastic processes obtained by the triangular transformations method may also be obtained by the parameter dependence (not conversely), but the possibility of a nice statistical and simulation analysis as provided by the transformations is sometimes lost. This was the reason both methods were introduced. Any of the two is very general.

The patterns employed allow us to define wide classes of conditional probability distributions of any term X_t, given realizations $x_1, \ldots, x_{t-1}$ of all past terms $X_1, \ldots, X_{t-1}$ of the defined stochastic processes.

Notice, that such conditional distributions are very seldom explicitly given in efficient forms in the literature. The classical exception lies within the pattern of the multivariate normal case. The obtained conditional distributions are then used for further construction of joint probability distributions of all the random vectors $(X_1, \ldots, X_t)$, $t = 2, 3, \ldots$ if an initial distribution of X_1 is given.

Perhaps the most amazing fact that follows is the easy possibility of defining non-Markovian (as well as the Markovian) stochastic processes incorporating long pasts, and still analytically tractable. Additionally, the method of parameter dependence allows us to include into the model, typically occurring in practice, 'state random variables' that describe a "stochastic environment" in which the processes evolve over time.

The generality of these new models (from a financial perspective) inclined us rather to concentrate on the formulation of fundamental ideas as beginning to possibly new theories. Therefore, in order to avoid unnecessary dissipation, the number of examples was purposefully limited. Statistical analysis problems of the new stochastic models are only mentioned. Also references are limited, somewhat, especially because the results presented are possibly at first in a financial setting. However, somewhat similar, from a pure mathematical point of view, but generally different results were published in (Filus & Filus, 2008).

II. DEFINING TRANSFORMATIONS

Consider a sequence of log returns R_t of a single asset, $t = 0, 1, \ldots, T$; (Tsay, 2005), as given by the following sequence $T = 1, 2, \ldots$ of transformations:

$$R_0 = {}_0$$

$$R_1 = V_1(R_0)X_1 + B_1(R_0)$$

$$R_2 = V_2(R_0, R_1)X_2 + B_2(R_0, R_1)$$

$$R_T = V_T(R_0, R_1, \ldots, R_{T-1})X_T + B_T(R_0, R_1, \ldots, R_{T-1}),$$

$T = 1, 2, \ldots$, (1) where the random variables $X_1, \ldots, X_T$ are assumed to be independent and identically distributed. This is then a general white noise pattern which is a source of randomness for the considered log returns $R_1, \ldots, R_T, \ldots$. V_0 represents a nonnegative constant initial value, while the functions $V_1, \ldots, V_T$ are arbitrary positive and piecewise continuous with respect to each argument. If the variance of each random variable X_t is 1, then $V_1, \ldots, V_T$ will have the "conditional volatilities" interpretation conditioned on realizations of past returns $R_0, R_1, \ldots$ prior to a given R_t. Also conditioned on the same realizations of the past returns are the conditional expectations

$$E[R_t | R_0, R_1, \ldots, R_{t-1}] = B_t(R_0, R_1, \ldots, R_{t-1})$$

where $B_1, \ldots, B_T$ are arbitrary, piecewise continuous with respect to each argument, functions of realizations of past returns.

Example. The functions $V_t(\ )$ and $B_t(\ )$ (t = 1, … ,T) may be arbitrary continuous. However, in practical applications one could choose, for example, the following simple functions: $V_t(r_0, r_1, \dots, r_{t-1}) = 1 + a_0r_0^2 + a_1r_1^2 + \dots + a_{t-1}r_{t-1}^2$, $B_t(r_0, r_1, \dots, r_{t-1}) = b_0r_0 + b_1r_1 + \dots + b_{t-1}r_{t-1}$,

where the coefficients $a_0, a_1, \dots, a_{t-1}$ are real nonnegative and $b_0, b_1, \dots, b_{t-1}$ are arbitrary real. These coefficients are to be statistically estimated.

Also, if appropriate, one can choose as model:

$$V_t(r_0, r_1, \dots, r_{t-1}) = \exp[\, a_0r_0^2 + a_1r_1^2 + \dots + a_{t-1}r_{t-1}^2] \text{ and}$$

$$B_t(r_0, r_1, \dots, r_{t-1}) = \exp[b_0r_0 + b_1r_1 + \dots + b_{t-1}r_{t-1}]$$

with arbitrary real coefficients $a_0, a_1, \dots, a_{t-1}$ and $b_0, b_1, \dots, b_{t-1}$. Other examples of such functions can easily be given.

Returning to the main subject, notice that the sequence of the random vector transformations $(X_1, \dots, X_T) \square (R_1, \dots, R_T)$ (T = 1, 2, …) defined by (1), is the pseudoaffine version of sequence of triangular transformations $R^T \square R^T$, (Filus & Filus & Arnold, 2010). Here it is proposed to apply them as a general financial model_for values of log returns. This model can be seen as a slightly different version of time series, and is proposed to be named *"triangular model"***.** Realize that all the transformations (1) are easily invertible, and their inverses are given as follows:

$$R_0 = X_0,$$

$$X_1 = [\, R_1 - B_1(R_0)\,] \,/\, V_1(R_0)$$

$$X_2 = [\, R_2 - B_2(R_0, R_1)\,] \,/\, V_2(R_0, R_1)$$

$$X_T = [R_T - B_T(R_0, R_1, \dots, R_{T-1})\,] \,/\, V_T(R_0, R_1, \dots, R_{T-1})$$

T = 1, 2, … . (1*) For realizations $x_1, \dots, x_T$ and $r_0, r_1, \dots, r_T$ of the underlying random variables, denoted by the corresponding capital letters, the jacobians, $J_T(r_1, \dots, r_T) = \partial(x_1, \dots, x_T) \,/\, \partial(r_1, \dots, r_T)$, have the simple form of the inverse of the volatilities' products

$$J_T(r_0, r_1, \dots, r_{T-1}) = [V_1(r_0)\, V_2(r_0, r_1) \dots V_T(r_0, r_1, \dots, r_{T-1})\,]^{-1}, \text{ (2) for each } T = 1, 2, \dots .$$

One can see that if the sequence of probability densities (pdf) of the random vectors $(X_1, \dots, X_T)$ is known (which is mostly the case), then from (1*) and (2) one immediately can derive the corresponding sequence of joint pdfs of the random vectors of the returns $(R_1, \dots, R_T)$, T = 1, 2, … .

In such a way, one defines a wide class of stochastic processes $\{R_T\}_{T = 1, 2, \dots}$. (The Kolmogorov consistency theorem easily applies to this case.)

Consider these processes as *"modified time series"* processes for log returns $R_1, R_2, \dots$. Clearly, the model given by (1) is heteroscedastic as the underlying conditional volatilities, $V_t(r_0, r_1, \dots, r_{t-1})$, t = 1, 2, … (conditioned on elementary events $R_0 = V_0 = r_0, R_1 = r_1, \dots, R_{t-1} = r_{t-1}$), are, in general, distinct.

It follows from (1) that the introduced model is, in general, not Markovian but still analytically tractable.

Actually, when using model (1) one can incorporate in each conditional pdf $g_T(r_T \mid r_1, \dots, r_{T-1})$ (at present time T) all the past information on the returns, and underlying calculations are still performable.

However, this computational advantage is overshadowed by limitations of a statistical nature. As T grows, the number of parameters to be estimated also grows without bounds, so some restrictions on the past must be provided. For that one can apply the notion of *k-Markovianity* that limits the past to the last k observations (k = 1, 2, ...). The case k = 1 means the ordinary Markovianity.

The general k-Markovian version of model (1) can be defined as the following sequence of transformations:

$$R_0 = X_0$$

$$R_1 = V_1(R_0)X_1 + B_1(R_0)$$

$$R_2 = V_2(R_0, R_1)X_2 + B_2(R_0, R_1)$$

$$R_j = V_j(R_0, R_1, \dots, R_{j-1})X_j + B_j(R_0, R_1, \dots, R_{j-1}) \text{ if } j-1 \le k$$

$$R_t = V_t(R_{t-k}, \dots, R_{t-1})X_t + B_t(R_{t-k}, \dots, R_{t-1}) \text{ if } t-1 \ge k$$

$$R_T = V_T(R_{T-k}, \dots, R_{T-1})X_T + B_T(R_{T-k}, \dots, R_{T-1}) \quad (3)\ k = 1, 2, \dots, T = 1, 2, \dots, k < T.$$

The k-Markovian conditional pdfs of $R_t \mid R_0, R_1, \dots, R_{t-1}$ as derived from (3) are given by: $g_t(r_t \mid r_1, \dots, r_{t-1})$ if $t-1 \le k$ and $g_t(r_t \mid r_{t-k}, \dots, r_{t-1})$ if $t-1 \ge k$.

Thus, in this setting, the (conditional) distribution of the present asset log return R_T only depends on the last k moments (months, years) in the past. The earlier times are considered irrelevant and are neglected.

Nevertheless, even in the case k = 2 (bi-Markovian) the amount of information incorporated in the stochastic model is significantly bigger than in the Markovian case, so one may expect more accurate predictions.

3. Examples

The following examples are based on (1) and (3).

Example 1. Assume that, for each T, the random variables $X_1, \dots, X_T$ are independent, each having the standard normal N(0, 1) pdf.

Using standard calculations based on the knowledge of (1*) and (2) one first obtains the (unconditional) normal pdf $g_1(r_1) = N[\, B_1(R_0), V_1(R_0)\,]$ for R_1 and then for each t = 2, 3, ... ,T one obtains the conditional pdf: $g_t(r_t \mid r_1, \dots, r_{t-1})$

$$= [V_t(r_0, r_1, \dots, r_{t-1})\sqrt{2\pi}\,]^{-1}\exp[-(1/2)\{(\mathbf{r_t} - B_T(r_0, r_1, \dots, r_{t-1}))\,/\,V_t(r_0, r_1, \dots, r_{t-1})\}^2]. \quad (4)$$

Realize that the latter conditional pdf is normal with respect to the single variable r_t. The joint probability density $g_T(r_1, \dots, r_T)$ for each random vector $(R_1, \dots, R_T)$, T = 2, 3, ... , is given by the common formula: $g_T(r_1, \dots, r_T) = g_1(r_1)\,\Pi_{t=1}^{T} g_t(r_t \mid r_1, \dots, r_{t-1})$, **(5)** where $g_t(r_t \mid r_1, \dots, r_{t-1})$ is given by (4).

The so obtained T-dimensional pdf is the FF-normal (former name "pseudonormal"), (Kotz & Balakrishnan & Johnson, 2000).

Example 2.

Consider the following "pseudolinear" part of the pseudoaffine transformation (1) which one obtains by setting in (1) all the "pseudotranslation" coefficients $B_t(R_0, R_1, \dots, R_{t-1})$ to zero. One then has the pseudolinear transformations:

$$R_0 = X_0$$

$$R_1 = V_1(R_0)X_1$$

$$R_2 = V_2(R_0, R_1)X_2$$

$$R_T = V_T(R_0, R_1, \dots, R_{T-1})X_T \quad \textbf{(6)} \quad T = 1, 2, \dots .$$

Investigate how the transformations (6) act on set of independent *Pareto* distributed random variables X_t (t = 1, 2, ... ,T; T = 1, 2, ...) so, in this case, the expected values of X_t' s are positive.
Recall that the Pareto density is given by

$f_t(x_t) = 1 / \beta\,(1 + x_t / \beta\gamma)^{1+\gamma}$, (7) where β and γ are positive real parameters.
Using (6), for every t = 1, ... ,T, express $\mathbf{x_t}$ as

$$x_t = r_t / V_{t-1}(r_0, r_1, \dots, r_{t-1}) \text{ (assuming } V_{t-1}(r_0, r_1, \dots, r_{t-1}) \neq 0).$$

Also realize, that the jacobian of inverse to (6) equals to the inverse product: $J_T(r_0, r_1, \dots, r_{T-1}) = [V_1(r_0)\, V_2(r_0, r_1) \dots V_T(r_0, r_1, \dots, r_{T-1})]^{-1}$.

As the next step, one obtains (for each t = 1, 2, ... ,T) the conditional pdfs $g_t(r_t | r_0, r_1, \dots, r_{t-1})$ of each rv R_t, given the past realizations $r_0, r_1, \dots, r_{t-1}$ of the rvs $R_0, R_1, \dots, R_{t-1}$, as follows:

$$g_t(r_t | r_0, r_1, \dots, r_{t-1}) = f(x_t) \,|\, \partial x_t / \partial r_t |$$

$$= f(r_t / V_{t-1}(r_1, r_2, \dots, r_{t-1})) \,|\, V_{t-1}(r_1, r_2, \dots, r_{t-1}) |^{-1}$$

$$= 1 / \{ \beta \,|\, V_{t-1}(r_1, r_2, \dots, r_{t-1}) | \,[\, 1 + r_t / \beta \,|\, V_{t-1}(r_1, r_2, \dots, r_{t-1}) | \,\gamma\,]^{1+\gamma} \}. \quad (8)$$

So, the effect of each t^{-th} line in transformation (6) on the rv X_t is to change its Pareto density (7) for the (conditional) Pareto density (8) of R_t.

The two Pareto densities (7) and (8) only differ by the scale parameters, namely**:** β in (7) was transformed into the product $\beta \,|\, V_{t-1}(r_1, r_2, \dots, r_{t-1}) \,|$ in (8).

Given the conditional densities (8) one obtains the joint density of each random vector $(R_0, R_1, \dots, R_T)$, T = 1, 2, ... using formula (5). In such a way the "Pareto stochastic process" $\{R_T\}_{T=1, 2, \dots}$ is well defined.

Example 3.

In the same way as for the independently Pareto distributed random variables $X_1, \dots, X_T$, (T = 1, 2, ...), one can apply transformation (6) to any sequence of independent identically, and exponentially distributed random variables that will be denoted by the same symbols X_t's.

If, for any t = 1, 2, … , $g_t(x_t)$ is the exponential density of X_t given by the expression $(1/\theta)\exp[-x_t/\theta]$ then it can easily be verified that the corresponding conditional density of $R_t|\ R_o, R_1, \dots, R_{t-1}$ will be given as follows: $h_t(r_t|\ r_o, r_1, \dots, r_{t-1}) = (1/\theta\ |\ V_{t-1}(r_o, r_1, \dots, r_{t-1})\ |)\exp[-r_t/\theta\ |\ V_{t-1}(r_o, r_1, \dots, r_{t-1})\ |]$. It is then clear that as in Example 2, the parameters θ is multiplied by the "coefficient" $|\ V_{t-1}(r_o, r_1, \dots, r_{t-1})\ |$.

The same actually will happen with the parameter σ in Example 1, if one would assume all the random variables X_t in (1) are normal $N(0, \sigma)$. Also in this case, the parameter σ will be turned to the conditional volatility of R_t: $\sigma\ |\ V_{t-1}(r_o, r_1, \dots, r_{t-1})\ |$.

This regularity for the parameter transformations will be applied in the next section.

III. PARAMETER DEPENDENCE MODELS

4.1 In all three examples in the previous section transformation (1) or (6) were used in order to obtain the conditional densities, say, $\varphi_t(r_t|\ r_o, r_1, \dots, r_{t-1})$ describing the stochastic dependence of the return R_t on the past.

Realize that in this derivation the underlying operations only result in changing the value of a parameter of the given density of X_t, into other value that depends on the past return values $r_o, r_1, \dots, r_{t-1}$.

This observation opens the way for the method of conditioning (on values $r_o, r_1, \dots, r_{t-1}$), which is significantly more efficient than the method of triangular transformations (1) or (6). This method, called the "parameter dependence", is presented in (Filus & Filus, 2012) and (Filus & Filus, 2013).

In the considered framework one can describe this method as follows.

Suppose there is given a sequence of independent random variables (now, instead of X_t, denoted by R_{f_t} t = 1, 2, …) all having the same arbitrary probability density $f_t(r_t; \alpha)$, $\alpha \in A$. In this situation any past in this artificial "no memory process" has no influence on the current density $f_t(r_t; \alpha)$ of R_{ft}.

The density depends on a constant (original) scalar or vector parameter α. Instead of applying transformation (1) or (6) to the random vectors $(R_{f1}, \dots, R_{fT})$ one can "directly transform" each density $f_t(r_t; \alpha)$ into a conditional density $\varphi_t(r_t|\ r_o, r_1, \dots, r_{t-1})$ of $R_t|\ r_o, r_1, \dots, r_{t-1}$ just by setting the parameter α of $f_t(r_t; \alpha)$ to "become" a function of the values $r_o, r_1, \dots, r_{t-1}$.

In such a way one defines the sequence of conditional pdfs by the formula: $\varphi_t(r_t|\ r_o, r_1, \dots, r_{t-1}) = f_t(r_t; \alpha_t(r_o, r_1, \dots, r_{t-1}))$, t = 1, 2, … (9) which, for an arbitrary function $\alpha_t(r_o, r_1, \dots, r_{t-1})$, defines a legitimate density with respect to r_t if all the values $\alpha_t(r_o, r_1, \dots, r_{t-1})$ still belong to the set A of the parameters α of $f_t(r_t; \alpha)$. Each sequence of the so obtained conditional densities $\{\varphi_t(r_t|\ r_o, r_1, \dots, r_{t-1})\}_{t=1,2,\dots}$ defines a corresponding stochastic process $\{R_t\}_{t=1,2,\dots}$.

The parameter dependence method allows for relatively free choice for the functions $\alpha_t(r_o, r_1, \dots, r_{t-1})$ and therefore the class of the so obtained stochastic processes is much wider than that obtained by the triangular transformation from the same sequence of independent random variables X_t or R_{ft}. On the other hand, the factor that, in applications, often may limit the range of choices of the functions $\alpha_t(r_o, r_1, \dots, r_{t-1})$ is reality.

Every "educative guess" for such a function must be statistically verified. So, first of all, the chosen function itself usually has its own parameters (parametric approach) that must be estimated by any statistical method such as, for example, the maximum likelihood method. Then the properly arranged parametric hypothesis should be verified. Finally the choice of the best fitting to data

function $\alpha_t(r_o, r_1, \dots, r_{t-1})$ should be based on statistical methods as to be the best one from several candidates (the choices made in the beginning). This then should be declared as the final model.

4.2 It is common (Tsay, 2005), that the general stochastic model for log returns of a given single asset from a portfolio is a joint probability distribution

$$P(R_1 < r_1, \dots, R_T < r_T \mid Y_1, \dots, Y_k) = G_T(r_1, \dots, r_T; Y_1, \dots, Y_k)$$

$$= G_1(r_1; Y_1, \dots, Y_k)\, \Pi_{t=2}{}^{T} G_t(r_t \mid r_1, \dots, r_{t-1}; Y_1, \dots, Y_k) \qquad (10)$$

where $G_1(r_1; Y_1, \dots, Y_k)$ is the cdf of the random variable R_1 and, for $t = 2, 3, \dots, T$, $G_t(r_t \mid r_1, \dots, r_{t-1}; Y_1, \dots, Y_k)$ is the conditional distribution function of R_t, given realizations $r_1, \dots, r_{t-1}$ of the random variables $R_1, \dots, R_{t-1}$.

However, the above joint and conditional distributions also depend on the state random variables $Y_1, \dots, Y_k$ that summarize the "environment" in which asset return is determined, see (Tsay, 2005), page 13.

One can apply the parameter dependence method to define the conditional distribution functions $P(R_1 < r_1, \dots, R_T < r_T \mid y_1, \dots, y_k)$, where $y_1, \dots, y_k$ are (measured) realizations of the states $Y_1, \dots, Y_k$.

For that it is enough to set parameter $\alpha_t(r_o, r_1, \dots, r_{t-1})$ **(**which already determines the conditional distribution $G_t(r_t \mid r_1, \dots, r_{t-1})$ **)** to be additionally dependent on the values $y_1, \dots, y_k$. Thus, for a given t, the conditional distribution of $R_t \mid r_1, \dots, r_{t-1}; y_1, \dots, y_k$ will be determined by a parameter(s) $\alpha_t(\,)$ of R_t's distribution as follows:

$G_t(r_t \mid r_1, \dots, r_{t-1}; y_1, \dots, y_k) = G_t(r_t; \alpha_t(r_1, \dots, r_{t-1}; y_1, \dots, y_k))$. (11) If the values (realizations) $y_1, \dots, y_k$ are measured then the joint distribution (10) is already determined. If not, one needs to have joint probability density $f(y_1, \dots, y_k)$ of the random vector $(Y_1, \dots, Y_k)$. It seems that often one may assume stochastic independence of the components $Y_1, \dots, Y_k$ of this vector.

Finally, as typically, it may be needed to multiply the resulting G_T's distribution (10) conditioned on $y_1, \dots, y_k$ by the density $f(y_1, \dots, y_k)$.

As an example of the parameter function $\alpha_t(r_1, \dots, r_{t-1}; y_1, \dots, y_k)$ one may consider the following:

$$\alpha_t(r_1, \dots, r_{t-1}; y_1, \dots, y_k) = \alpha\,(1 + a_1 r_1^2 + \dots + a_{t-1} r_{t-1}^2) \exp[\, b_1 y_1 + \dots + b_k y_k\,],$$

where α is the constant original parameter of the density $f_t(r_t; \alpha)$ of the random variable R_{ft} (Recall, $\{R_{ft}\}_{t = 1, 2, \dots}$ is the original stochastic process with the independent terms). Furthermore, $a_1, \dots, a_{t-1}$ and $b_1, \dots, b_k$ are real coefficients. Obviously, when all the coefficients $b_1, \dots, b_k$ are small enough then the impact of the states $y_1, \dots, y_k$ on the parameter **(**so on the conditional distribution**)** is insignificant.

According to my knowledge, the above application of the parameter dependence method to incorporate the random states $Y_1, \dots, Y_k$ impact on the returns' distributions is not yet present in literature.

Final Remark

The core achievement when employing either of the two methods, is opening the way for easy constructions of the conditional probability distributions of $X_t \mid X_1, \dots, X_{t-1}$, given in compact analytical forms ready for the calculations. Underlying calculations can be analytical or, if necessary, relatively simple numerical. Having the conditional distribution functions (11) in analytical forms allows for extending many classical *regression models,* usually being in the form of conditional expectation, say, $E[\, R_t \mid r_1, \dots, r_{t-1}; y_1, \dots, y_k\,]$, by replacing them with the full probability distribution

London Journal of Research in Science: Natural & Formal

(11). Notice that the latter regression is the expected value of (11) so it is only part of the wider model considered here. In what is called *"enforced regression"* (Filus & Filus, 2014), the numerical characteristics like conditional expectations or covariance coefficients can be replaced by richer functional characteristics such as the conditional distributions or joint probability distributions respectively. This idea is, apparently, different from that (nonparametric) considered by (Koenker & Bassett, 1978), and followers. For a wider discussion of this subject, see (Filus & Filus, 2014).

REFERENCES

1. J. K. Filus & L. Z. Filus, Parameter Dependence as 'Weak Transformation'; Method of Construction of Multivariate Probability Densities, Biometrie und Medizinische Informatik Greifswalder Seminarberichte, Heft 23 Statistical and Biometrical Challenges, Theory and Applications, 133 – 147, 2014.
2. J. K. Filus & L. Z. Filus, A Method for Multivariate Probability Distributions Construction via Parameter Dependence, Communications in Statistics: Theory and Methods, Vol. 42, Num. 4, 15, 716-721, 2013.
3. J. K. Filus & L. Z. Filus, Multivariate "Pseudodistributions" as Natural Extension of the Multivariate Normal Density Pattern – Theory, American Institute of Physics Conference Proceedings 1479, Numerical Analysis and Applied Mathematics, Vol. 1479, 1417-1420, 2012.
4. J. K. Filus & L. Z. Filus, B. C. Arnold, Families of multivariate distributions involving "triangular" transformations, Communications in Statistics - Theory and Methods, Volume 39, Issue 1, 107-116, 2010.
5. J. K. Filus & L. Z. Filus, Construction of New Continuous Stochastic Processes, Pak. J. Statistics, Vol. 24(3), 227-251, 2008
6. R. Koenker & G. W. Bassett, Regression Quantiles, Econometrica, 46, pp 33-50, 1978.
7. S. Kotz & N. Balakrishnan & N. L. Johnson, Continuous Multivariate Distributions, Volume 1. Second Edition. J. Wiley & Sons, Inc, New York, pp 217-218, 2000.
8. R. S. Tsay, Analysis of Financial Time Series, Second Edition.
9. J. Wiley & Sons, Inc, 2005.

Single Slit to Curve-Single Slit, Double Slit to Curve-Double Slit to Non-Parallel-Double Slit to Non-Parallel-Curve-Double Slit Experiments - Photo Wave Phenomena

Hui Peng

ABSTRACT

Feynman (1956) called the double slit experiment "... contains the only mystery. We cannot make the mystery go away by 'explaining' how it works". The photons are described by probability wave functions. The wave functions collapse to photons when landed on detector. However, the collapse of the wave function leads to the inconsistent/incomplete of the quantum mechanics (Penrose, 2022). In this article, we confirm that the diaphragm does not change the nature of the light passing through it. Then we perform multi experiments to show that, before and after passing through the diaphragm, the light is photons, not waves. It is photons that produce the interference pattern, we refer to it as "PhotoWave Phenomena". We show for the first time the novel phenomena, new mysteries: (1) a same single produces the non-diffraction pattern near the diaphragm, which gradually evolves to the orthogonal diffraction patterns; (2) a curve-single slit produces the non-diffraction pattern near the diaphragm, which gradually evolves to Hourglass-shape patterns.

Keywords: double slit, pattern evolution, Particle pattern, Transition pattern, Non-interference pattern, non-parallel double slit, hybrid pattern, curved-double slit, Arc interference pattern, Point-symmetry interference pattern, non parallel-curve-double slit, Butterfly-shape pattern, Optical Butterfly phenomena.

Classification: LCC Code: QC793.5.P8

Language: English

Great Britain Journals Press

LJP Copyright ID: 925673
Print ISSN: 2631-8490
Online ISSN: 2631-8504

London Journal of Research in Science: Natural & Formal

Volume 24 | Issue 13 | Compilation 1.0

Single Slit to Curve-Single Slit, Double Slit to Curve-Double Slit to Non-Parallel-Double Slit to Non-Parallel-Curve-Double Slit Experiments - Photo Wave Phenomena

Hui Peng*

ABSTRACT

Feynman (1956) called the double slit experiment "... contains the only mystery. We cannot make the mystery go away by 'explaining' how it works". The photons are described by probability wave functions. The wave functions collapse to photons when landed on detector. However, the collapse of the wave function leads to the inconsistent/incomplete of the quantum mechanics (Penrose, 2022). In this article, we confirm that the diaphragm does not change the nature of the light passing through it. Then we perform multi experiments to show that, before and after passing through the diaphragm, the light is photons, not waves. It is photons that produce the interference pattern, we refer to it as "PhotoWave Phenomena". We show for the first time the novel phenomena, new mysteries: (1) a same single slit produces the non-diffraction patternn near the diaphragm, which gradually evolves to the orthogonal diffraction patterns; (2) a curve-single slit produces the non-diffraction pattern near the diaphragm, which gradually evolves to Hourglass-shape patterns; (3) a double slit produces the non-interference patterns near the diaphragm, which gradually evolves to the orthogonal interference patterns; (4) a non-parallel-double-slits produces the non-wave patterns near the diaphragm, which gradually evolves to the hybrid patterns; (5) a curved-double slit produces Arc-interference pattern near the diaphragm and Point-symmetry interference patterns near/on the detector; (6) Non-parallel-curve-double slit produces Butterfly-shape interference patterns; (7) simple differences in the shapes of slits lead to the profound differences in the pattern evolutions and in the final patterns, we referred to which as "Optical-Butterfly phenomena". We referred to above novel phenomena as PhotoWave phenomena. The PhotoWave phenomena support Penrose's statement. To explain completely/consistently PhotoWave phenomena is a challenge. PhotoWave experiments provide the comprehensive phenomena for further developing theoretical model to study the nature of the light, the complementarity principle, and the light wave theories.

Keywords: double slit, pattern evolution, Particle pattern, Transition pattern, Non-interference pattern, non-parallel double slit, hybrid pattern, curved-double slit, Arc interference pattern, Point-symmetry interference pattern, non parallel-curve-double slit, Butterfly-shape pattern, Optical Butterfly phenomena.

Contents

London Journal of Research in Science: Natural & Formal

5. PhotoWave phenomena: Double slit to Curved double slit

6. PhotoWave phenomena: double slit to non-parallel-curve-double slit

7. Summary and conclusion

I. INTRODUCTION

Historically, the study of the nature of light reached basically two concepts: wave and particle.

(1) Light is waves only: In 1690, C. Huygens established the wave theory of light [1].

(2) Light is particles only: In 1704, Newton established corpuscles theory [2].

(3) Light is waves only: In 1801, Young's double slit experiment [3] and Arago experiment [4] revived Huygens' wave theory.

(4) Light is Photons: In 1905, Einstein quantized light as photons to interpret "Photoelectric effect" [5].

(5) Wave-Particle duality: In 1927, to coordinate particle concept and wave concept of light, Bohr proposed the complementarity principle that stating that the wave and particle phenomena cannot be observed simultaneously

[6]. Until 1951, wave-particle duality of the light still puzzled Einstein, he wrote "All these 50 years of conscious brooding have brought me no nearer to the answer to the question: What are light quanta?" [7].

(6) Mystery of double slit: In 1956, Feynman called the double slit experiment "a phenomenon [...] has in it the heart of quantum mechanics. In reality, it contains the only mystery. We cannot make the mystery go away by 'explaining' how it works" [8].

(7) Light is Probability waves: a photon is described by a probability wave function which collapses to photon when one measures it [9].

(8) Penrose's Statement: In 2022, R. Penrose in an interview stated: "this is not something that people normally even recognize as a problem I mean they do but they shove it under the carpet which is known as the collapse of the wave function. Now you see current quantum mechanics strictly speaking is an inconsistent theory that is rather brutal way of saying what Einstein and Schrodinger and even Dirac said that quantum mechanics is incomplete" [10].

Three standard explanations of the normal double slit experiments are: (1) The classical optical wave; (2) The electromagnetic (EM) wave; (3) The probability wave function description.

In this article, we show (1) several novel phenomena which are new mysteries; (2) the nature and characteristics of the patterns of the parallel-double slit, non-parallel-double slit, curved-double slit, and non-parallel-curve double slit are distance-dependent, angle-dependence, curvature-dependence, respectively. Novel experiments show that the light is Photons not only in Photoelectric effect, but in the classical wave experiments. Namely *the light is photons, not waves, before and after passing through the double-slit. It is Photons that produce the non-wave patterns near diaphragms and wave patterns near/on the screen*. We referred to it as *"PhotoWave Phenomena"* [11,12]. Thus, no need to introduce both the wave-particle duality and the collapse of wave functions to interpret photons in measurement.

PhotoWave phenomena support Penrose's statement.

Let us summarize the evolution of the understand of the nature of the light (Table 1): (1) Light is waves only; to (2) light is both waves and photons; to (3) light is photons only [12].

Table 1: Comparison: Light as waves, as photons, as both,

	Light is Waves only	Wave-Particle duality	Light is Photons only
Wave pattern	*Light as waves* produces wave pattern	*Light as waves* produces wave pattern: Wave function collapsing on detector	*Light as Photons* produces wave patterns: *PhotoWave phenomena*
Photon effect		*Light as Photons* produces Photoelectric effect	*Light as Photons* produces Photoelectric effect

PhotoWave phenomena challenge the wave nature of the light, wave-particle duality, Bohr's complementarity principle, and the wave function collapse. It is a challenge to consistently interpretate the PhotoWave phenomena We provide novel experiments/PhotoWave phenomena for further theoretical development.

II. FOUR ZONES AND POSTULATES

2.1. Four Zones

Let us divide the space between the source and screen into four Zones (Figure 2.1) [13].

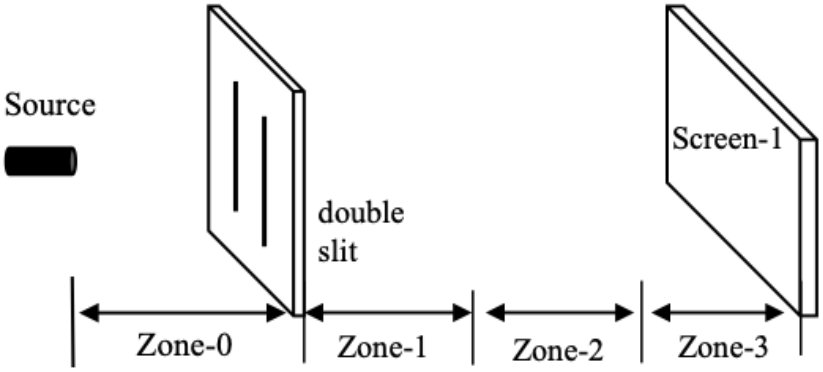

Figure 2.1: Four Zones

(1) *Zone-0:* between the source and the double slit, in which the pattern is non-wave, i.e., the light is photons before passing through the double slit;

(2) *Zone-1:* near the double slit, in which the patterns are *non-interference*, referred to the patterns as the *Particle pattern*;

(3) *Zone-3:* near the screen, in which the patterns are *Interference/diffraction patterns*;

(4) *Zone-2*: transition Zone, between Zone-1 and Zone-3; in which Particle patterns in Zone-1 evolve to the Interference Pattern in Zone-3, referred to the patterns in Zone-2 as *Transition patterns* that are also the *non interference pattern*.

2.2. Postulates

The wave-description of double-slit experiment is: *the light is waves, before and after passing through the double-slit*. In this article, we experimentally show: t*he light is photons, before and after passing through the double slit* [14], we refer to it as the photon-description of double-slit experiment.

Combining above two descriptions, we propose:

Postulate-1: the diaphragm, e.g., slide of double slit, does not change the nature of the light passing through it. Postulate-1 can be applied to quantum particles as well, such as electrons, etc.
Let us apply Postulate-1 to two descriptions of the double slit experiments:

Wave-description: the light is waves in the double slit experiments. Utilizing four Zones, the standard interpretation of Young's double-slit experiment can be rewritten as:

(1) *the light is waves* in Zone-0, i.e., *before passing* through the diaphragm, the light is waves.

(2) *the light is waves* in Zone-1, Zone-2 and Zone-3, i.e., *after passing* through the diaphragm and before landing on the detector, the light is waves.
(3) *the light is photons measured* on the detector.

The concept of the collapse of wave functions is necessary to explain the light landing on detector as particles.

Photon-description: the light is photons in the double slit experiments. It is photons that produce both the non interference patterns and interference patterns, we referred to it as "PhotonWave Phenomenon". Utilizing four Zones and Postulate-1, Photon-description states the following:

(1) *the light is Photons* in Zone-0, i.e., before passing through the diaphragm, the light is Photons.
(2) *the light is Photons* in Zone-1, Zone-2 and Zone-3, i.e., after passing through the diaphragm and before landing on the detector, the light is Photons.
(3) *the light is Photons* on the detector.

The concept of the collapse of wave functions is no longer needed, which support Penrose's statement. *Postulate-1* can be rewritten as: In Zone-0 and in Zone-1/Zone-2/Zone-3, the light has the same nature, as well the quantum particles.

Example-1: if we experimentally show that the light is photons in Zone-0, then the light is photons in Zone-1/Zone 2/Zone-3 as well.

Example-2: if we experimentally show that the light is photons in Zone-1, then the light is photons in Zone-0/Zone 2/Zone-3 as well.

Photon-description indicates that each fringe of the interference pattern on a detector is formed independently and partially. We have experimentally confirmed this indication [15,16].

We experimentally confirm "PhotonWave Phenomenon" in the article. However, we need to theoretically interpret the phenomenon of photons producing the wave patterns, the "PhotonWave Phenomenon".

Postulate-2 on convex lens

To study the details of the pattern evolution, we utilize the convex lens by placing the lens at different positions between the diaphragm and detector, so the light patterns arriving at the input surface of the lens are different. For the experiments, the original image is that when the light just comes out

the diaphragm. The input image is the pattern arriving at the input surface of the lens placed a distance away. Both the original image and the input image are different. To utilize the convex lens to study the evolution of patterns, we propose Postulate-2 of Lens. Postulate-2 contain three sub-Postulates:

Postulate-2.1: the convex lens enlarges the input image that arrives at the input surface; *Postulate-2.2:* The convex lens breaks/stops the evolution of the patterns;

Postulate-2.3: The convex lens does not change the nature of the input pattern.

Experiments in this article confirm Postulate-2.

Next, we show the universal phenomena that, the nature and the characteristics of the patterns depend on distance from the diaphragm, e.g., of the double slit/cross double slit. Namely in Zone-1, Zone-2 and Zone-3, the patterns are Particle patterns, Transition patterns and Interference patterns, respectively, i.e., in Zone-1 and Zone-2, the light is photons, and thus, in Zone-3, the light is photons that form the interference patterns. In the same classical wave experiment, the non-interference patterns evolve to the interference patterns, which is a mystery.

2.3. Experimental Setup

Experimental setup: Figure 2.2 shows Experimental setup without lens. Figure 2.3 shows Experimental setup with lens. For Experiments in this article, we utilize Experimental setup of Figure 2.2 and Figure 2.3.

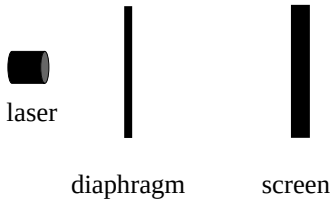

Figure 2.2: Experimental setup

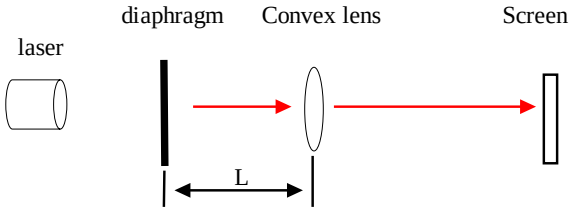

Figure 2.3. Experimental setup with lens . (a)

III. PHOTOWAVE PHENOMENA: SINGLE SLIT TO CROSS-SINGLE SLIT TO CURVE-SINGLE SLIT

In Section 3, we show the novel phenomenon of non-diffraction pattern evolving to diffraction patterns and then, show that the phenomenon is universal.

3.1. Single slit to cross-single slit to Curve-single slit

The single slit is one of the fundamental experiments in classical optics. We extend the single slit to the cross-single slit, and to the curve-single slit/cross-curve-single slit (Figure 3.1).

Figure 3.1: Diaphragm of single slit, curve-single slit and cross-curve-single slit

3.2. Single slit/cross single slit and pattern evolutions

The double slit has been extended to the cross double slits that have much more variations. We extend the single slit to the cross single slits. Then perform the single slit/cross-single slit experiments:

Experiment-3.1: Single slit experiment:

Experiment-3.2: Single slit cross tilt single slit

Experiment-3.3: Single slit orthogonally cross single slit

Experiment-3.4: Single slit crossing two double slit

Experiment-3.5: Single slit crossing ring

By Experimental setup (Figure 2.3), Experiment-3.1 to Experiment-3.5 show: (1) the phenomenon of the non diffraction patterns evolving to the diffraction patterns; (2) the phenomenon of the pattern evolution is universal. The evolutions of non-diffracting pattern to the diffraction patterns of Experiment-3.1 to Experiment-3.5 are summarized in Table 2.

Table 2: Evolutions of patterns of cross single slit experiments

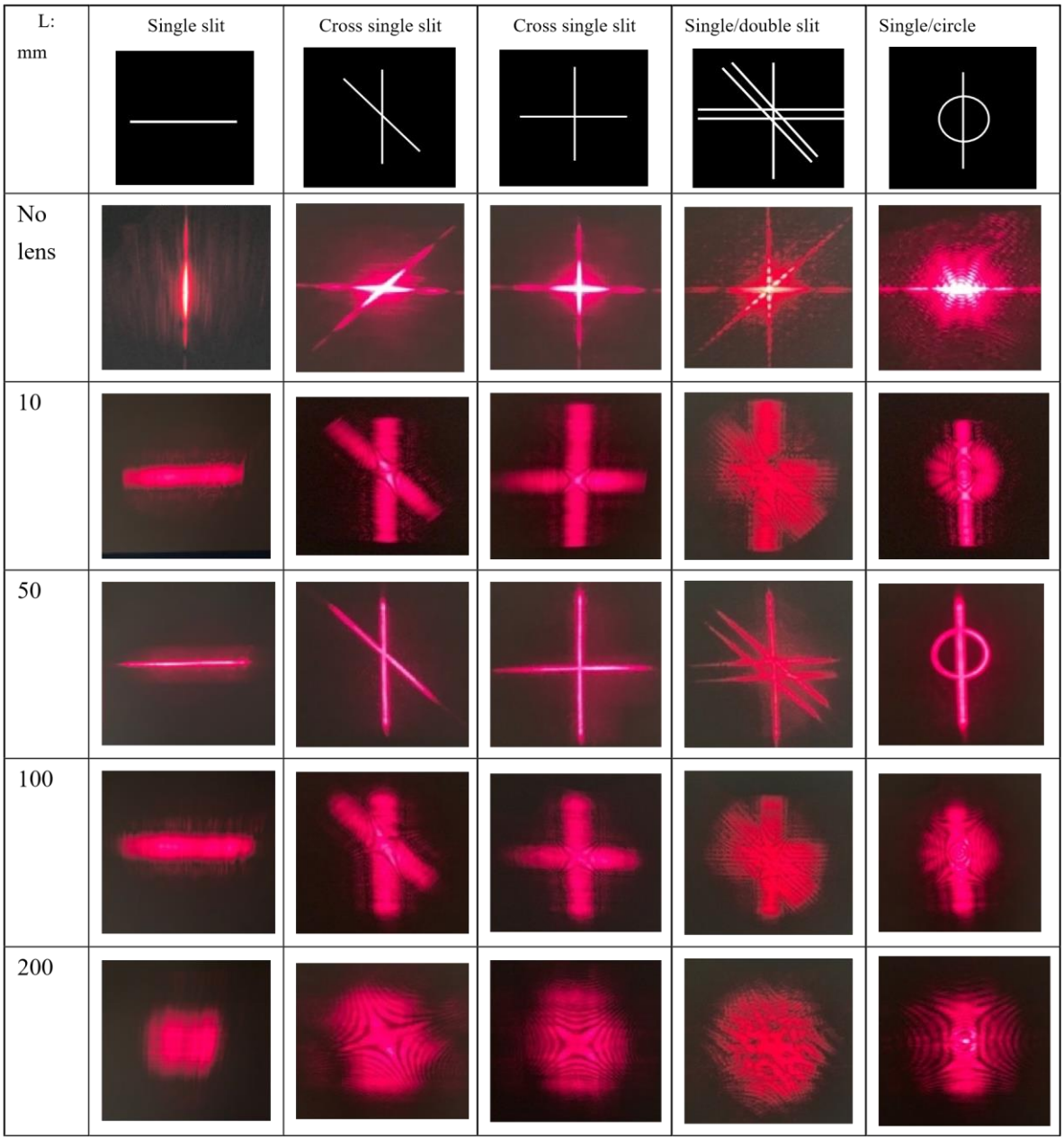

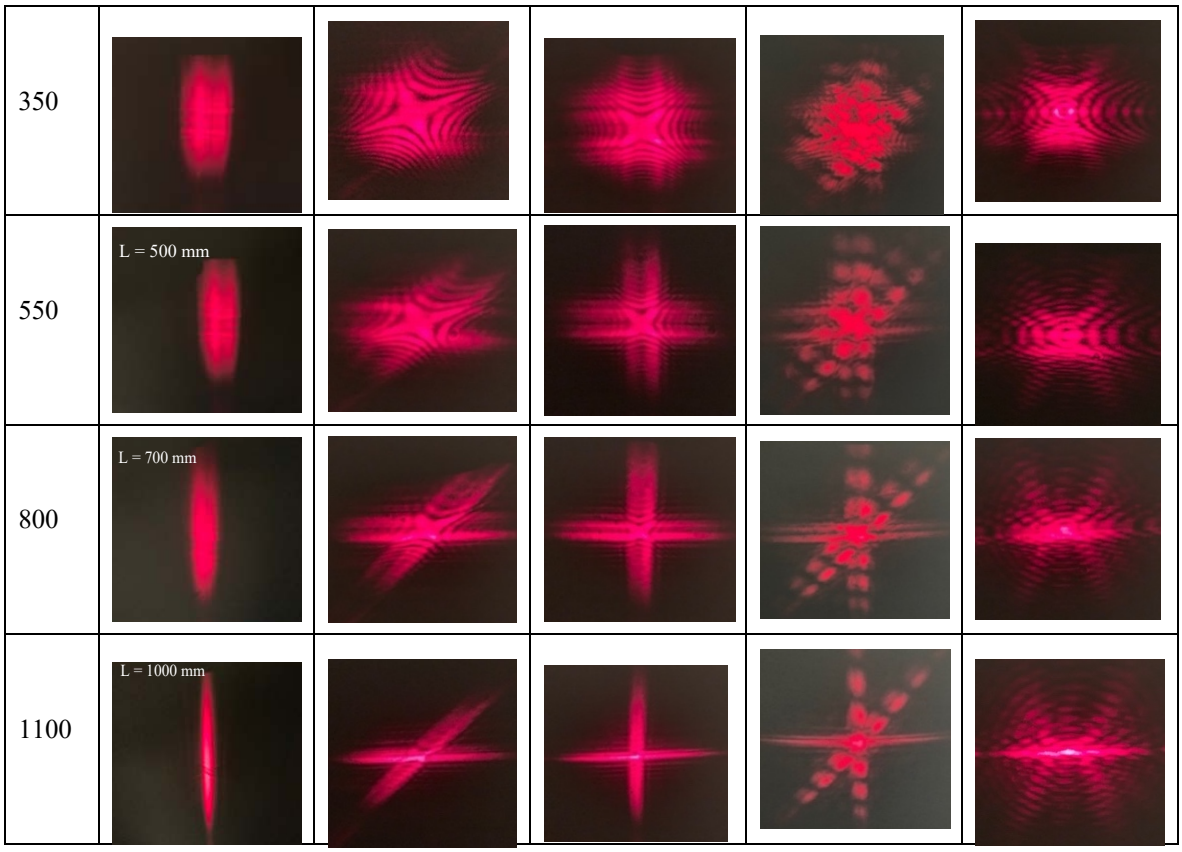

Observation: for all of Experiments

At L = 10 mm, the patterns are Pre-particle patterns

At L = 50 mm, the patterns are Particle patterns

At L = 100 to 800 mm, the patterns are Transition patterns

At L = 1100 and larger, the patterns are Diffraction and/or Interference patterns

Note: the evolution is gradually taking place, there is no clear cut between Particle patterns and Transition patterns, and between Transition patterns and the Diffraction patterns.

3.4. Curve-single slit and pattern evolution

We extend the single slit to the curve-single slits.

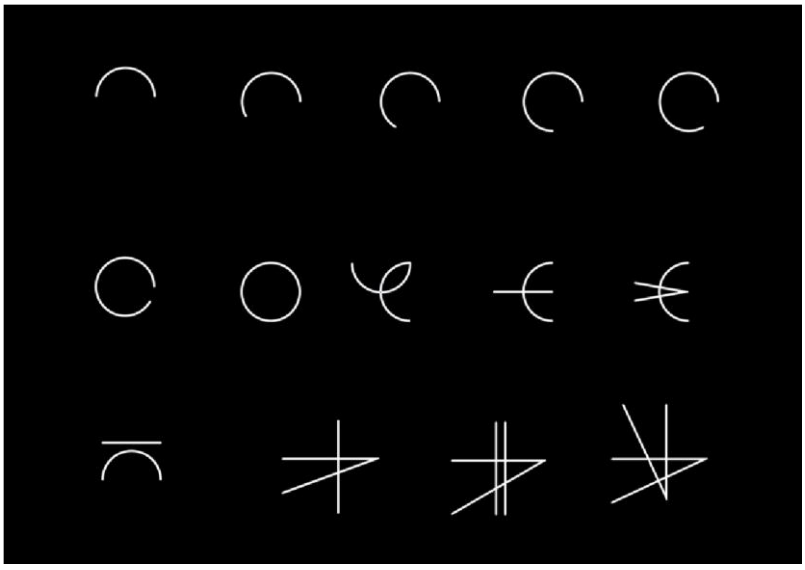

Figure 3.2: Curve-single slit and cross-single slit

Experiment-3.6: Curve-single slit experiment Utilizing Experimental setup of Figure 2.2, Figure 3.3 shows that the curve-single slit produces Hourglass-shape diffraction pattern.

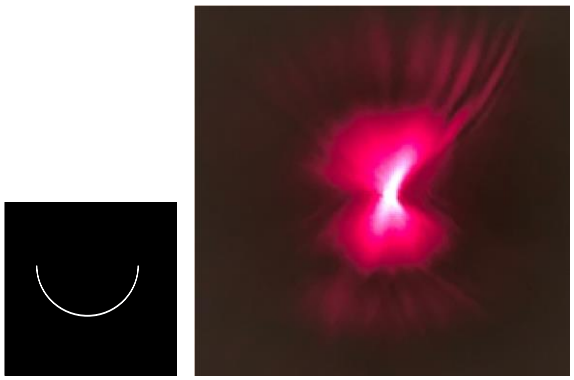

Figure 3.3: Hourglass-shape diffraction pattern of Curve-single slit

Using Experimental setup of Figure 2.3, Figure 3.4 shows the pattern evolution of curve-single slit

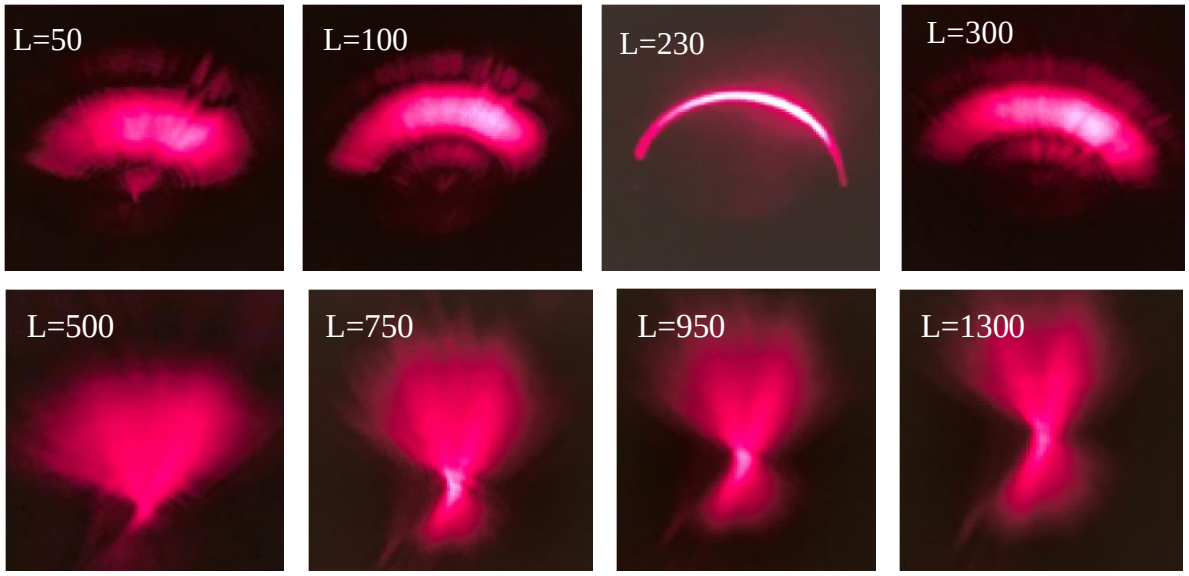

Figure 3.4: Pattern evolution of curve-single slit

Observation: Figure 3.4 shows the pattern evolution of the curve-single slit. At L=50 – 100 mm, we observe Pre particle patterns. At L = 230 mm, it is the typical Particle pattern. At L = 300 – 750 mm, we have Transition patterns. At L >300 mm, it is the pattern of the curve- single slit, referred to it as *Hourglass-shape pattern.*

3.5. Ring and pattern evolution

We extend the curve-single slit to the ring.

Experiment-3.7: (Figure 3.5 and 3.6):

Utilizing Experimental setup of Figure 2.2, Figure 3.5 shows that a ring produces the ring-shape interference patterns.

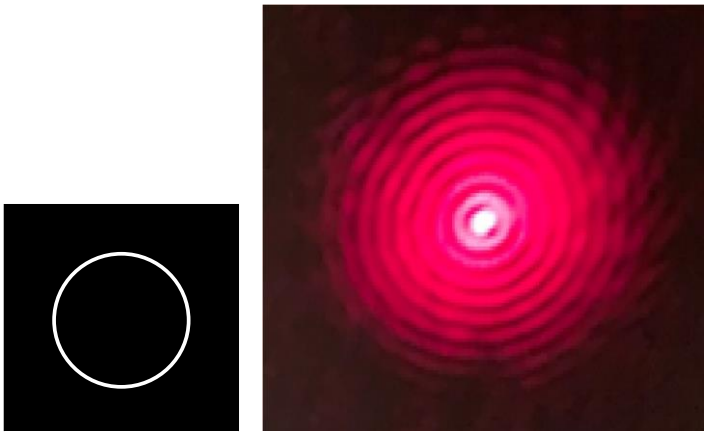

Figure 3.5: Ring and its pattern without lens

Utilizing Experimental setup of Figure 2.3, Figure 3.6 shows the pattern evolution of a ring.

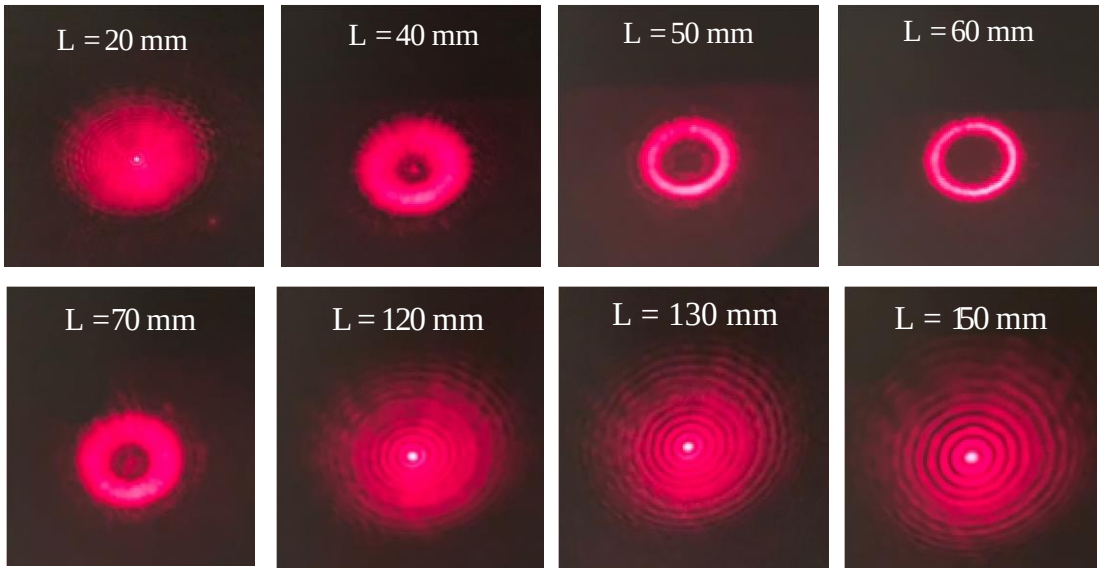

Figure 3.6: Evolution of patterns of ring experiment

Observation: When L = 60 mm, the pattern is the typical Particle pattern that is the image of the ring. Approximately, from L = 20 mm to L = 40 mm, the patterns are Pre-Particle patterns. At L >130, the photons produce Ring-shape Interference pattern.

Conclusion: Ring-shape Interference pattern has two characteristics:

(1) it is similar to Newton's ring interference pattern. However, difference is that Newton's ring is created by the reflection of light between two surfaces, typically a spherical surface and an adjacent touching flat surface.

(2) There is a spot at the center of the ring-shape interference pattern, which is similar to Arago spot/Poisson spot/Fresnel spot. However, difference is that Arago spot is at the center of a circular disc's shadow, not a ring.

3.6. Discussion

In Section 3, we show for the first time the novel PhotoWave phenomena/mystery:

(1) the pattern evolutions from the non-diffraction patterns to the diffraction patterns;

(2) the two evolutions taking place in the same experiments (e.g., Experiment-3.4): the non-interference pattern evolving to interference pattern, while non-diffraction pattern evolving to diffraction pattern simultaneously;

(3) The light is photons, not wave. It is photons that produce both the non-diffraction and diffraction patterns in the same experiment;

(4) PhotoWave phenomena are universal.

The patterns of the single slit, curve-single slit and ring are profoundly different (Table 3):

(1) a straight-line single slit produces the normal diffraction pattern;

(2) a curve-single slit produces Hourglass-shape pattern;

(3) a ring produces Ring-shape interference pattern with a spot at the center.

(4) A change in the shape of single slit alter the pattern evolution and the final pattern on the detector at larger distance.

Next let us compare both the pattern evolution and the final pattern on the detector (Table 3).

Table 3: Different patterns of single slit, curve-single slit and ring

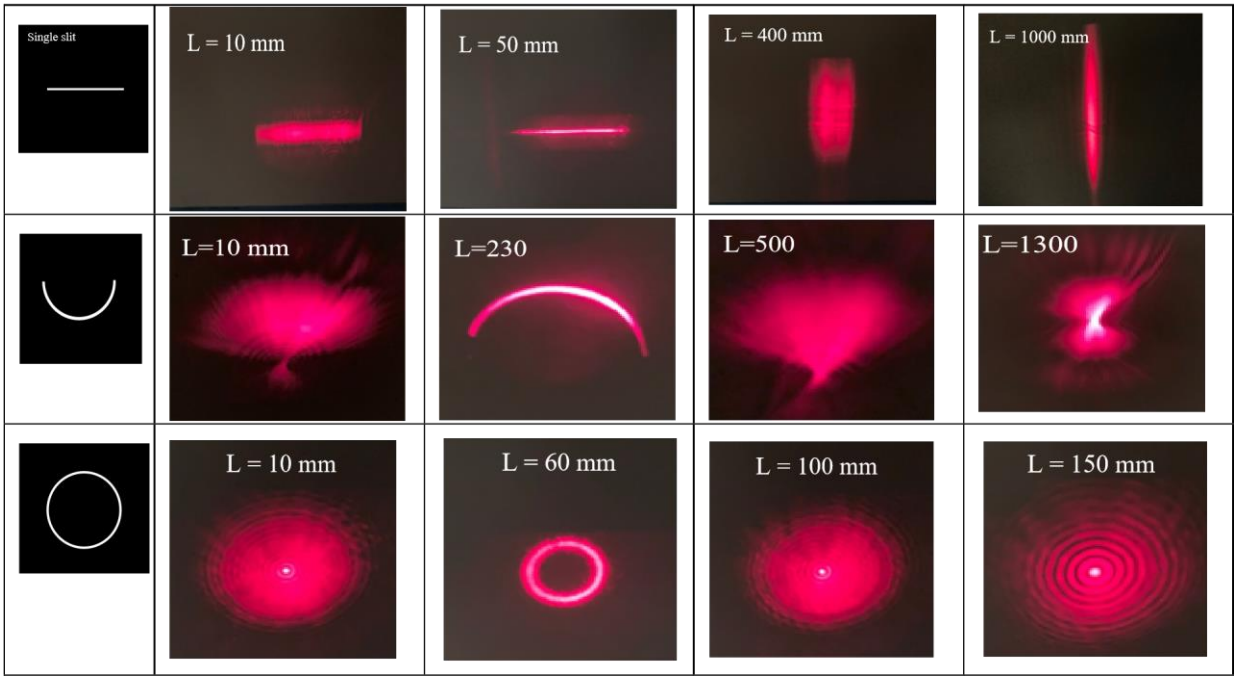

Conclusion:
Simple differences in the shapes of slits lead to the profound differences in the pattern evolutions and in the final patterns. The consistent and complete physical/mathematical interpretation is a challenge.

IV. PHOTOWAVE PHENOMENA: DOUBLE SLIT TO NON-PARALLEL DOUBLE SLIT

The double slit is one of the fundamental experiments in classical optics, where the two slits are parallel. We extend the parallel double slit to the non-parallel double slit and cross-non-parallel double slit (Figure 4.1). Non-parallel double slit of different angles (Figure 4.2) are utilized to show the angle dependence of pattern

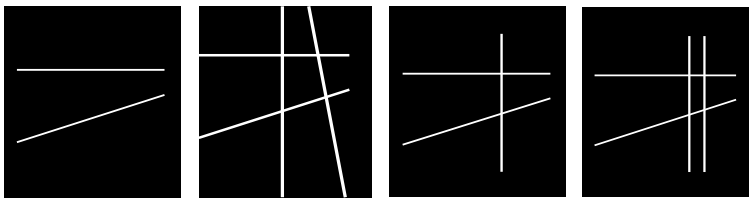

Figure 4.1: Diaphragm of non-parallel double slit/cross-non-parallel double slit

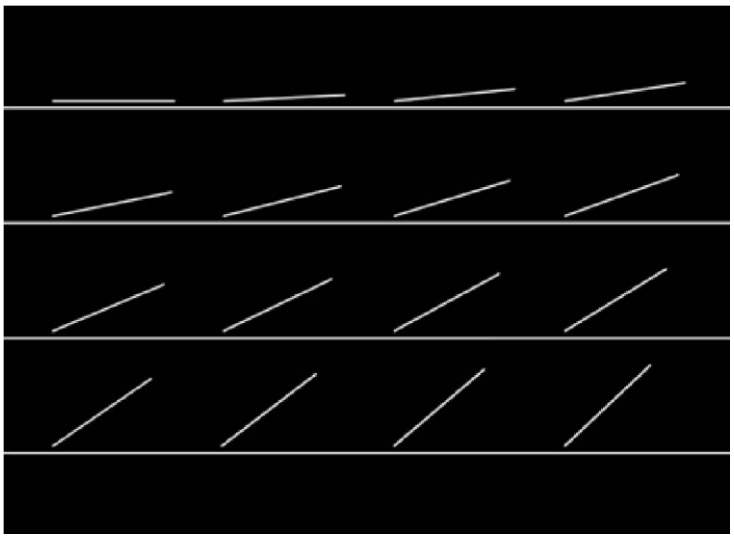

Figure 4.2: Diaphragm of non-parallel double slit of different angles

4.1. Non-parallel double slit: Hybrid pattern

We show for the first time the patterns of the non-parallel-double-slits: two non-parallel single slits produce Interference + Diffraction hybrid pattern, referred to it as the hybrid patterns.

Experiment-4.1.

The laser with beam-diameter 3 mm aims at the non-parallel-double-slits, as shown by the red circle in Figure 4.3. We set the distance between the diaphragm and the screen 1400 mm. The narrow-ends of two slit is 0.3 mm. As an example, the angle between two slits is 17.5°. Utilizing Experimental setup of Figure 2.2, Figure 4.3 shows that the non-parallel double slit produces the hybrid pattern

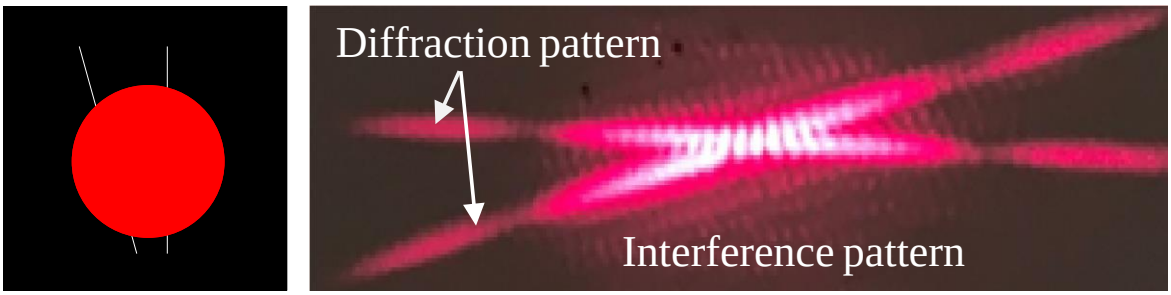

Figure 4.3: Interference pattern embedded in diffraction patterns

Observation: Figure 4.3 shows the non-parallel-double-slit and its novel pattern, i.e., the interference pattern embeds in the two diffraction patterns; we referred to the pattern as the Interference pattern + diffraction hybrid pattern or "Hybrid pattern". Two non-parallel slits produce two diffraction patterns respectively as they were independent single slit. While two slits produce the embedded interference pattern as they are a double slit.

Note: We show for the first time the mysterious phenomenon that the interference pattern embeds in the two diffraction patterns.

4.2. Pattern evolution: Photon producing patterns

Now, study the pattern-evolution of the non-parallel double slit.

Experiment-4.2

Experimental setup: Figure 2.3. The angle between two slits is 17.5°.

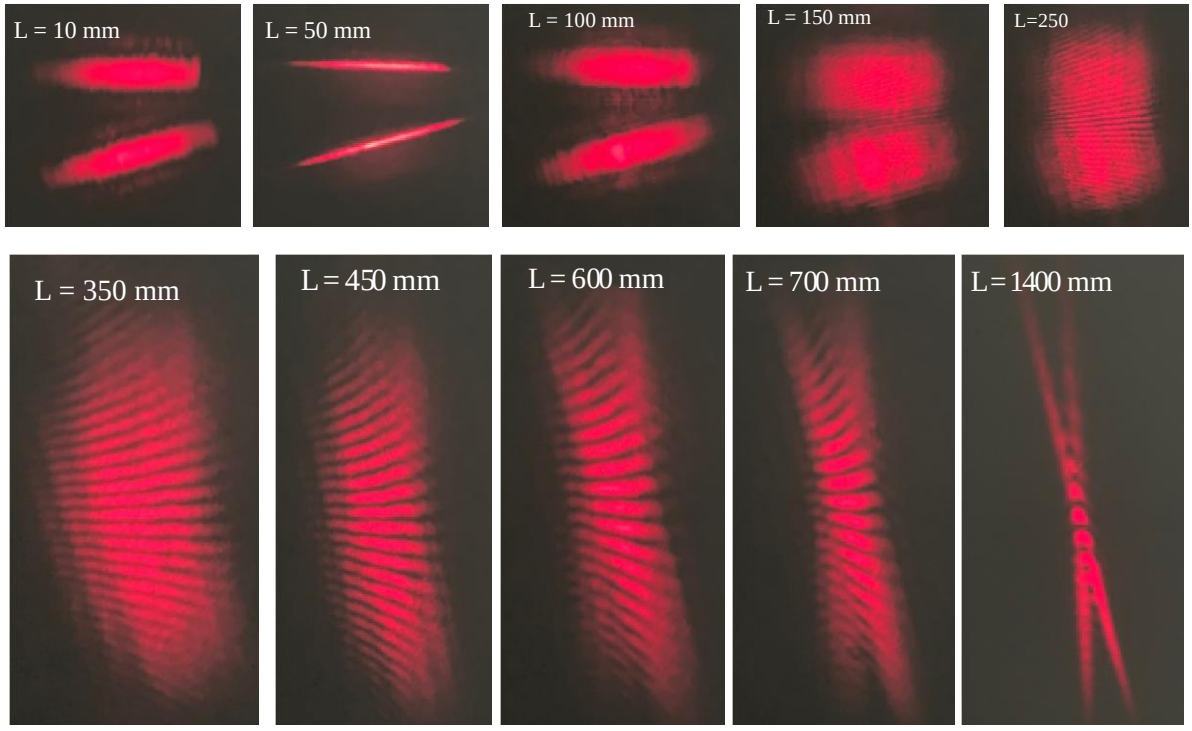

Figure 4.4: Pattern evolution of non-parallel double slit experiment

Observation: Figure 4.4 shows the pattern evolution. The patterns are the Particle patterns, at L = 10-100 mm. At *L* = 150-700 mm, we call the patterns Transition patterns. At *L* >300 mm, the patterns are the Interference.

4.3. Angle-dependence of patterns

Next, we show the phenomena: when the angle between two slits increases from the 0° to 45° and beyond, the interference pattern evolves to the partial interference + diffraction hybrid patterns and, finally, evolve to the crossing diffraction patterns. In the non-parallel-double slit experiments, the nature and the characteristics of the patterns depend not only on the distance from the diaphragm, but also on the angle between two slits.

Experimental setup: The laser with beam-diameter 3 mm aims at the non-parallel-double-slits, as shown by the red circle in Figure 4.3. The all distances between the bottom-ends of each tilt short slit and the horizontal long slits are 0.3 mm. Then, utilizing Experimental setup of Figure 2.2 and the diaphragm containing 16 double-slits with different angles: 0° - 45° (Figure 4.2), we show the angle-dependence of the patterns of the non-parallel double-slit experiments.

Experiment-4.3: 0° between two slits

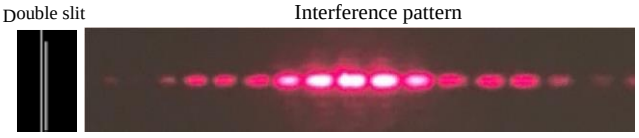

Experiment-4.4: 3° between two slits

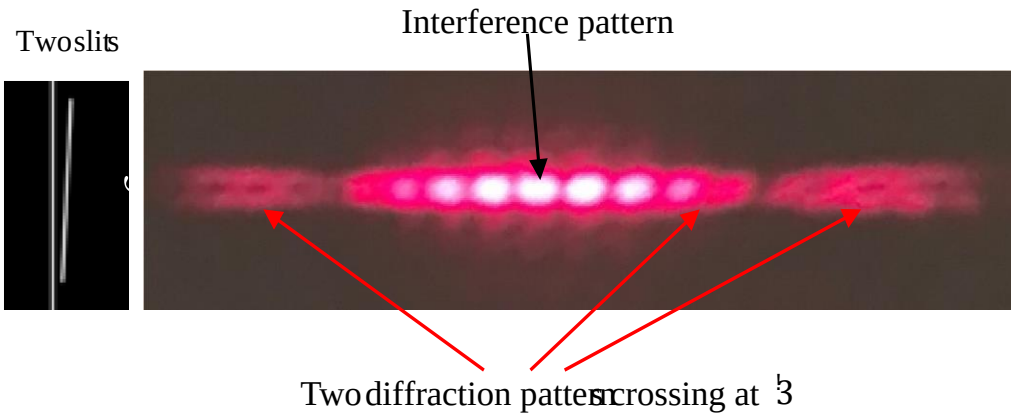

Experiment-4.5: 6° between two slits o

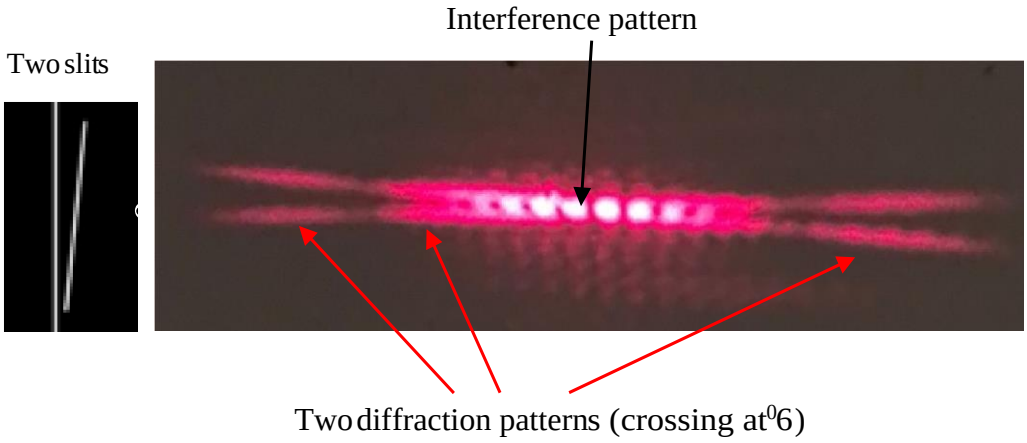

Experiment-4.6: 15° between two slits

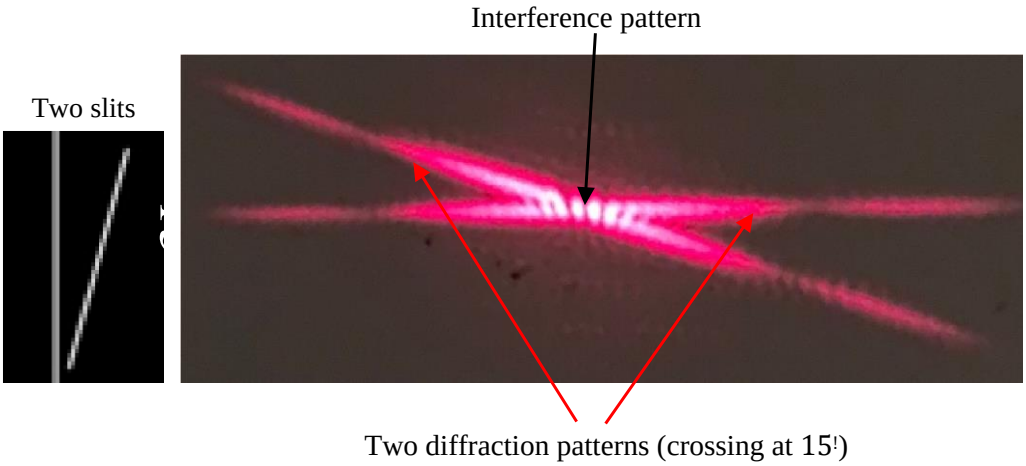

Experiment-4.7: 42° between two slits

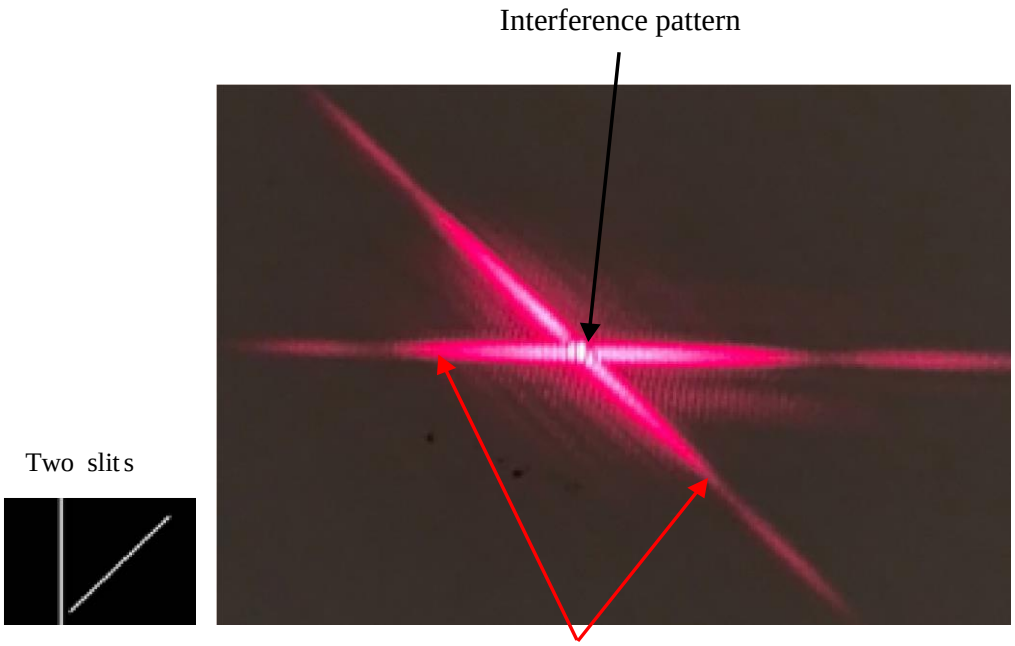

Two diffraction patterns (crossing at 42!)

Observation: there is the hybrid pattern at 42°.

Experiment-4 8: 45° between two slits

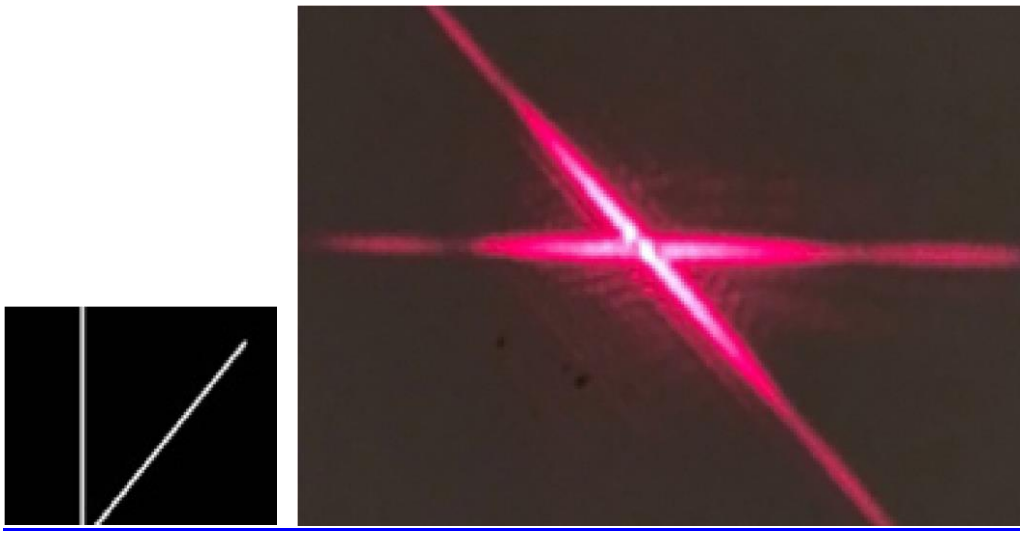

Observation: There is no hybrid pattern at 45°.

We show that when the angle between two slits is 0°, the pattern is the interference pattern; increase the angle between the two slits, the patterns are the hybrid pattern; at 45°, the pattern becomes the diffraction pattern. For certain angles, the non-parallel double slit produce the pattern that contains two diffraction patterns and the partial interference pattern embedded in the diffraction patterns, referred to it as the Interference + diffraction hybrid patterns or the hybrid patterns. The hybrid patterns depend on the angle between two slits.

4.4. Discussion

The hybrid pattern shows that the light is photons, not wave, and it is photons that produce the hybrid patterns, PhotoWave phenomena.

It is a challenge for the existing wave theories to interpret the hybrid pattern and thus, we suggest that the hybrid pattern indicates the interaction between photons.

The optical theory, EM theory and quantum probability theory cannot predict/explain this hybrid pattern and thus, are inconsistent/incomplete. A new theory is demanded.

V. PHOTOWAVE PHENOMENA: DOUBLE SLIT TO CURVED DOUBLE SLIT [20]

Now we extend the double slit to the curve-double slit and to the cross-curve-double slit (Figure 5.1). Then we study the pattern evolution of the curve-double slit, and the curvature-dependence of the patterns (Figure 5.2).

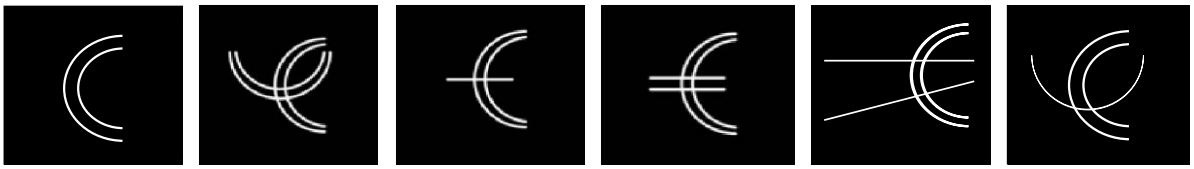

Figure 5.1: Diaphragm of curve-double slit and cross-curve-double slit

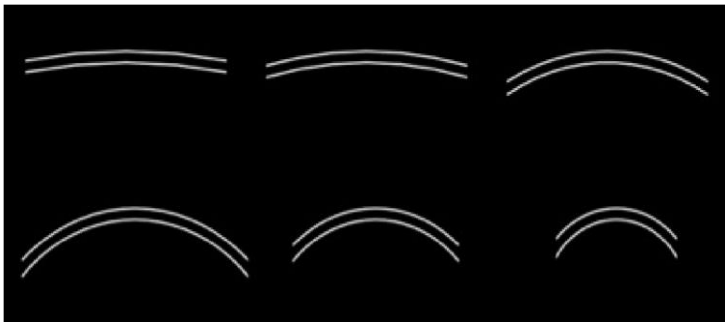

Figure 5.2: Diaphragm of curve-double slit of different angles

5.1. Curve-double slit: Arc-Shape and Point-Symmetry Interference Pattern

Cross double slit-1 Cross double slit-2 Ring

Experiment-5.1: Arc-shaped interference pattern and Point-symmetry interference pattern

Experimental setup: Utilizing Experimental setup of Figure 2.2, Figure 5.3 shows the curve-double slit and its Arc interference pattern and Point-symmetry interference pattern

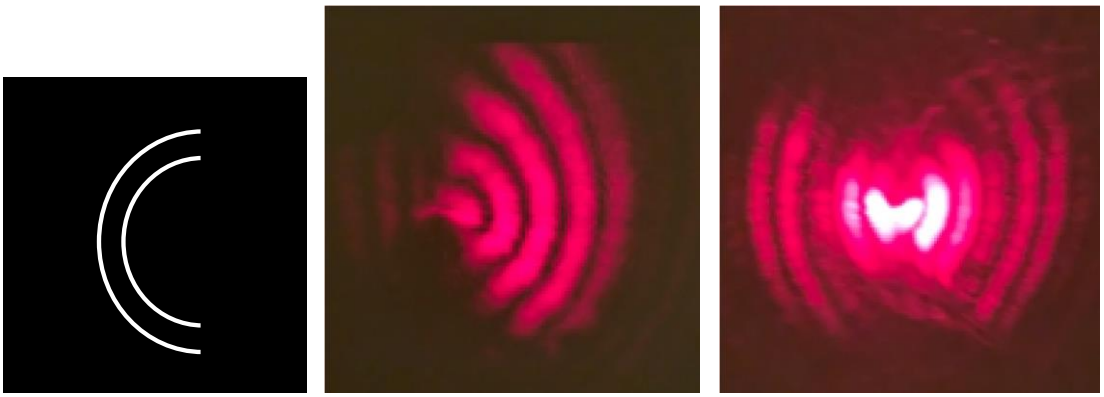

Figure 5.3: Arc-interference and Point-symmetry interference pattern

Observation: we observe Arc-shaped interference pattern near the curved-double slit and Point-symmetry interference pattern at detector (Figure 5.3).

5.2. Pattern Evolution: Photon producing Arc-shape and Point-symmetry interference patterns

To study the pattern evolution, we use Experimental setup in Figure 2.3: The lens is placed at different positions "L mm".

Experiment-5.2.

Experimental setup: Figure 2.3.

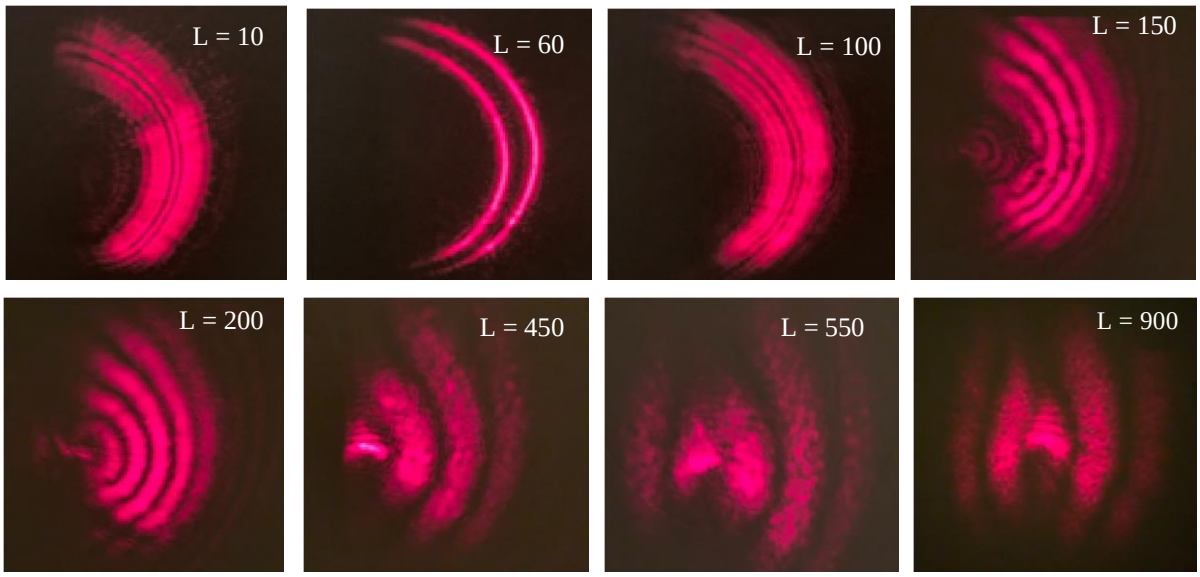

Figure 5.4: Pattern Evolution

Observation (Figure 5.4): we observe for the first time the following pattern and its evolution: L =10 mm, Pre-particle pattern; L = 60 mm, Particle pattern; L =100 -150 mm, Transition pattern-1; L =200 mm, Arc-shaped interference-pattern; L = 350 -550 mm, Transition pattern-2; L = 900 mm and larger, Point-Symmetry-interference-pattern

Conclusion: the light is photons, not waves.

Note: the evolution gradually takes place, there is no clear cut: (1) between Pre-Particle patterns and Particle patterns; (2) between Particle patterns and Transition patterns-1; (3) between Transition patterns-1 and Arc interference-patterns; (4) between Arc-interference-patterns and Transition patterns-2; and (5) between Transition patterns-2 and Point-Symmetry-interference-patterns.

5.3. Curvature-dependence of Pattern

Experiment-5.3: Utilizing Experimental setup (Figure 2.2), Figure 5.5 shows the curvature-dependence of the patterns of the curved-double slit.

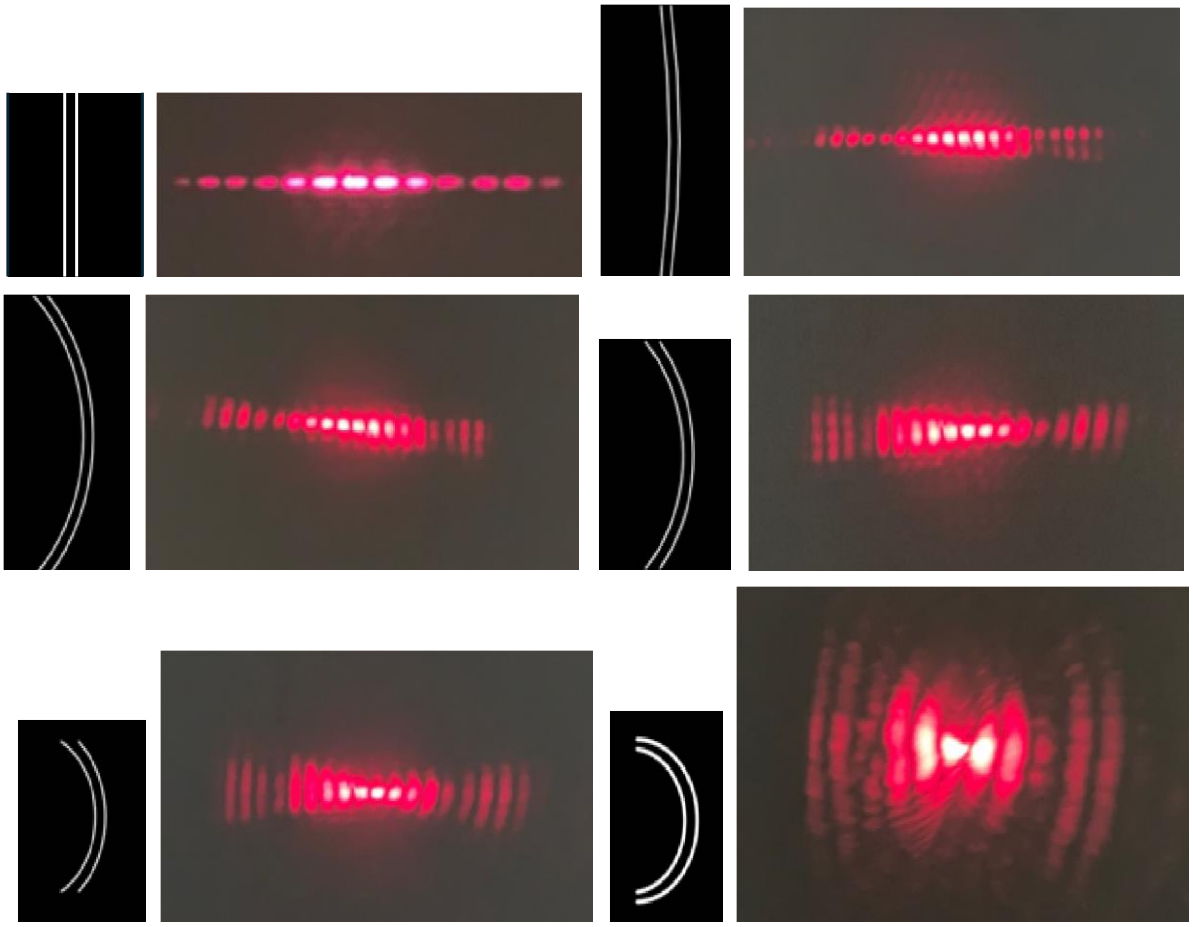

Figure 5.5: Curvature-dependent patterns of curved double slit

Observation: Figure 5.5 shows the curvature-dependence of the patterns of the curved double slit experiments.

5.4. Single-slit crossing curve-double-slit

5.4.1. Single slit crossing curve-double slit

Experiment-5.4: single slit crossing curve-double slit

Experimental setup: Utilizing Experimental setup of Figure 2.2, Figure 5.6 shows that a Single slit crossing curve double slit produces a pattern of a diffraction pattern crossing a Point-symmetry interference patter at detector.

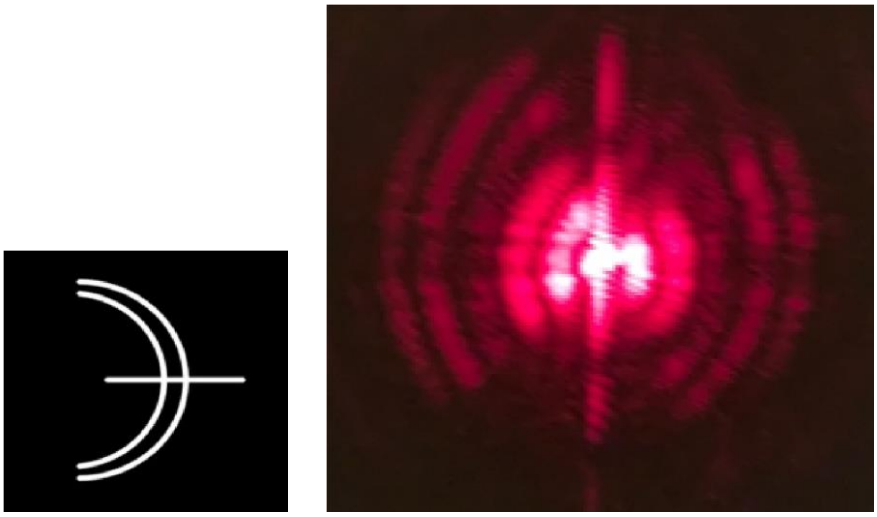

Figure 5.6: Single slit crossing curve-double slit

5.4.2. Pattern evolution

Experiment-5.5: Pattern evolution of Single slit crossing curve-double slit

Experimental setup: Figure 2.3.

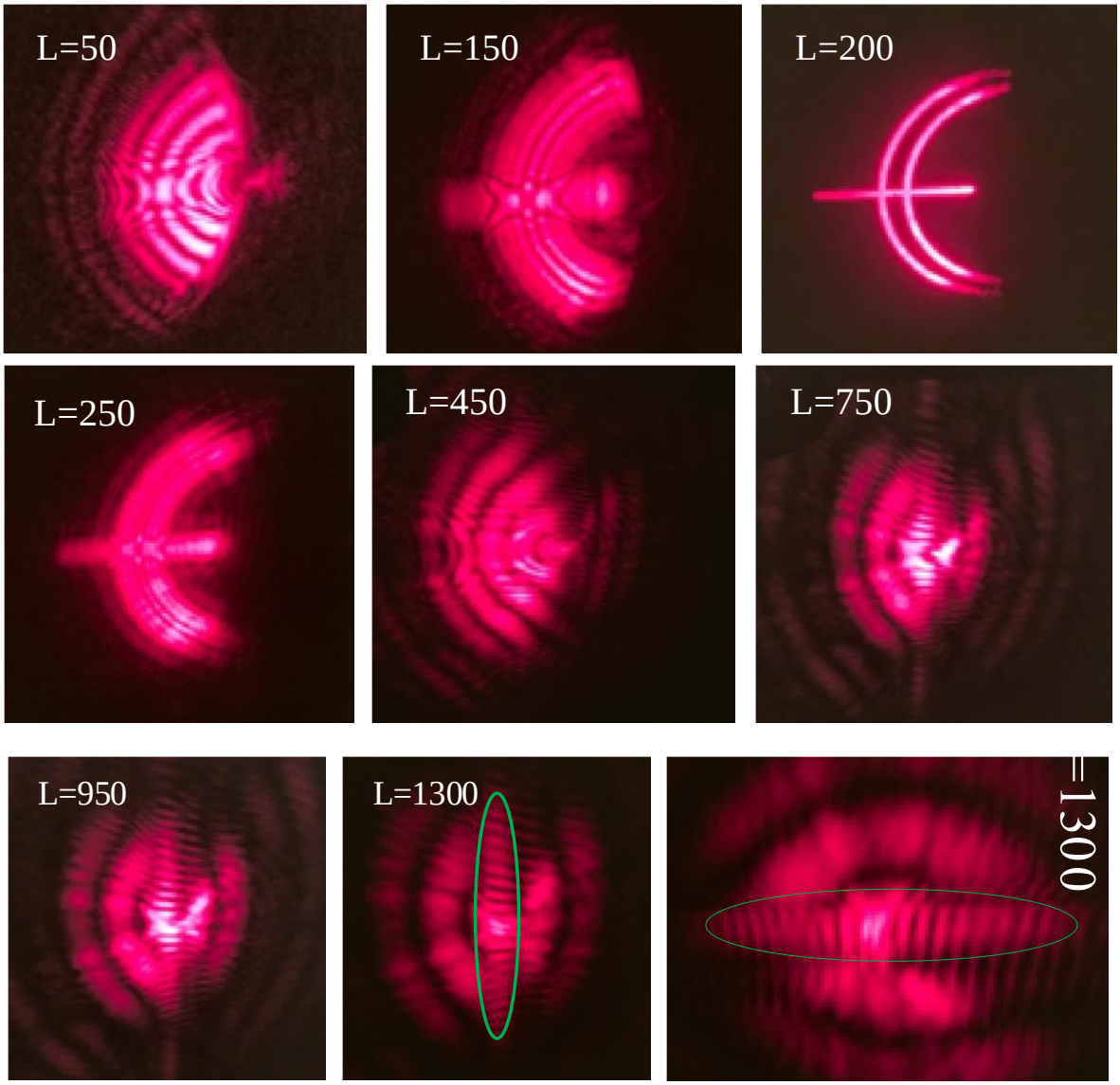

Figure 57: Pattern evolution

Observation (Figure 5.7): we observe Arc-shape interference pattern at L = 50 mm, Transition pattern at L = 150 mm, Particle pattern at L = 200 mm, Transition pattern at L = 250 mm, Arc-shape interference pattern at L = 450 mm, Point-symmetry interference pattern at L = 750-1300 mm.

Note: as shown by the green oval at L = 1300 mm, the single slit produces an interference pattern, but a diffraction pattern. The right of Figure 5.7 *shows the enlarged interference pattern due to single slit*.

5.5. Double slit crossing curve-double slit

5.5.1. Double slit crossing curve-double slit

Experiment-5.6: double slit crossing curve-double slit

Experimental setup: Fig. 2.2

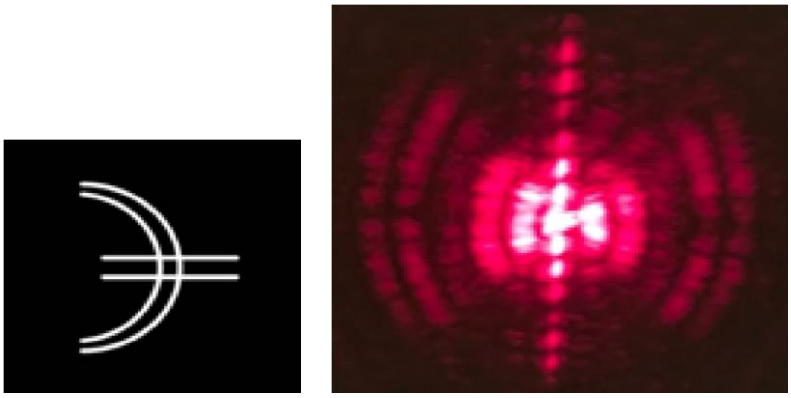

Fig. 5.8: Double slit crossing curved double slit and pattern

Observation (Fig. 5.8): the right is the vertical interference pattern crossing the Point-symmetry interference pattern.

5.5.2. Pattern evolution

Experiment-5.7:

Experimental setup: Fig. 2.3.

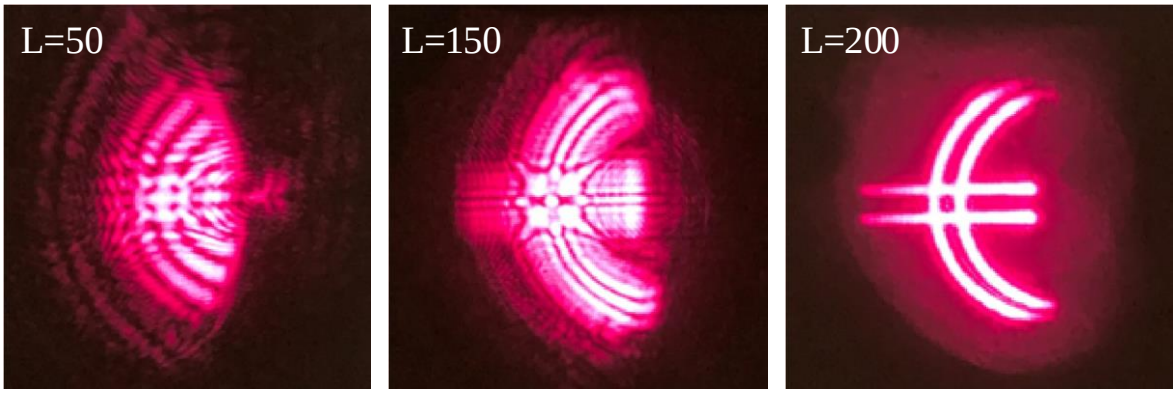

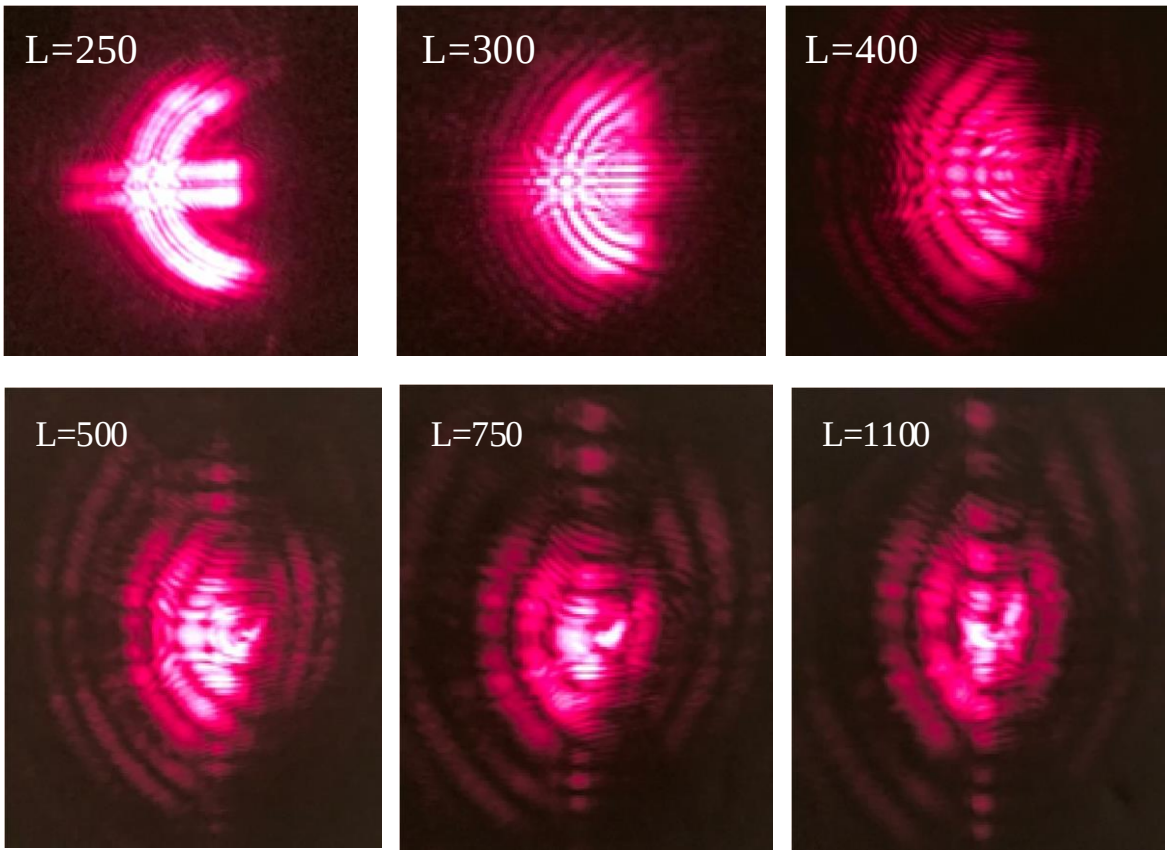

Fig. 5.9: Pattern evolution of double slit crossing curve-double slit

Observation (Fig. 5.9): we observe Arc-shape interference pattern at L = 100-150 mm, Particle pattern at L = 200 mm, Transition pattern at L = 250 mm, Arc-shape interference pattern at L = 300 mm, interference pattern crossing Point-symmetry interference pattern at L = 500-1100 mm.

5.6. Curve-double slit crossing curve-double slit

5.6.1. Curve-double slit crossing curve-double slit

Experiment-5.8: curve-double slit crossing curve-double slit (Figure 5.10)

Experimental setup: Fig. 2.2

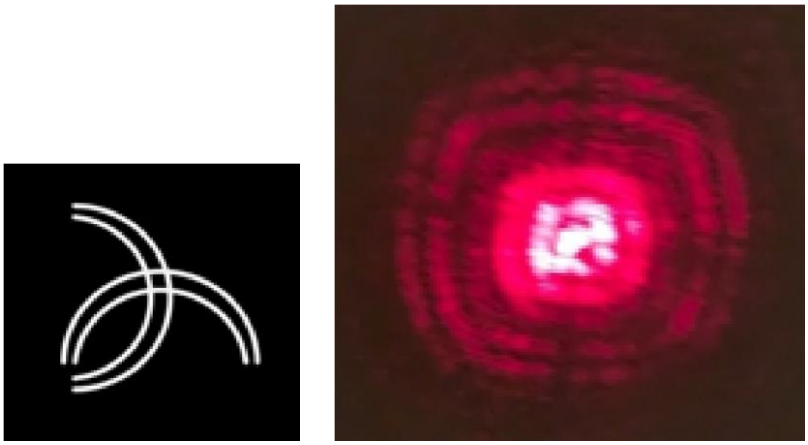

Fig. 5.10: curve-double slit crossing curve-double slit and pattern

Observation (Fig. 5.10): the right is the interference pattern, we referred to it as Square-shape interference pattern.

5.6.2. Pattern evolution

Experiment-5.9: curve-double slit crossing curve-double slit

Experimental setup: Fig. 2.3

Figure 5.11: shows the pattern evolution of curve-double slit crossing curve-double slit

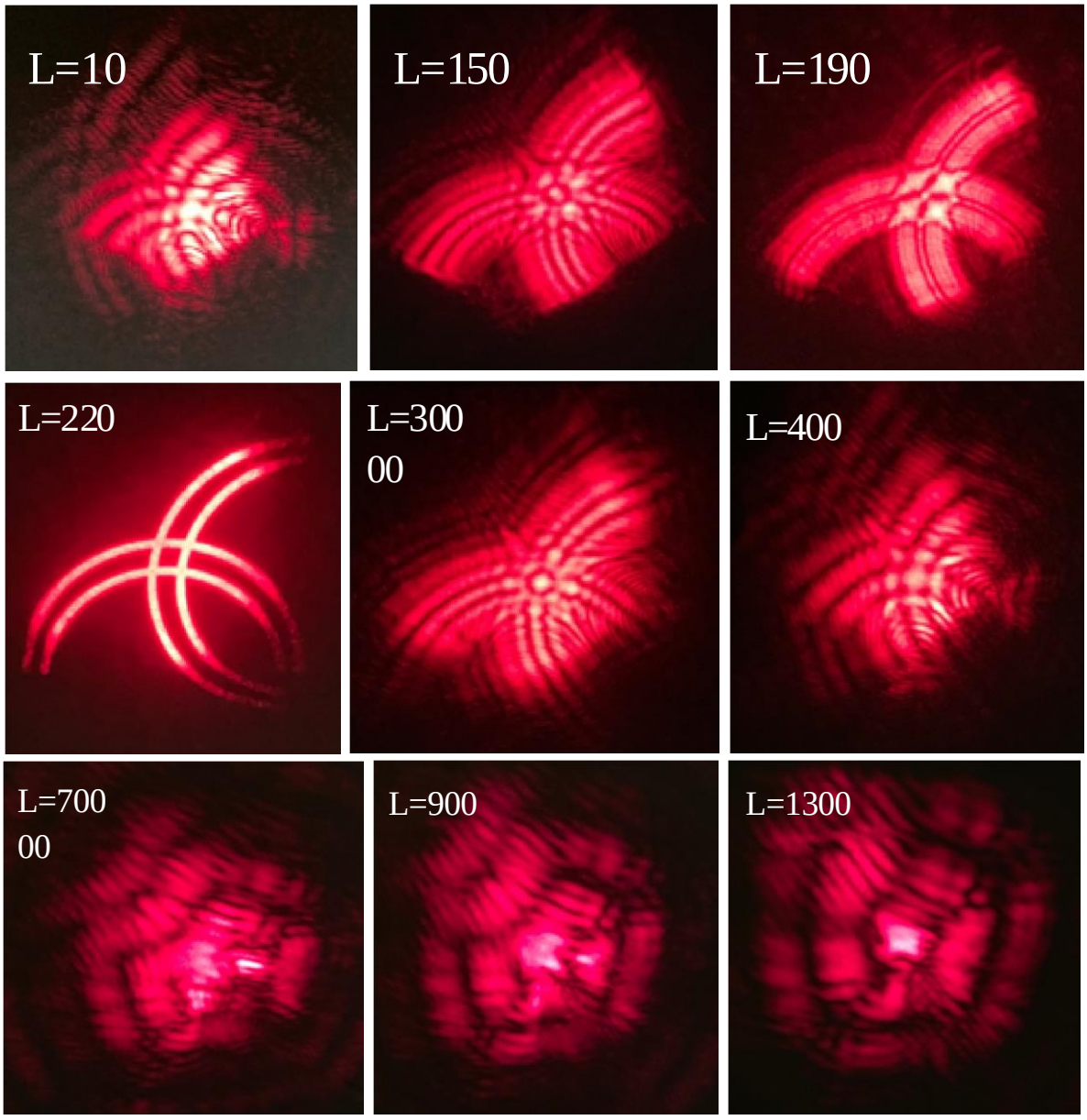

Fig. 5.11: . Pattern evolution

Observation (Figure 5.11): Patterns at L=10-190 mm are Pre-particle patterns. At L=220 mm, it is the typical Particle pattern. At L=300-700 mm, patterns are Transition patterns. At L >900 mm, pattern become the interference patterns, referred to it as Square-shape interference patterns.

5.7. Discussion

By preforming the curve-double slit experiments, we show Arc-shape interference-pattern and Point-Symmetry interference-patterns. For Curve-double slit crossing curve-double slit experiments, we observe Square-shape interference pattern.

Cross-double slit has two straight double slit; double- slit-crossing-curve-double-slit has one straight double-slit and one curve-double-slit; curve-double-slit-crossing- curve-double-slit has two curve-double -slit. Next let us Cross double slit-1 Cross double slit-2 Ring compare both the pattern evolution and the final pattern on the detector.

Table 4: Comparison of cross-double slit, double slit crossing curve-double slit andcurve-double slit crossing curve-double slit

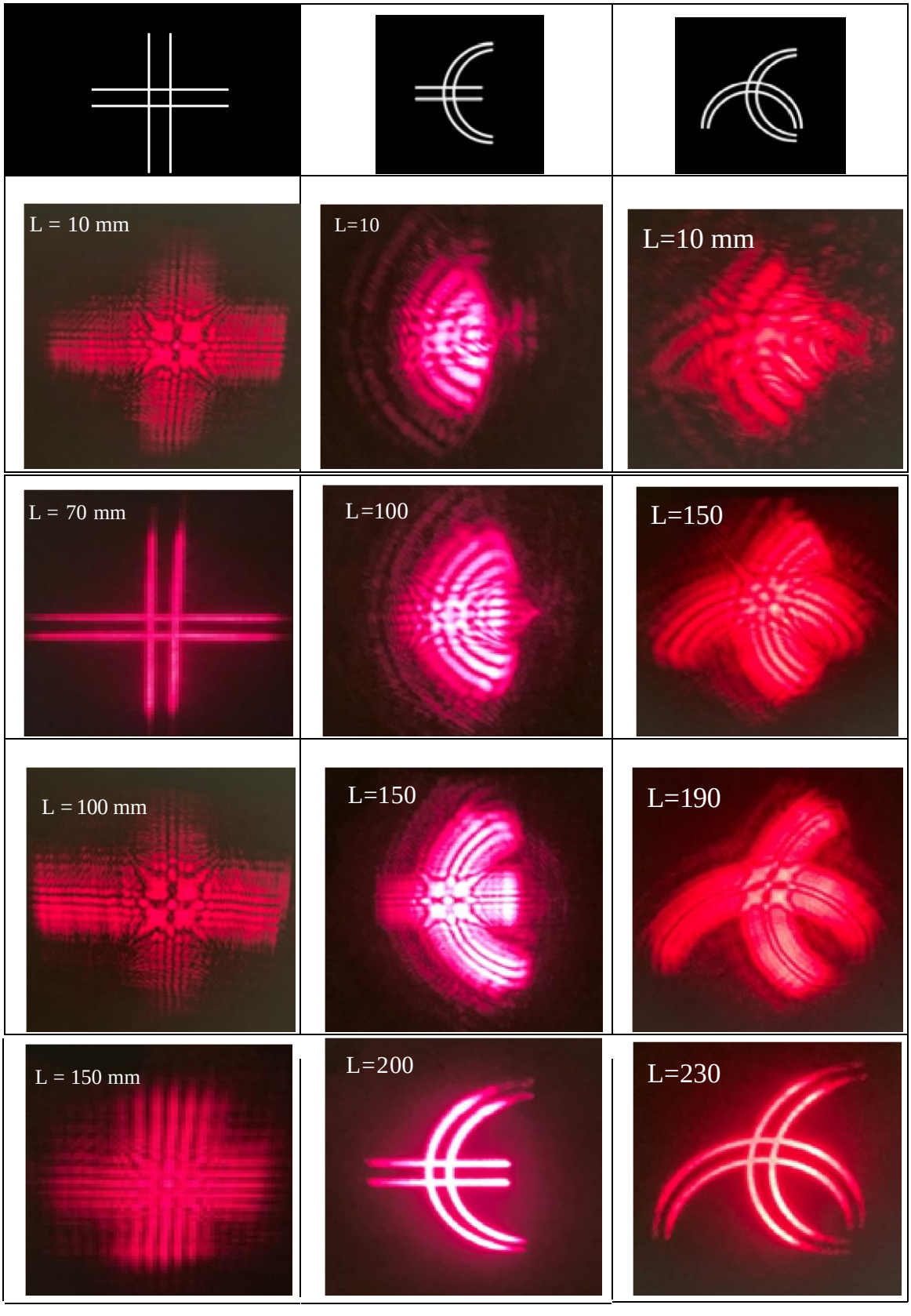

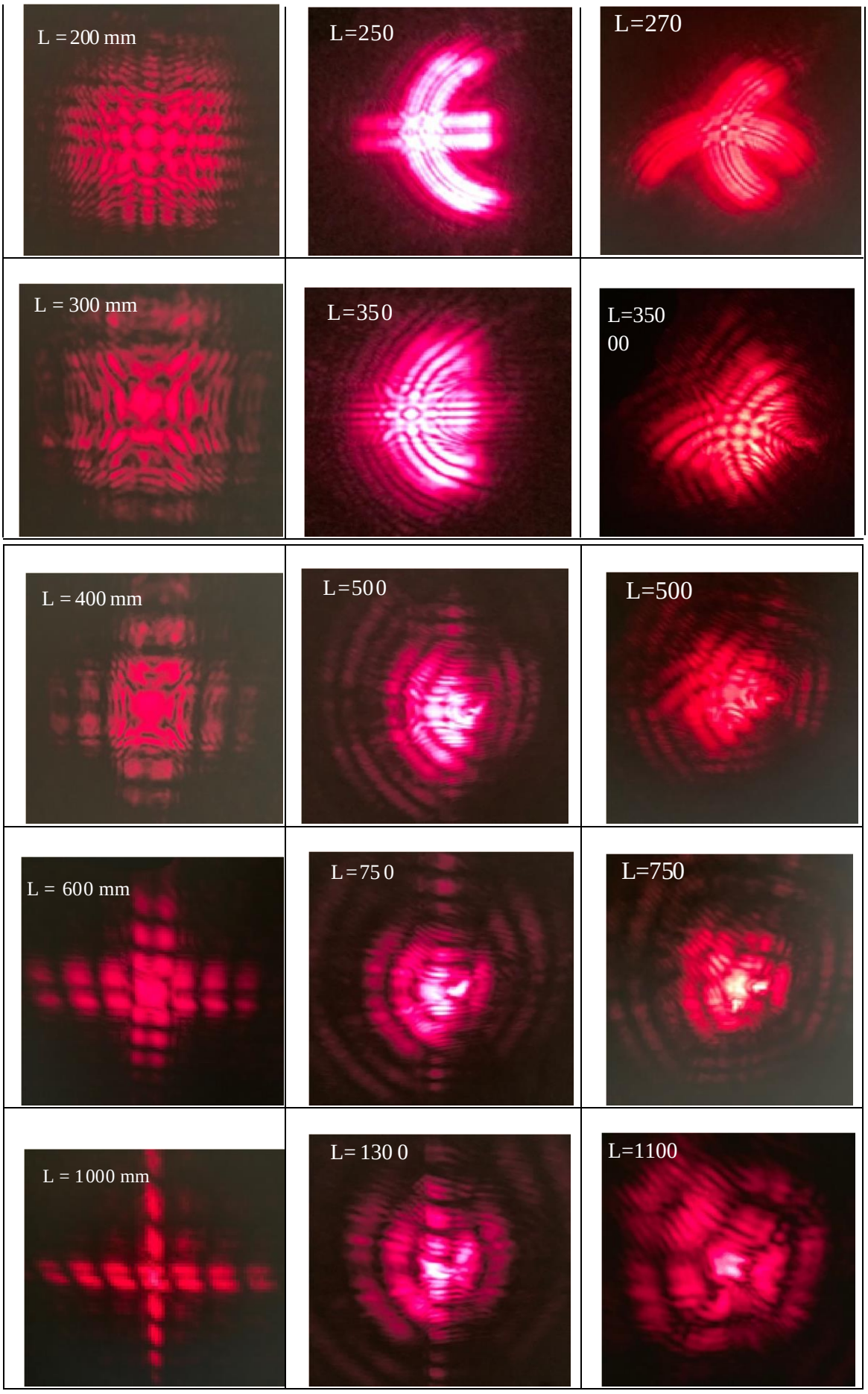

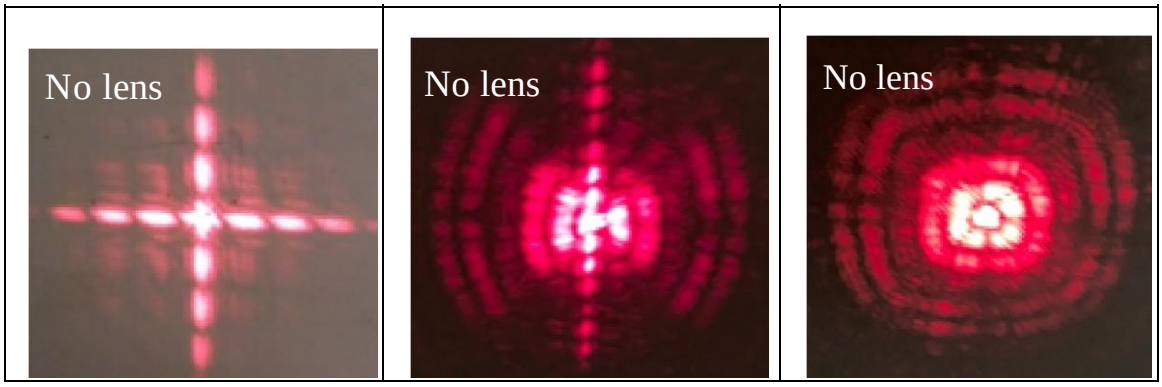

Differences in the shapes of slits lead to the profound differences in the pattern evolutions and in the final patterns.

VI. PHOTOWAVE PHENOMENA: DOUBLE SLIT TO NON-PARALLEL-CURVE-DOUBLE SLIT

6.1. Non-parallel-curve-double slit: Butterfly-shape interference pattern

Now we extend the non-parallel-double-slit or curve-double-slit to the non-parallel-curve-double-slit (top of Figure 6.1) and then, study its pattern evolution (Figure 6.2), and the curvature-dependence of the patterns (Table 4).

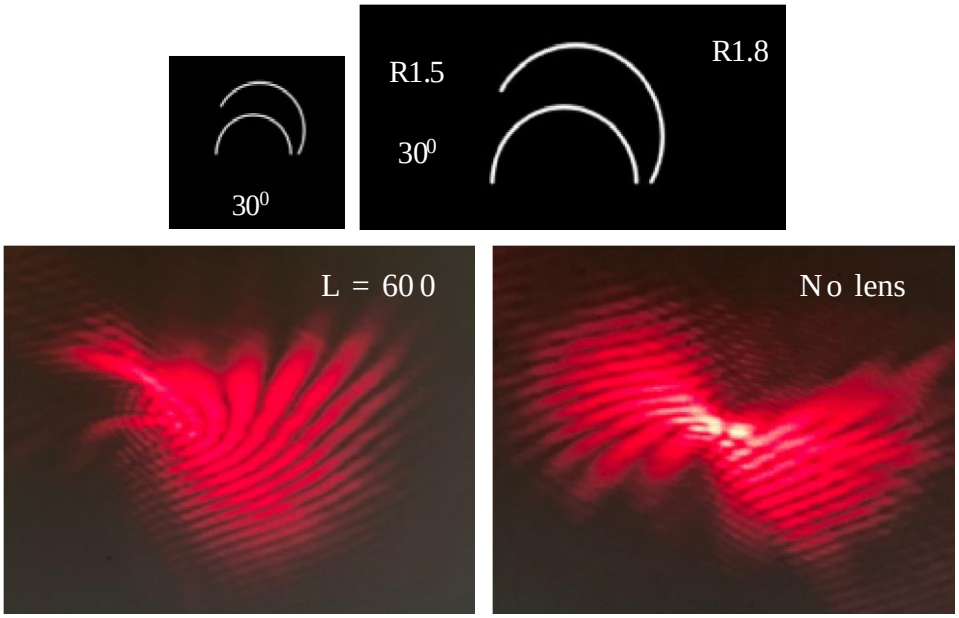

Figure 6.1: Non-parallel-curve-double slit and Butterfly-shape patterns

Observation: Figure at L = 600 mm shows a "Resting-Butterfly-shape interference pattern" or "close-wing Butterfly" pattern. The right of Figure 6.1 shows a "Flying-Butterfly-shape interference patterns" or "open-wing Butterfly" pattern.

6.2. Pattern Evolution: Photons producing Butterfly-shape interference pattern Experiment-6.1

(Fig. 6.2): pattern evolution

Experimental setup: Fig. 2.3.

Figure 6.2 shows the pattern evolution of the non-parallel-curve-double slit.

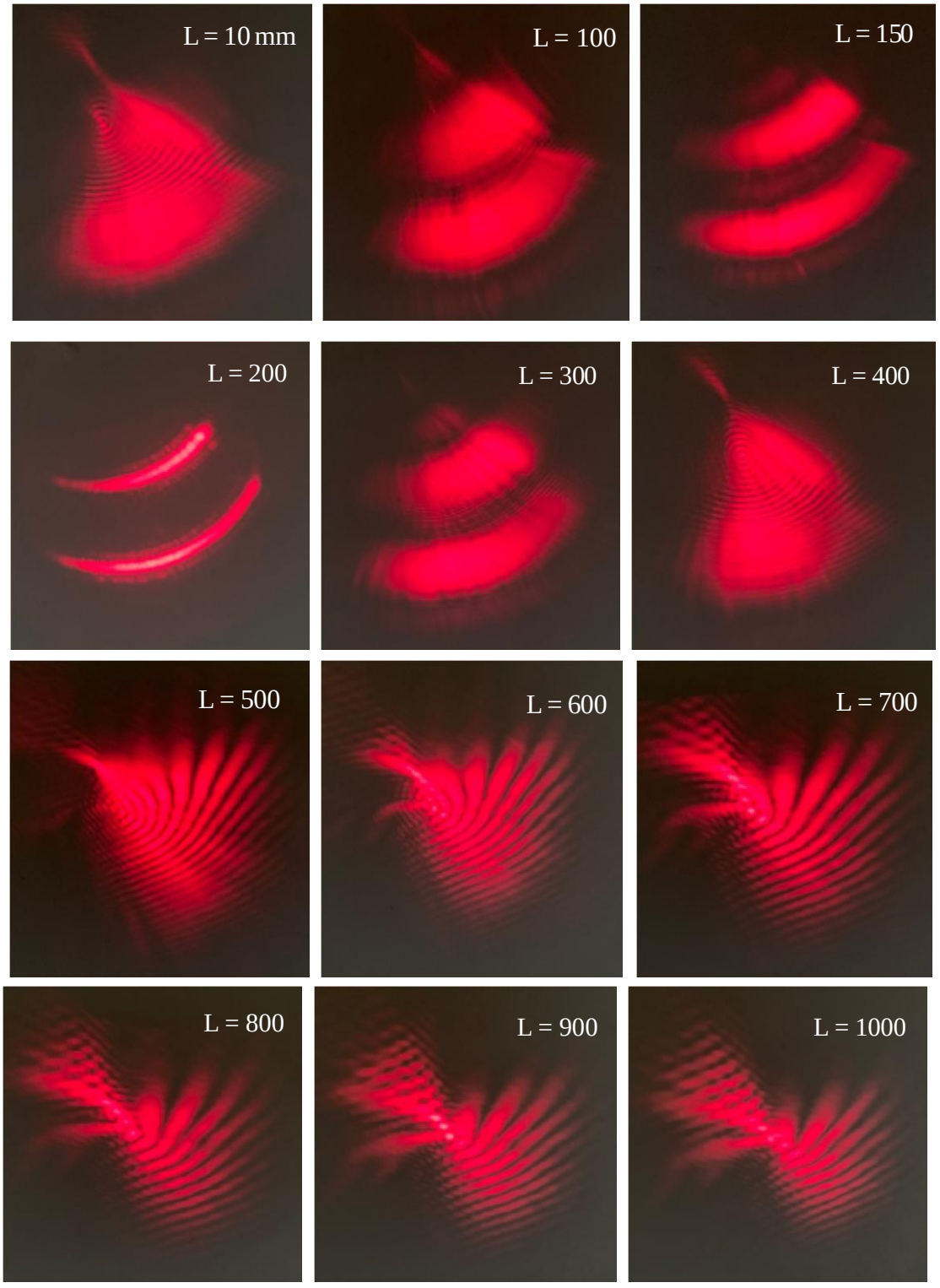

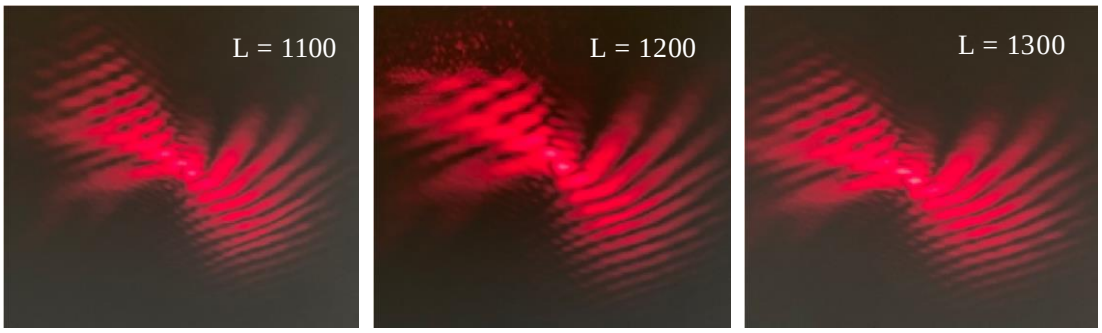

Fig. 6.2: Pattern evolution

Observation (Fig. 6.2):

Figures at L = 10-100 mm shows Pre-particle patterns; at L = 150-200 mm, showing Particle pattern, the image of the non-parallel curved double slit; at L = 300 - 400 mm, showing Transition patterns; at L = 500-600 mm, showing Resting-Butterfly-shape interference pattern; at L = 700 - 1000 mm, showing Transition patterns; at L = 1100-1300 mm, showing Flying-Butterfly-shape interference patterns.

We refer to the patterns at L = 500-600 mm as a "Resting-Butterfly-shape interference pattern" or "close wing Butterfly" pattern; while the pattern at L = 1300 mm as a "Flying-Butterfly-shape interference patterns" or "open wing Butterfly" pattern.

Note: the patterns gradually evolve, so there is no clear cut between patterns.

6.3. Angle-Dependence of Butterfly Patterns

Now let us study the Angle-Dependence of Butterfly Patterns (Fig. 6.3).

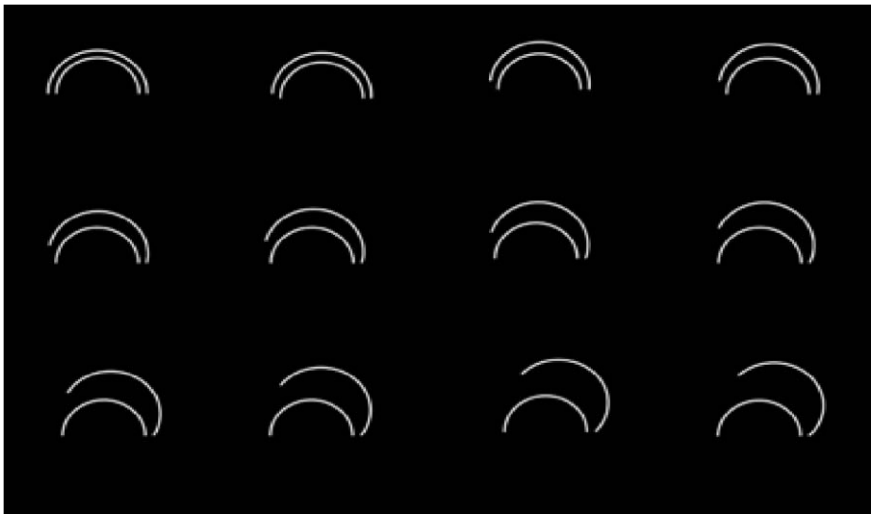

Figure 6.3: Diaphragm of non-parallel-curve-double slit with different angle Table 5 shows the Angle-Dependence of Butterfly Patterns.

Table 5: Patterns of Non-parallel-curve-double slit of different angles

	L = 200 mm	L = 500 mm	L = 1300 mm
0_0		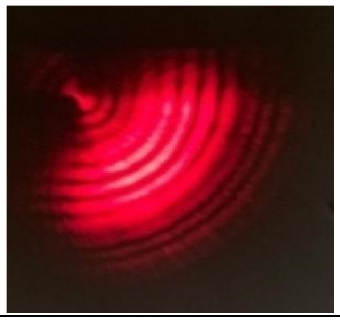	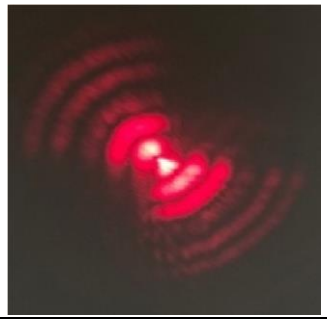
3_0		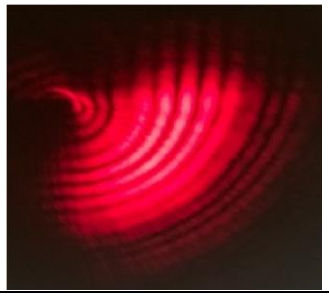	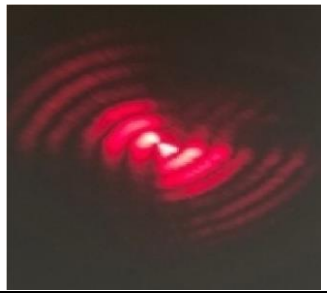
9^0	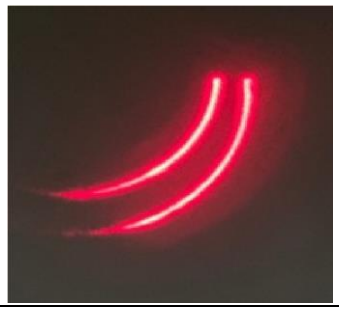	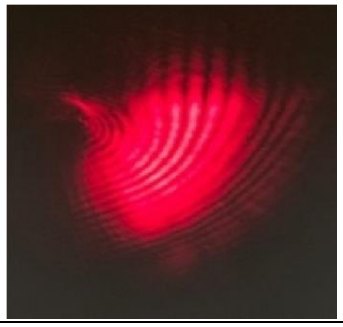	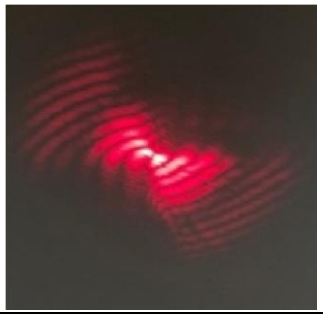
15_0		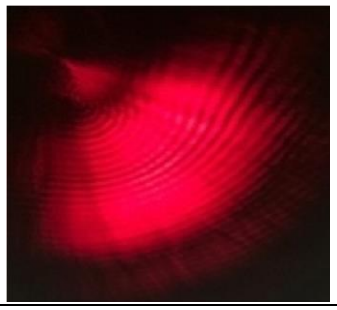	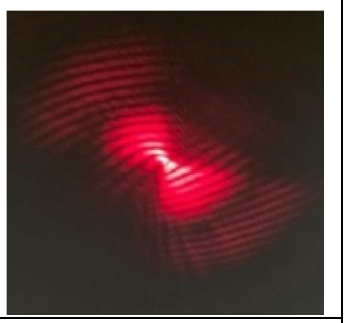
24_0	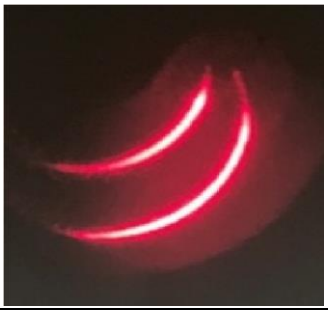	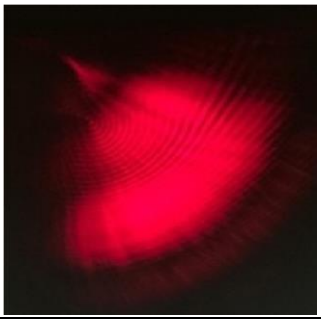	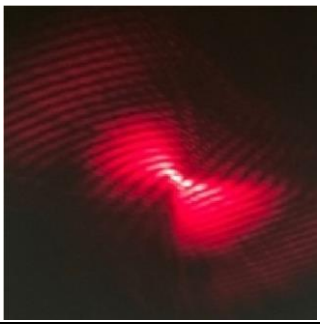

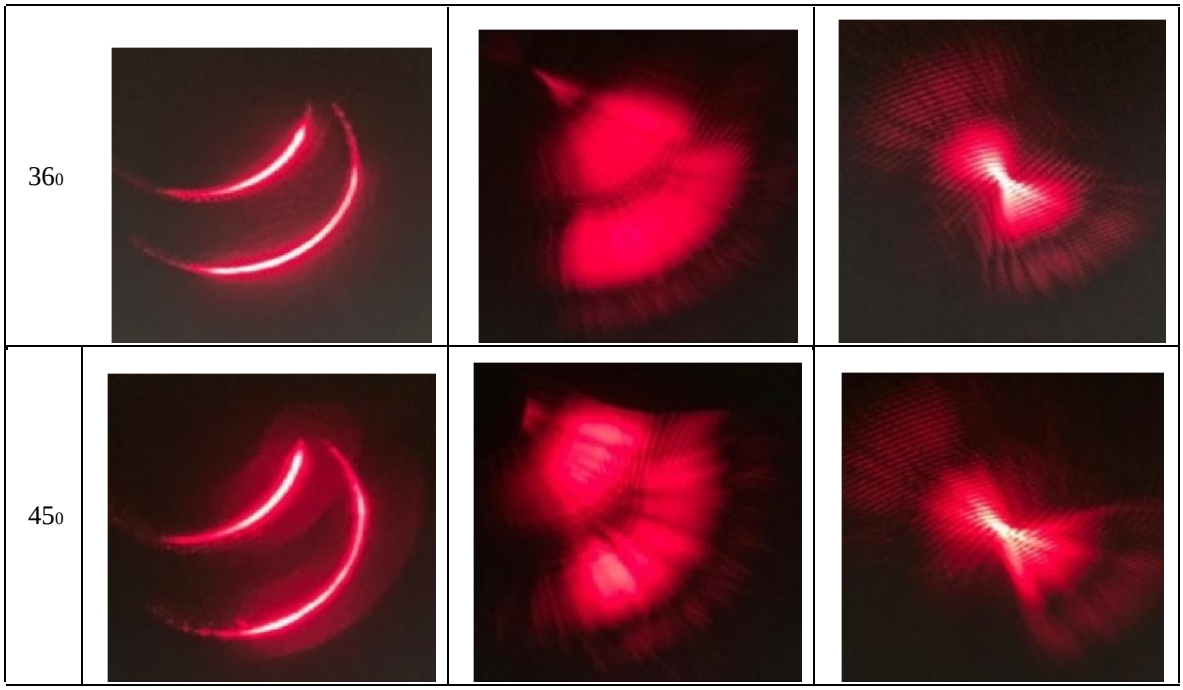

Observation: Figures on the column of L = 200 mm show the Particle patterns. Figures on the column of L = 500 mm show how the patterns of "Butterfly at rest" evolve with angles between two curves. Figures on the column of L = 1300 mm show how the patterns of "Butterfly at flying" evolve with angles between two curves.

6.4. Discussion

We proposed and performed the non-parallel-curve-double slit experiments, which show both the non diffraction/non-interference patterns (such as Pre-particle patterns, Particle patterns, Transition patterns), and the Butterfly-shape interference patterns.

The coexistence of the non-diffraction/non-interference patterns and Butterfly-shape interference patterns in the same experiment indicates that it is photons that produce both the non-diffraction/non-interference patterns, and the Butterfly-shape interference patterns, referred to it as Photo-Wave experiments/phenomena. To completely and consistently interpret PhotoWave phenomena is a challenge.

VII. SUMMARY AND CONCLUSION

We experimentally show, for the first time:
(1) the light is photons in:

(a) the classical experiments, e.g., the single slit, cross single slit, double slit, cross double slit, single slit crossing double slit experiments;
(b) the novel experiments, e.g., curve-single slit, ring, the non-parallel-double slit, curve-double slit, and nonparallel-curve-double slit experiments;
(2) It is the photons that produce both non-wave patterns and wave patterns in the same experiment, referred to it as PhotonWave phenomena;
(3) PhotonWave phenomena are universal;
(4) PhotonWave phenomena show new mysteries of physical optics, in addition to Feynman's mystery of the double slit experiment;

It is not necessary to introduce the concept of "collapse of the wave function" in PhotonWave phenomena; which supporting Penrose's statement.

PhotonWave phenomena shown in this article include:

*) Non-wave patterns in traditional wave experiments

*) Non-wave patterns evolve to wave patterns in same Experiment; Coexistence of wave pattern and non-wave pattern in same experiment

) Hourglass shape patterns) Ring-shape interference patterns

*) Interference pattern embedded in diffraction pattern, refer to it as Hybrid patterns

*) Angle-dependence of hybrid patterns

*) Arc interference pattern and Point-symmetry interference pattern in same experiment;

) Curvature-dependence of Arc interference pattern and Point-symmetry interference pattern) Butterfly-shape interference patterns

Theory:

No need of the concept of collapse of wave function to explain the double slit experiment;

No need of wave-particle duality to explain both Photoelectric Effect and PhotoWave Phenomena

It is a challenge to consistently/completely explain PhotoWave Phenomena shown in Section 3-6. A consistent/complete theory of quantum optics/physical optics is demanded.

Simple differences in the shapes of slits lead to the profound differences in the final patterns (Table 6) and in the 1 pattern evolutions. We refer to the phenomena as *Optical Butterfly Effect*, which shows the sensitive dependence on initial shapes. Optical Butterfly Effect is an analogy of "Chaos Butterfly Effect".

Table 6: Comparison of different slits and their patterns

Slit	Patterns		Slit	Patterns
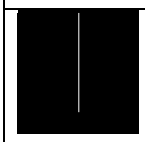	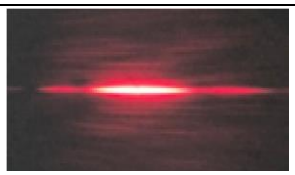		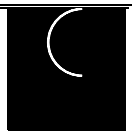	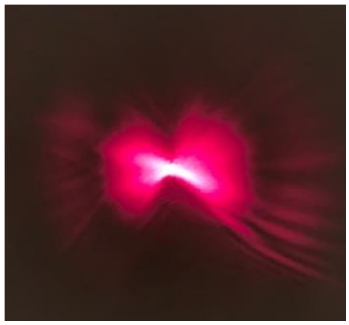
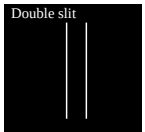	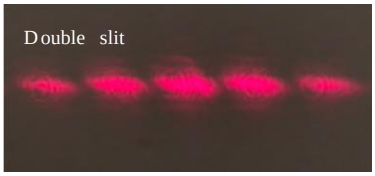		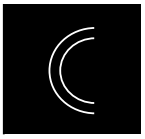	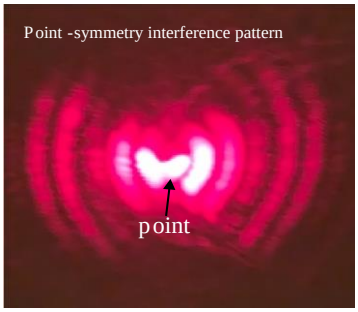

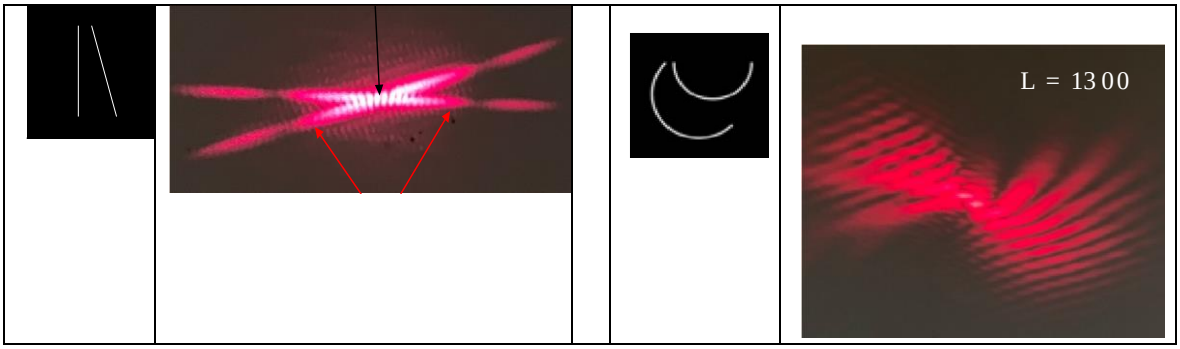

Appendix: Interpretation of Hybrid pattern

A1. Mechanism Interpretation of Hybrid Patterns of Non-Parallel-Double Slit

In the double slit experiment, the two slits are parallel. Figure 4.3 shows that two non-parallel slits produce two diffraction patterns respectively as they were two independent single slits. While the two non-parallel slits produce two partial interference patterns as they formed a double slit. The two partial interference patterns are embedded in two diffraction patterns respectively, we referred to it as the Hybrid pattern.

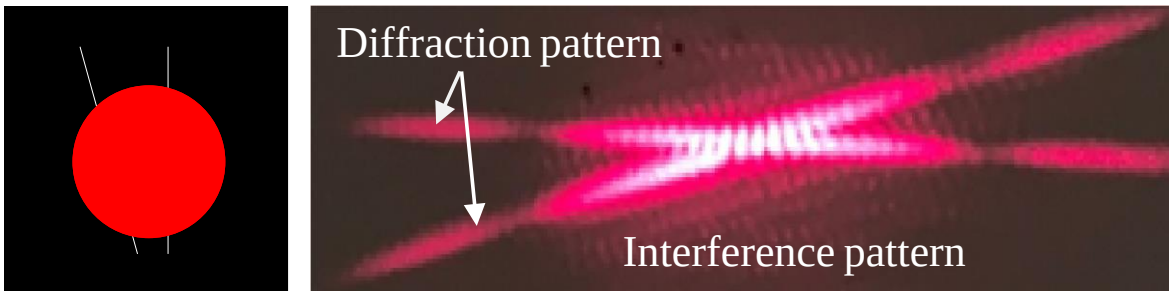

Figure 4.3: hybrid pattern

Now we interpret the mechanism of producing the "Hybrid pattern" of the non-parallel-double slit.

A1.1. Treating non-parallel double slit as two independent single slits: tilt Slit-1 and vertical Slit-2

First, let us consider a non-parallel double slit as two independent single slits as show in Figure A1.

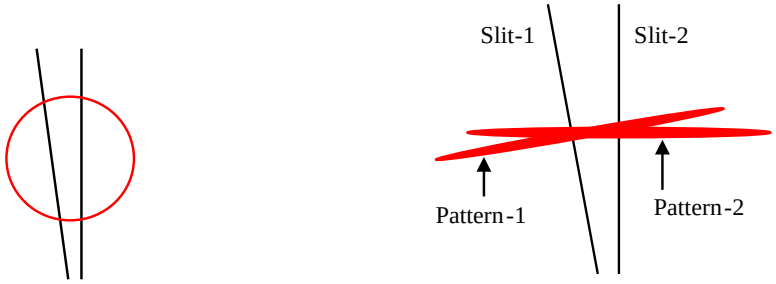

Figure A1, Non-parallel-double slit: Slit-1 and Slit-2 and their diffraction patterns

The red circle indicates the spot of the laser beam on the non-parallel-double slit. If the tilt Slit-1 and the vertical Slit-2 were two independent single slits, then Slit-1 would produce the diffraction Pattern-1; while Slit-2 would produce the diffraction Pattern-2. Pattern-1 and Pattern-2 are perpendicular to Slit-1 and Slit-2 respectively.

Pattern-1 and Pattern-2 (Figure A1) are part of the Hybrid pattern (Figure 4,3).

Obviously, Pattern-1 and Pattern-2 in Figure A1 are different from the Hybrid pattern in Figure 4,3, which indicate that Slit-1 and Slit-2 cannot be considered only as two independent single slits.

A1.2. Treating tilt Slit-1 as multi-small Slit-1-1, and vertical Slit-2 as single slit

We have shown that in a traditional double slit experiment, the light propagates as photons, and it is the photons that produce the interference pattern [17,18], the PhotoWave phenomenon.

To interpret the Hybrid pattern of a non-parallel-double slit, let us utilize the PhotoWave concept and introduce multi *"auxiliary lines" as sub-Slits*.

Since the dimension of a photon is Zero, we can divide the tilt Slit-1 into large number of small segments denoted as single Slit-1-1, such that, for each photon, each single Slit-1-1 can be consider as a slit paralleling to the vertical Slit-2. Namely each single Slit-1-1 and Slit-2 can be considered as a parallel double slit.

The large number of small single Slit-1-1 are represented by red *"auxiliary lines"* (Figure A2). Therefore, some of photons passing through the Slit-1-1/Slit-2-double-slit produce the interference Pattern-1-1, and some of photons passing through Slit-2 produce the diffraction Pattern-2 (Figure A2). Both the interference Pattern-1-1 and Pattern-2 are perpendicular to both Slit-1-1 and Slit-2 and thus, Pattern-1-1 and Pattern-2 are overlap, or, Pattern-1-1 embeds in Pattern-2.

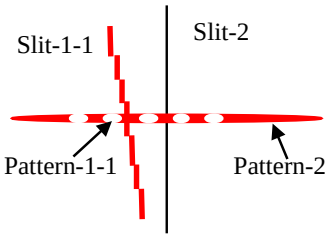

Figure A2: Slit-1-1 producing interference Pattern-1-1;

Slit-2 producing diffraction Pattern-2

Pattern-1-1 and Pattern-2 (Figure A2) are part of the Hybrid pattern (Figure 3).

Obviously, Pattern-1-1 and Pattern-2 in Figure A2 are different from the Hybrid pattern in Figure 3, which indicate that "Treating tilt Slit-1 as multi-small Slit-1-1 and vertical Slit-2 as single slit" is incomplete.

A1.3. Treating tilt Slit-1 as both single Slit-1 and multi-small Slit-1-1, and Slit-2 as single slit

Slit-1 still acts as a whole single slit and thus produces the diffraction Pattern-1 (Figure A3); while Slit-1-1/Slit 2-double-slit produces the interference Pattern-1-1; Slit-2 produces diffraction Pattern-2.Pattern-1 perpendiculars

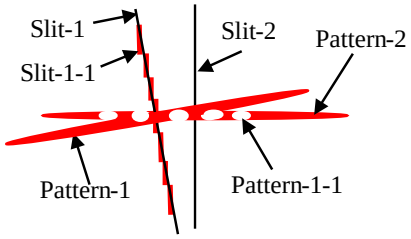

Figure A3: Slit-1-1/Slit-2-double-slit producing interference Pattern-1-1; Slit-1 producing Pattern-1; Slit-2 producing diffraction Pattern-2

Pattern-1-1, Pattern-1 and Pattern-2 (Figure A3) are part of the Hybrid pattern (Figure 4.3). Obviously, Pattern-1-1, Pattern-1 and Pattern-2 in Figure A3 are different from the Hybrid pattern in Figure 4.3, which indicate that "Treating tilt Slit-1 as both single Slit-1 and multi-small Slit-1-1 and Slit-2 as single slit" is still incomplete.

A1.4. Treating Slit-2 as multi-small Slit-2-1 and tilt Slit-1 as single slit

We have shown above that photons passing through the single Slit-1 produce the diffraction Pattern-1, and, combining with Slit-2, produces the interference Pattern-1-1.

Following the same concept/method, we can divide the Slit-2 into large number of small segments denoted as single Slit-2-1, such that, for each photon, each Slit-2-1 can be consider as a slit paralleling to Slit-1. Namely each pair of single Slit-2-1 and Slit-1 can be considered as a parallel double slit.

The large number of small single Slit-2-1 (Figure A4) are represented by red *"auxiliary lines"*. Therefore, some of photons passing through Slit-2-1/Slit-1-double-slit produce the interference Pattern-2-1, and some of photons passing through Slit-1 produce the diffraction Pattern-1 (Figure A4). Both the interference Pattern 2-1 and Pattern-1 are perpendicular to Slit-1 and thus, Pattern-2-1 and Pattern-1 are overlap, or, Pattern-2-1 embeds in Pattern-1.

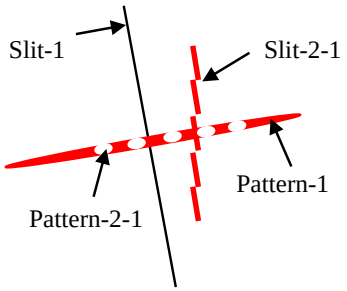

Figure A4: Slit-2-1/Slit-1 producing interference Pattern-2-1;
Slit-1 producing diffraction Pattern-1

Pattern-2-1 and Pattern-1 (Figure A4) are part of the Hybrid pattern (Figure 3).

Obviously, Pattern-1 and Pattern-2-1 in Figure A4 are different from the Hybrid pattern in Figure 4.3, which indicate that "Treating slit-2 as multi-small Slit-2-1 and tilt Slit-1 as single slit" is still incomplete.

A1.5. Treating Slit-1 as single Slit-1 and Slit-2 as both a single Slit-2 and multi-small Slit-2-1

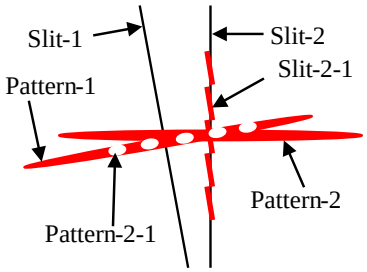

Figure A5: Slit-2-1/Slit-1 produces interference Pattern-2-1; Slit-2 produces diffraction Pattern-2
Slit-1 produces diffraction Pattern-1

Slit-1 acts as a whole single slit and produces the diffraction Pattern-1; while Slit-2-1 and Slit-1 form a double slit and thus produce the interference Pattern-2-1; Slit-2 produces the diffraction Pattern-2 (Figure A5). Both Pattern-1 and Pattern-2-1 perpendicular to Slit-1 and thus, Pattern-2-1 and Pattern-1 are overlap, or, Pattern-2-1 embedded in Pattern-1.

Pattern-2, Pattern-2-1 and Pattern-1 (Figure A5) are part of the Hybrid pattern (Figure 4.3). Obviously, Pattern-1, Pattern-2 and Pattern-2-1 in Figure A5 are different from the Hybrid pattern in Figure 4.3, which indicate that "Treating Slit-1 as single Slit-1 and Slit-2 as both a single Slit-2 and multi-small Slit-2-1" is still incomplete.

A1.6. Treating Slit-1 as both a single Slit-1 and multi-small Slit-1-1 and Treating Slit-2 as both a single Slit-2 and multi-small slit-2-1

In Figure A6, we keep auxiliary line Slit-1-1 and auxiliary line Slit-2-1, in addition to Slit-1 and Slit-2. Then we have the Hybrid pattern which is the same as that in Figure 4.3.

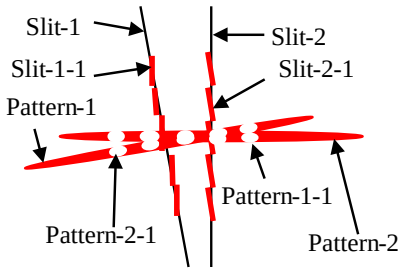

Figure A6: Slit-2-1/Slit-1 produce interference Pattern-2-1; Slit-2 produces diffraction Pattern-2
Slit-1-1/Slit-2 produce interference Pattern-1-1; Slit-1 produces diffraction Pattern-1

Now, let us delete the auxiliary line Slit-1-1, the auxiliary line Slit-2-1, Slit-1 and Slit-2 in Figure A6, we finally show the Hybrid pattern (Figure A7), which is the same as that in Figure 4.3.
Pattern-1

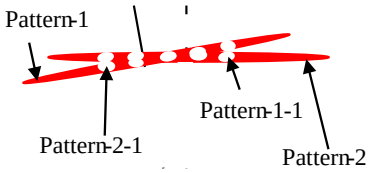

Figure A7: Hybrid pattern of non-parallel-double slit

The combination of Slit-1 and Slit-2 produces the interference Pattern-1-1 and the interference Pattern-2-1. Slit-1 produces the diffraction Pattern-1. Slit-2 produces the diffraction Pattern-2.

A2. Math Description

In this Section, we mathematically describe the "Hybrid pattern" of the non-parallel-double slit. The interference Pattern-1-1 and Pattern-2-1 can be mathematically described by either the classical formulars P or modified formular [19]

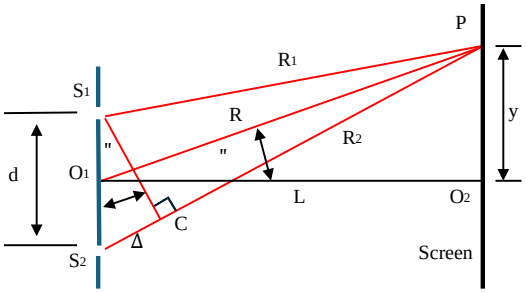

$$y \approx L\frac{n\lambda}{\#} \quad \text{or} \quad y + \frac{d}{\$} \approx L\frac{n\lambda}{\#}$$

or modified formular [19]

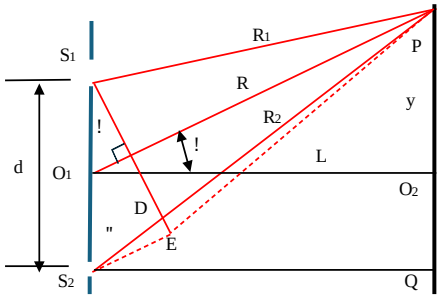

$$y \approx L\frac{n\lambda}{d}\frac{1}{\sqrt{1-(n\lambda/d)^2}}$$

A3. Conclusion

By utilizing the PhotoWave concept and the auxiliary lines Slit-1-1 and the auxiliary lines Slit-2-1 in the non parallel double slit experiment, we interpret the mechanism of how the Hybrid pattern is produced. Based on the interpretation, we propose the math description of the Hybrid pattern.

REFERENCES

1. C. Huygens, “Traité de la Lumière”, published in Leyden by Van der Aa, French. (1690).
2. I. Newton, “Opticks: or, a treatise of the reflexions, refractions, inflexions and colours of light”, London. (1704).
3. T. Young, "The Bakerian lecture. Experiments and calculation relative to physical optics”, Philosophical Transactions of the Royal Society of London. 94: 1–16. doi:10.1098/rstl.1804.0001. S2CID 110408369 (1804).
4. “Arago spot”, WikipediA
5. A. Einstein, “On a Heuristic Point of View Concerning the Production and Transformation of Light”, Ann. der Physik, Vol. 17, pp132-148 (1905).
6. N. Bohr, "The Quantum Postulate and the Recent Development of Atomic Theory". Nature. **121** (3050): 580–590. Bibcode:1928Natur.121.580B. doi:10.1038/121580a0. (1928)
7. S. Rashkovskiy, “Is a rational explanation of wave-particle duality possible?”, arXiv 1302.6159 [quant-ph]. (2013).
8. R. Feynman, R. Leighton, and M. Sands, “The Feynman Lectures on Physics” (Addison-Wesley, Reading), Vol. 3. (1965)
9. R. Penrose, "On Gravity's role in Quantum State Reduction". *General Relativity and Gravitation*. ***28*** *(5): 581–600*. doi:10.1007/BF02105068. ISSN 0001-7701. *(1996)*.

10. R. Penrose, “Why Quantum Mechanics Is an Inconsistent Theory | Roger Penrose & Jordan Peterson”. YouTube. (2022)
11. H. Peng, “Photoelectric Effect to Photowaves Phenomena --- New Phenomena Requiring Interpretation” TechRxiv. DOI: 10.36227/techrxiv.22659172.v1 (2023).
12. H. Peng, "New experiments/phenomena in optics: photoelectric effect to photowave phenomena," Proc. SPIE 12723, Seventeenth Conference on Education and Training in Optics and Photonics: ETOP 2023, 127231F doi: 10.1117/12.2670639. (June 2023);
13. H. Peng, “Mystery of double slit experiments ---non-interference patterns and interference patterns showing on screen simultaneously”. TechRxiv. Preprint. https://doi.org/10.36227/techrxiv. 21754220.v1 (2022).
14. H. Peng, “Incompleteness of Wave Interpretations of Double Slit and Grating Experiments.” International Journal of Physics, vol. 10, no. 3: 154-173. doi: 10.12691/ijp-10-3-4. (2022).
15. H. Peng, “Experimental Study of Mystery of Double Slit --- Comprehensive Double Slit Experiments. International Journal of Physics, vol. 9, no. 2: 114-127. doi: 10.12691/ijp-9-2-6. (2021).
16. H. Peng, “Double Slit to Cross Double Slit to Comprehensive Double Slit Experiments’. Research Square, preprint. DOI: https://doi.org/10.21203/rs.3.rs-555223/v1 (2021).
17. Hui Peng, “Double Slit to Cross Double Slit to Comprehensive Double Slit Experiments”, Research Square preprint, DOI: https://doi.org/10.21203/rs.3.rs-555223/v1. May 2021.
18. Hui Peng, “Advances in Optical Experiments Demanding New Optical Theory ---Non-Interference Pattern Evolving to Interference Pattern, Non-Diffraction Pattern Evolving to Diffraction Pattern and Two Non-Diffraction Patterns Evolving to Diffraction-Interference-Hybrid Pattern”. TechRxiv. DOI: 10.36227/techrxiv.170421443. 30332791/v1 December, 2023.
19. Hui Peng, “Logical Weaknesses in Classical Geometry Model of Deriving Math Formular of Double Slit Experiment --- A New Geometry Model Avoids Logical Weakness”. Optica Open. Preprint. https://doi.org/10.1364/opticaopen.27499023.v2. November 2024.

This page is intentionally left blank

The Innovative Development of the IFRS17 Formulated Brighton Mahohoho Inflation-Adjusted Automated Actuarial Loss Reserving Model: Harnessing Advanced Random Forest Techniques for Enhanced Data Analytics in Fire Insurance

Brighton Mahohoho

ABSTRACT

This paper presents the development and implementation of the IFRS17 Formulated Brighton Mahohoho Inflation-Adjusted Automated Actuarial Loss Reserving Model, lever-aging advanced Random Forest techniques to enhance data analytics in fire insurance.

The methodology encompasses the simulation of synthetic fire insurance data with key variables such as claim frequency, severity, and inflation rates. Exploratory Data Analysis (EDA) and data visualization techniques were employed to assess relationships and trends, aligning the model with IFRS17 compliance standards. Random Forest regression models were developed to predict claim frequency, severity, and inflation adjustments, integrating these predictions to estimate future loss reserves. Robust evaluation metrics, including Mean Absolute Error (MAE), Mean Squared Error (MSE), and Root Mean Squared Error (RMSE), ensured model accuracy.

Keywords: IFRS 17 regulations,random forest,automated loss reserves,fire insurance.

Classification: LCC Code: HG205

Language: English

Great Britain Journals Press

LJP Copyright ID: 925674
Print ISSN: 2631-8490
Online ISSN: 2631-8504

London Journal of Research in Science: Natural & Formal

Volume 24 | Issue 13 | Compilation 1.0

The Innovative Development of the IFRS17 Formulated Brighton Mahohoho Inflation-Adjusted Automated Actuarial Loss Reserving Model: Harnessing Advanced Random Forest Techniques for Enhanced Data Analytics in Fire Insurance

Brighton Mahohoho

ABSTRACT

This paper presents the development and implementation of the IFRS17 Formulated Brighton Mahohoho Inflation-Adjusted Automated Actuarial Loss Reserving Model, lever-aging advanced Random Forest techniques to enhance data analytics in fire insurance.

The methodology encompasses the simulation of synthetic fire insurance data with key variables such as claim frequency, severity, and inflation rates. Exploratory Data Analysis (EDA) and data visualization techniques were employed to assess relationships and trends, aligning the model with IFRS17 compliance standards. Random Forest regression models were developed to predict claim frequency, severity, and inflation adjustments, integrating these predictions to estimate future loss reserves. Robust evaluation metrics, including Mean Absolute Error (MAE), Mean Squared Error (MSE), and Root Mean Squared Error (RMSE), ensured model accuracy. Stress testing and scenario analysis were conducted to assess the model's resilience under various conditions. Key IFRS17 metrics such as Present Value of Future Cash Flows (PVFCF), Risk Adjustments, and Contractual Service Margins (CSM) were calculated, offering a comprehensive approach to actuarial loss reserving.

Keywords: IFRS 17 regulations,random forest, automated loss reserves,fire insurance.

Author: University of Zimbabwe, Department of Mathematics & Computational Sciences, 630 Churchill drive, Mt Pleasant, Harare, Zimbabwe.

I. INTRODUCTION

In recent years, the implementation of IFRS 17 has transformed financial reporting within the insurance sector, particularly emphasizing the need for accurate loss reserving (International Accounting Standards Board, 2019). This study introduces the Brighton Mahohoho Inflation-Adjusted Automated Actuarial Loss Reserving Model, which employs advanced random forest techniques to enhance data analytics in fire insurance. The model aims to address the complexities of loss reserving under IFRS 17, considering inflation adjustments that are critical for accurate financial forecasting [5].

London Journal of Research in Science: Natural & Formal

The Brighton Mahohoho model integrates inflation-adjusted parameters with automated actuarial processes to produce more reliable loss reserves. Random forest techniques, a subset of machine learning, are employed to analyze complex datasets, identifying patterns and correlations that traditional models may overlook [1]. This innovative approach enhances predictive accuracy and adaptability, vital in an ever-evolving regulatory environment. The rationale for this study is underscored by the increasing complexity of insurance contracts and the significant implications of accurate loss reserving under IFRS 17 [2]. As inflation impacts reserve calculations, there is a critical need for methodologies that can dynamically adjust to economic changes. By leveraging random forest techniques, this model provides a robust framework that aligns with the rigorous demands of modern actuarial science.

The Brighton Mahohoho model can be applied in various contexts within the fire insurance sector, allowing insurers to refine their loss reserving processes. By automating data analysis and incorporating real-time inflation adjustments, insurers can improve accuracy in financial statements and enhance decision-making processes regarding premium setting and risk management [4].This study is crucial for the actuarial field as it demonstrates the application of advanced machine learning techniques to improve loss reserving accuracy. The findings could influence best practices in the industry, encouraging a shift towards data-driven decision-making and regulatory compliance, ultimately contributing to the financial resilience of insurance companies [6].

1.1. Actuarial Loss Reserve Methods

Loss reserving is a fundamental aspect of actuarial science, dealing with the estimation of the reserves necessary to cover future claims. Accurate reserving is crucial for maintaining the financial health of an insurance company [7].Loss reserving methods can be categorized broadly into two classes: deterministic methods and stochastic methods.Deterministic loss reserving methods rely on historical data and fixed parameters to predict future claim liabilities. Common deterministic methods include the Chain-Ladder method and the Bornhuetter-Ferguson method.

1.1.1. Chain Ladder Method: The Chain-Ladder Model is a popular method in actuarial science for estimating the reserves needed for unpaid claims. This method relies on historical claim development patterns to predict future claims. The main idea is to analyze cumulative claim amounts over different accident years and development lags to estimate future liabilities.

Table 1: Cumulative Claims Data

Accident Year	Development Lag 1	Development Lag 2	...	Development Lag n
1	$C_{1,1}$	$C_{1,2}$	...	$C_{1,n}$
2	$C_{2,1}$	$C_{2,2}$	...	$C_{2,n}$
$\vdots$	$\vdots$	$\vdots$	$\vdots$	$\vdots$
m	$C_{m,1}$	$C_{m,2}$	...	$C_{m,n}$

The Table 1 presented is a triangular array that organizes cumulative claims data $C_{i,j}$, where i denotes the accident year and j signifies the development lag. The entries $C_{i,j}$ represent the cumulative amount of claims reported for accident year i up to development lag j.The year in which the claims occurred. For example, $i = 1$ represents the earliest accident year, while $i = m$ signifies the most recent.The time intervals since the claims were reported. For instance, $j = 1$ corresponds to the first development period, while $j = n$ refers to the last.

The total claims amount accumulated for accident year i by development lag j. The entries in the table can be expressed as:

$$C_{i,j} = \sum_{k=1}^{j} C_{i,k}$$

where $C_{i,k}$ represents the incremental claims reported in development lag k.

The primary assumption of the Chain-Ladder Model is that the development factors f_j remain stable across different accident years. These factors provide an estimate of how cumulative claims grow from one development period to the next. They can be defined mathematically as:

$$f_j = \frac{\sum_{i=1}^{m-j} C_{i,j+1}}{\sum_{i=1}^{m-j} C_{i,j}} \quad (j = 1, 2, \ldots, n-1)$$

This formula captures the average growth of cumulative claims from lag j to $j+1$, effectively measuring the relationship between claims in successive development periods.

Using the estimated development factors, future cumulative claims for accident years that have not yet fully developed can be projected. For any i (accident year) and j (development lag) where $j > n$, we can use the following recursive relationship:

$$C_{i,j} = C_{i,j-1} \cdot f_{j-1} \quad (i = 1, \ldots, m-j,\ j = 2, \ldots, n)$$

This equation states that the projected cumulative claims at development lag j for accident year i can be estimated by taking the cumulative claims from the previous lag $j-1$ and multiplying it by the estimated development factor f_{j-1}.

Proposition: *The cumulative claims $C_{i,j}$ are non-decreasing for all i and j, where i denotes the accident year and j denotes the development year.*

Proof: We define the cumulative claims $C_{i,j}$ as follows:

$$C_{i,j} = \sum_{k=0}^{j} C_{i,k}$$

where $C_{i,k}$ represents the claims reported up to development year k for accident year i To show that $C_{i,j}$ is non-decreasing, we need to prove that:

$$C_{i,j} \leq C_{i,j+1} \quad \forall i, j$$

Expanding $C_{i,j+1}$:

$$C_{i,j+1} = \sum_{k=0}^{j+1} C_{i,k} = \sum_{k=0}^{j} C_{i,k} + C_{i,j+1}$$

$$C_{i,j+1} = C_{i,j} + C_{i,j+1}$$

Since $C_{i,j+1}$ represents the cumulative claims including the additional claims for the development year $j+1$, we have:

$$C_{i,j+1} \geq C_{i,j} \quad (\text{as } C_{i,j+1} \geq 0)$$

Thus, we conclude:

$$C_{i,j} \leq C_{i,j+1} \quad \forall i, j$$

This demonstrates that the cumulative claims $C_{i,j}$ are non-decreasing.

Claim: *As the number of accident years m increases, the estimates $C_{i,n}$ (for fully developed claims) converge to the true future cumulative claims due to the law of large numbers. The stability of the development factors implies that with sufficient data, the average behavior of claims will tend to stabilize, providing more reliable estimates:*

$$\lim_{m \to \infty} C_{i,n} \to C_{i,n}^*$$

where $C_{i,n}^*$ denotes the true cumulative claims for accident year i.

- Let $C_{i,n}$ be the estimate of cumulative claims for accident year i after n development years.
- Let $C_{i,n}^*$ be the true cumulative claims for accident year i after n development years.
- Let $D_{i,j}$ be the development factor from accident year i to accident year j.

Proof:We assume that the development factors $D_{i,j}$ are stable, meaning they do not fluctuate significantly over time. Additionally, the number of claims in each accident year is sufficiently large, allowing us to apply the law of large numbers.

The estimate of cumulative claims $C_{i,n}$ can be expressed in terms of development factors:

$$C_{i,n} = C_{i,0} \prod_{j=1}^{n} D_{i,j}$$

where $C_{i,0}$ is the initial claim amount for accident year i.

By the law of large numbers, as m increases, the average of the development factors converges to the expected value:

$$\lim_{m \to \infty} \frac{1}{m} \sum_{k=1}^{m} D_{i,j} = \mathbb{E}[D_{i,j}]$$

for each j.

Consequently, as m approaches infinity, the estimates for cumulative claims converge to:

$$\lim_{m \to \infty} C_{i,n} = C_{i,0} \prod_{j=1}^{n} \mathbb{E}[D_{i,j}]$$

The true cumulative claims $C_{i,n}^*$ can similarly be expressed as:

$$C_{i,n}^* = C_{i,0} \prod_{j=1}^{n} D_{i,j}^*$$

where $D_{i,j}^*$ are the true development factors.

Under the assumption of stability of development factors, we can state that:

$$\mathbb{E}[D_{i,j}] = D_{i,j}^*$$

for large m.

Thus, we have:

$$\lim_{m\to\infty} C_{i,n} = C_{i,0} \prod_{j=1}^{n} D_{i,j}^{*} = C_{i,n}^{*}$$

We conclude that:

$$\lim_{m\to\infty} C_{i,n} \to C_{i,n}^{*}$$

This demonstrates that as the number of accident years increases, the estimates for cumulative claims converge to the true future cumulative claims due to the law of large numbers and the stability of the development factors.

The mathematical framework surrounding the Chain-Ladder Model, encapsulated in the triangular table format, offers a systematic approach to estimating unpaid claims reserves. Through the stability of development factors and the non-decreasing nature of cumulative claims, actuaries can derive reliable projections for future liabilities, critical for effective financial management in insurance.

Algorithm 1 Chain-Ladder Method

Input: Cumulative claims triangle $C_{i,j}$ Calculate development factors: **for**$j = 1$ to $n-1$ $f_j = \frac{\sum_{i=1}^{n-j} C_{i,j+1}}{\sum_{i=1}^{n-j} C_{i,j}}$ Project future claims: **for**$i = 1$ to n **for**$j = 1$ to $n-i$ $C_{i,j+1} = C_{i,j} \cdot f_j$ Output: Estimated total claims

Let $C_{i,j}$ denote the cumulative claims up to development year j for accident year i. The development factor f_j is given by:

$$f_j = \frac{\sum_{i=1}^{n-j} C_{i,j+1}}{\sum_{i=1}^{n-j} C_{i,j}} \tag{1.1}$$

Theorem*If the claims develop consistently, then the Chain-Ladder method converges to the true reserve.*

Proof:
Let $C_{i,j}$ denote the cumulative claims amount at development year j for accident year i. The Chain-Ladder method estimates the reserve using the following formula:

$$\hat{R}_i = C_{i,n} + \sum_{j=i+1}^{n} \hat{C}_{i,j}$$

where $\hat{C_{i,j}}$ is the estimated cumulative claim for accident year i at development year j. We define the development factors f_j as:

$$f_j = \frac{\sum_{i=1}^{n-j} C_{i,j+1}}{\sum_{i=1}^{n-j} C_{i,j}}, \quad j = 1, 2, \ldots, n-1$$

The estimated cumulative claims can then be expressed recursively as:

$$\hat{C}_{i,j} = C_{i,j-1} \cdot f_{j-1} \quad \text{for } j = i+1, \ldots, n$$

Assuming consistency in development, we assert that:

$$C_{i,j} = C_{i,j-1} \cdot f_{j-1} + \epsilon_{i,j} \quad \text{where } \epsilon_{i,j} \to 0 \text{ as } n \to \infty$$

Consequently, the reserve estimate can be expressed as:

$$\hat{R}_i = C_{i,n} + \sum_{j=i+1}^{n} C_{i,j-1} \cdot f_{j-1}$$

As n increases, and if the claims develop consistently, we have:

$$\lim_{n\to\infty} \hat{R}_i = \lim_{n\to\infty} \left(C_{i,n} + \sum_{j=i+1}^{n} C_{i,j-1} f_{j-1} \right) = R_i$$

where R_i is the true reserve for accident year i.

Thus, we conclude that:

$$\lim_{n\to\infty} \hat{R}_i = R_i$$

This completes the proof that the Chain-Ladder method converges to the true reserve when claims develop consistently.

1.1.2. Bornhuetter-Ferguson Method: The Bornhuetter-Ferguson (BF) method is a fundamental technique used in actuarial science for estimating reserve liabilities in insurance. The method is particularly useful when dealing with incomplete data, allowing actuaries to incorporate prior information in their estimations (Bornhuetter & Ferguson, 1972).

Let:

- C_i = cumulative claims at development year i,
- E_i = expected claims at development year i,
- f_i = development factor from year i to $i+1$.

The expected claims can be calculated as:

$$E_i = \text{Ultimate Loss} \times \text{Loss Development Factor}$$

Where the Ultimate Loss U is a key parameter in the BF method, typically estimated based on historical data.

Algorithm 2 Computation of Reserves Using Development Factors

Input: C: Cumulative claims to date f: Ultimate claims estimate D: Development factors n: Number of accident years

Output:

- Reserves

Initialize:

- $U_i = f_i$ (for each accident year i)

for $i = 1$ to n Calculate the development factors:

$$D_j = \frac{C_{i,j}}{C_{i,j-1}} \quad \text{for } j = 2, 3, \ldots, n$$

for $i = 1$ to n Compute the expected cumulative claims:

$$E_{i,j} = U_i \cdot D_2 \cdot D_3 \cdots D_j$$

for $i = 1$ to n Compute the reserves for each accident year:

$$R_i = E_{i,n} - C_{i,n}$$

Return: Reserves $R = (R_1, R_2, \ldots, R_n)$

The BF method can be formulated as a weighted average of the observed and expected claims:

$$C_i = (1 - \alpha) \times C_i + \alpha \times E_i$$

where α is a weighting factor that reflects the confidence in prior information versus the actual data [17].

Proposition 1: *The Bornhuetter-Ferguson (BF) method provides an unbiased estimator of the ultimate loss under specific conditions.*

Proof: Assume that the prior estimates are unbiased, and the development factors are consistent across all periods. Under these assumptions, we can prove the proposition as follows.

Let C_i represent the cumulative losses at development period i, and E_i represent the expected losses at development period i. We aim to show that:

$$\mathbb{E}[C_i] = \mathbb{E}[E_i] \quad \text{for all } i. \tag{1.2}$$

Given that the prior estimates E_i are unbiased, it follows that:

$$\mathbb{E}[E_i] = U_i \quad \text{for all } i, \tag{1.3}$$

where U_i represents the ultimate loss for development period i.

Let d_i represent the development factors. The development factor for period i is defined as the ratio of cumulative losses between two successive development periods:

$$d_i = \frac{C_{i+1}}{C_i}. \tag{1.4}$$

Under the assumption of consistent development factors, the expectation of cumulative losses follows the relationship:

$$\mathbb{E}[C_{i+1}] = d_i \cdot \mathbb{E}[C_i]. \tag{1.5}$$

By applying equations (1.3) and (1.5), we conclude that:

$$\mathbb{E}[C_i] = \mathbb{E}[E_i] \quad \text{for all } i, \tag{1.6}$$

proving that the BF method provides an unbiased estimator of the ultimate loss under the given conditions.

■

Claim: *The Bornhuetter-Ferguson (BF) method converges to the true ultimate loss as more data becomes available, assuming the underlying development patterns remain stable.*

Proof:To prove this, let C_i represent the cumulative losses at development period i, and let U represent the true ultimate loss. The BF method combines prior estimates with actual observations, adjusting for the expected development.

The estimate of the ultimate loss $\hat{U}_i$ at development period i using the BF method is given by:

$$\hat{U}_i = C_i + (1 - F_i) \cdot E_i, \tag{1.7}$$

where:

- C_i is the cumulative reported loss at development period i,
- F_i is the cumulative development factor up to period i,
- E_i is the expected loss for the remaining development.

As more data becomes available, i.e., as $i \to n$ (where n is the final development period), the cumulative development factor $F_i \to 1$. This implies that the observed data accounts for the entire development, leaving no need for further estimates.

$$\lim_{i \to n}(1 - F_i) = 0.$$

Substituting this into equation (1.7), we get:

$$\lim_{i \to n} \hat{U}_i = \lim_{i \to n} (C_i + (1 - F_i) \cdot E_i) = C_n. \tag{1.8}$$

At $i = n$, C_n is the cumulative loss at the final development period, which equals the true ultimate loss:

$$C_n = U. \tag{1.9}$$

The assumption that the underlying development patterns remain stable ensures that the development factors F_i follow a predictable pattern, so as more development periods are observed, the estimate $\hat{U}_i$ becomes increasingly accurate.

From equations (1.8) and (1.9), we conclude that:

$$\lim_{i \to n} \hat{U}_i = U, \tag{1.10}$$

showing that the BF method converges to the true ultimate loss as more data becomes available.

■

The Bornhuetter-Ferguson method offers a robust framework for estimating reserves in insurance, blending historical experience with current data. Its ability to adapt to varying degrees of uncertainty makes it a critical tool for actuaries .

Stochastic methods incorporate randomness into the modeling of claims reserves. This approach allows for a range of possible outcomes, providing a distribution of reserve estimates.

1.1.3. Bootstrap Method: The Bootstrap method is a powerful statistical tool employed in loss reserving to estimate both reserves and the uncertainty surrounding these estimates. The technique was first introduced by [24] and has since found wide applications in non-life insurance for predicting future liabilities and quantifying the risk associated with reserve estimates. This method involves resampling residuals to simulate alternative versions of the loss development triangle, which are then used to calculate a range of possible reserve outcomes. The goal is to generate a distribution of reserve estimates to assess variability and confidence intervals.

The Bootstrap approach in loss reserving leverages the underlying development factors used in traditional chain-ladder methods. By resampling the residuals from the development triangles, this method assumes that the variability of past data is reflective of the variability that can be expected in the future.

Given a development triangle of cumulative claims data, the chain-ladder technique estimates future claims by multiplying observed claims in each development period by a set of development factors. The Bootstrap method goes a step further by resampling residuals to create alternative possible versions of the triangle and obtain a distribution of reserve estimates.

Let $C_{i,j}$ be the cumulative claim in accident year i and development year j. The standard chain-ladder model estimates the development factors f_j such that:

$$C_{i,j+1} = f_j C_{i,j}, \quad \text{for } i = 1, 2, \ldots, n-1 \text{ and } j = 1, 2, \ldots, n-i.$$

The development factor f_j is typically estimated as:

$$f_j = \frac{\sum_{i=1}^{n-j} C_{i,j+1}}{\sum_{i=1}^{n-j} C_{i,j}}.$$

The residuals $e_{i,j}$ in the chain-ladder model are calculated as:

$$e_{i,j} = \frac{C_{i,j+1} - f_j C_{i,j}}{C_{i,j}}.$$

The key assumption in the Bootstrap method is that these residuals follow the same distribution, and they can be resampled to generate alternative claims triangles.

proposition :*The Bootstrap method produces an unbiased estimate of the reserve under the assumption that the resampled residuals are independent and identically distributed (i.i.d.).*

*proof*We begin by considering the *chain-ladder model*, which assumes that the cumulative claims $C_{i,j}$ for accident year i and development year j follow a multiplicative structure. Denote the cumulative claims by:

$$C_{i,j} = f_j \cdot C_{i,j-1} + \varepsilon_{i,j}, \tag{1.11}$$

where f_j are the development factors, and $\varepsilon_{i,j}$ represents the residuals.

In the Bootstrap method, residuals $\varepsilon_{i,j}$ are resampled to generate new sets of claims data. Let $\hat{C}_{i,j}$ denote the bootstrapped claim amounts for accident year i and development year j. These are calculated as:

$$\hat{C}_{i,j} = f_j \cdot \hat{C}_{i,j-1} + \hat{\varepsilon}_{i,j}, \tag{1.12}$$

where $\hat{\varepsilon}_{i,j}$ are the resampled residuals.

Given that the original model in equation (1.11) assumes multiplicative development factors, resampling residuals from $\varepsilon_{i,j}$ preserves this structure. Specifically, the resampled data $\hat{C}_{i,j}$ retain the multiplicative form of the original chain-ladder model, ensuring that:

$$\mathbb{E}\left[\hat{C}_{i,j}\right] = \mathbb{E}\left[C_{i,j}\right]. \tag{1.13}$$

The unbiasedness of the bootstrap reserve estimate follows from the fact that the expected value of the resampled claims data $\hat{C}_{i,j}$ is equal to the expected value of the original claims data $C_{i,j}$. Assuming that the residuals $\varepsilon_{i,j}$ are independent and identically distributed (i.i.d.), we have:

$$\mathbb{E}\left[\hat{\varepsilon}_{i,j}\right] = \mathbb{E}\left[\varepsilon_{i,j}\right] = 0, \tag{1.14}$$

which implies that:

$$\mathbb{E}\left[\hat{C}_{i,j}\right] = f_j \cdot \mathbb{E}\left[\hat{C}_{i,j-1}\right] = f_j \cdot \mathbb{E}\left[C_{i,j-1}\right]. \tag{1.15}$$

By applying this recursively over all development years j, the expected value of the bootstrap reserve estimate $\hat{R}$ is equal to the expected value of the original reserve estimate R. Therefore, the bootstrap method provides an unbiased estimate of the reserve:

$$\mathbb{E}\left[\hat{R}\right] = \mathbb{E}\left[R\right]. \tag{1.16}$$

This completes the proof.

□

Lemma:*If the residuals $e_{i,j}$ are independent, the bootstrap replicates will reflect the true variability of the reserves.*

Proof:We start by assuming that the residuals $e_{i,j}$ are independent and identically distributed (i.i.d). Let us consider a model where the reserve R is estimated as a function of observed data, typically through:

$$R = f(X, \theta) + e$$

where $f(X, \theta)$ represents the deterministic part of the model with parameters θ, and e denotes the residuals.

To apply the bootstrap method, we generate B bootstrap replicates $\hat{R}^{(b)}$, for $b = 1, 2, \ldots, B$, using:

$$\hat{R}^{(b)} = f(X, \hat{\theta}^{(b)}) + e^{(b)}$$

where $\hat{\theta}^{(b)}$ are the parameter estimates from the bootstrap sample, and $e^{(b)}$ are the bootstrap residuals.

The variability of the reserves is derived from the variability of the residuals $e_{i,j}$. Since we assume independence of the residuals, the bootstrap replicates $\hat{R}^{(b)}$ will reflect the true variability of the reserves. The variance of the bootstrap estimate $\hat{R}^{(b)}$ is:

$$\mathrm{Var}(\hat{R}^{(b)}) = \mathrm{Var}(f(X, \hat{\theta}^{(b)})) + \mathrm{Var}(e^{(b)}) \tag{1.17}$$

Due to the independence assumption of $e_{i,j}$, the bootstrap residuals $e^{(b)}$ accurately replicate the original data's residual distribution. Therefore, the second term in Equation (1.17), $\mathrm{Var}(e^{(b)})$, converges to the true variability of the original residuals as $B \to \infty$. Thus, the total variability of the reserves, captured by the bootstrap process, accurately reflects the true variability of the reserves.

□

claim: *The Bootstrap method enhances the estimation of confidence intervals by providing a non-parametric way to estimate the distribution of reserve estimates.*

The Bootstrap method, introduced by [25], is a powerful resampling technique used for estimating the distribution of a statistic, particularly in cases where the underlying distribution is unknown. For reserve estimation in actuarial science, it enables the construction of confidence intervals without assuming a parametric form for the data's distribution. We shall now proceed to prove how this method enhances the estimation of confidence intervals.

theorem Let $\hat{R}$ be the reserve estimate based on a sample $\{X_1, X_2, \ldots, X_n\}$. Using the Bootstrap method, the confidence interval for $\hat{R}$ is given by the empirical distribution of bootstrapped reserve estimates $\hat{R}_b$.

Proof;Let $\{X_1, X_2, \ldots, X_n\}$ represent the observed data from which the reserve estimate $\hat{R}$ is calculated. The key idea of the Bootstrap method is to resample the observed data with replacement to generate multiple bootstrapped samples $\{X_1^*, X_2^*, \ldots, X_n^*\}$. For each bootstrapped sample, we compute a new reserve estimate $\hat{R}_b$. Repeating this process B times yields the set of bootstrapped reserve estimates:

$$\hat{R}_1, \hat{R}_2, \ldots, \hat{R}_B \tag{1.18}$$

The empirical distribution of the bootstrapped reserve estimates approximates the true sampling distribution of $\hat{R}$, which is generally unknown. Using this empirical distribution, we can construct a confidence interval for $\hat{R}$ by selecting appropriate percentiles from the set of bootstrapped estimates.

For a $(1-\alpha)\times 100\%$ confidence interval, the lower and upper bounds are given by the $\frac{\alpha}{2}$ and $(1-\frac{\alpha}{2})$ percentiles of the bootstrapped reserve estimates, respectively:

$$\left(\hat{R}_{\frac{\alpha}{2}}, \hat{R}_{1-\frac{\alpha}{2}}\right) \tag{1.19}$$

This non-parametric approach bypasses the need for assumptions about the form of the underlying distribution of reserve estimates, making it highly flexible. Additionally, the Bootstrap method accounts for the variability in the data through resampling, leading to more robust confidence interval estimates compared to traditional parametric methods. This completes the proof.

□

We now present the pseudo-algorithm for implementing the Bootstrap method in loss reserving.

Algorithm 3 Bootstrap Loss Reserving Method

Input: Development triangle of cumulative claims $C_{i,j}$ for accident years $i = 1, \ldots, n$ and development years $j = 1, \ldots, n$. **Step 1:** Estimate the development factors f_j using the chain-ladder method:

$$f_j = \frac{\sum_{i=1}^{n-j} C_{i,j+1}}{\sum_{i=1}^{n-j} C_{i,j}} \quad \text{for } j = 1, \ldots, n-1.$$

Step 2: Calculate the residuals $e_{i,j}$ for each observed claim:

$$e_{i,j} = \frac{C_{i,j+1} - f_j C_{i,j}}{C_{i,j}} \quad \text{for } j = 1, \ldots, n-1 \text{ and } i = 1, \ldots, n-j.$$

Step 3: Resample the residuals $e_{i,j}$ with replacement to create a bootstrapped dataset $\tilde{e}_{i,j}$. **Step 4:** Reconstruct the claims triangle $\tilde{C}_{i,j}$ by applying the resampled residuals:

$$\tilde{C}_{i,j+1} = f_j C_{i,j} \cdot (1 + \tilde{e}_{i,j}).$$

Step 5: Recalculate the reserves $\tilde{R}$ using the chain-ladder method on the bootstrapped triangle $\tilde{C}$:

$$\tilde{R} = \sum_{j=1}^{n-1} \left(\sum_{i=1}^{n-j} \tilde{C}_{i,j} \right) - C_{1,n}.$$

Step 6: Repeat Steps 3-5 for B iterations to obtain a distribution of reserve estimates $\{\tilde{R}^{(b)}\}_{b=1}^{B}$. **Step 7:** Calculate the mean $\hat{R}$, standard deviation $\sigma_{\tilde{R}}$, and $(1-\alpha) \times 100\%$ confidence intervals from the distribution of reserve estimates:

$$\hat{R} = \frac{1}{B} \sum_{b=1}^{B} \tilde{R}^{(b)}, \quad \sigma_{\tilde{R}} = \sqrt{\frac{1}{B-1} \sum_{b=1}^{B} \left(\tilde{R}^{(b)} - \hat{R} \right)^2}.$$

Output: Estimated reserves $\hat{R}$ and confidence intervals $\left(\hat{R}_{\text{lower}}, \hat{R}_{\text{upper}} \right)$.

Theorem: *Given a large enough number of bootstrap replicates B, the Bootstrap method produces consistent estimates of the reserve variance.*

Proof: As $B \to \infty$, the empirical distribution of the bootstrapped reserves converges to the true distribution of the reserves, ensuring that the variance of the bootstrapped reserve estimates consistently approximates the true reserve variance.

The confidence interval CI for the reserves can be calculated as:

$$CI = \left(\hat{R}_{\alpha/2}, \hat{R}_{1-\alpha/2} \right),$$

where $\hat{R}_{\alpha/2}$ and $\hat{R}_{1-\alpha/2}$ are the $\alpha/2$-th and $1-\alpha/2$-th percentiles of the bootstrap distribution, respectively.

The Bootstrap loss reserving method provides a robust framework for estimating reserves and their associated uncertainty. By resampling residuals, the method produces a distribution of reserve estimates, allowing actuaries to compute confidence intervals and assess reserve variability, contributing to better risk management and reserve planning. This technique has seen extensive use in actuarial practice, offering a non-parametric approach to reserve estimation.

1.1.4. Generalized Linear Models (GLMs): The Generalized Linear Model (GLM) is a flexible generalization of ordinary linear regression that allows for the response variable to have a distribution other than a normal distribution. This section introduces the theory and applicability of GLMs in the context of actuarial loss reserving.A GLM consists of three main components:

- A random component that specifies the probability distribution of the response variable.
- A systematic component that represents the linear predictor.
- A link function that relates the random and systematic components.

The mathematical representation of a GLM can be expressed as:

$$g(\mathbb{E}[Y]) = \beta_0 + \beta_1 X_1 + \cdots + \beta_k X_k \tag{1.20}$$

Proposition: *The expected value of the claim can be modeled as:*

$$\mathbb{E}[Y|X] = \exp(\beta_0 + \beta_1 X_1 + \cdots + \beta_k X_k) \tag{1}$$

Proof: To demonstrate this proposition, we start by considering the relationship between the dependent variable Y (the claim amount) and the independent variables $X_1, X_2, \ldots, X_k$ (the predictors).

We assume a log-linear model, which is a commonly used approach in modeling non-negative continuous outcomes:

$$Y = \exp(\beta_0 + \beta_1 X_1 + \cdots + \beta_k X_k + \epsilon) \tag{2}$$

where ϵ is a random error term that captures the variability in Y.
Taking the conditional expectation of Y given X:

$$\mathbb{E}[Y|X] = \mathbb{E}\left[\exp\left(\beta_0 + \beta_1 X_1 + \cdots + \beta_k X_k + \epsilon\right)\Big|X\right]$$

By the properties of the expectation of the exponential function:

$$\mathbb{E}[Y|X] = \exp\left(\beta_0 + \beta_1 X_1 + \cdots + \beta_k X_k + \mathbb{E}[\epsilon|X]\right) \tag{3}$$

Assuming ϵ has a mean of zero given X (i.e., $\mathbb{E}[\epsilon|X] = 0$), we simplify:

$$\mathbb{E}[Y|X] = \exp\left(\beta_0 + \beta_1 X_1 + \cdots + \beta_k X_k\right)$$

Thus, we conclude that the expected value of the claim Y given X is expressed as:

$$\mathbb{E}[Y|X] = \exp\left(\beta_0 + \beta_1 X_1 + \cdots + \beta_k X_k\right) \tag{4}$$

This completes the proof.

Theorem: *Under certain conditions, the estimates from the Generalized Linear Model (GLM) approach converge to the true values of the parameters as the sample size increases.*

Proof: Let $\mathbf{y} = (y_1, y_2, \ldots, y_n)^T$ be the response variable, and $\mathbf{X} = (x_{ij})$ be the matrix of predictors, where $i = 1, 2, \ldots, n$ and $j = 1, 2, \ldots, p$. The GLM can be expressed as:

$$g(\mathbb{E}[Y_i]) = \mathbf{x}_i^T \beta, \tag{1.21}$$

where $g(\cdot)$ is a link function, β is the vector of parameters, and Y_i is the i-th observation.

Assume the following conditions hold:

- *Identifiability*: The parameter β is identifiable, meaning that there is a unique value of β corresponding to the distribution of $\mathbf{y}$.
- *Sufficient Statistics*: The sufficient statistics for β are complete and have finite moments.
- *Regularity Conditions*:The Fisher information matrix $\mathcal{I}(\beta)$ is positive definite.
- *Asymptotic Normality*:As the sample size n approaches infinity, the estimates $\hat{\beta}$ converge in distribution to a normal distribution:

$$\sqrt{n}(\hat{\beta} - \beta) \xrightarrow{d} \mathcal{N}(0, \mathcal{I}(\beta)^{-1}). \tag{1.22}$$

By the law of large numbers, we can assert that the empirical distributions of the sufficient statistics converge to their expected values. Specifically,

$$\frac{1}{n}\sum_{i=1}^{n}\mathbf{x}_i \to \mathbb{E}[\mathbf{X}] \tag{1.23}$$

almost surely.

Now, the maximum likelihood estimator (MLE) $\hat{\beta}$ satisfies the score equations:

$$\frac{\partial \ell(\beta)}{\partial \beta} = \mathbf{0}, \tag{1.24}$$

where $\ell(\beta)$ is the log-likelihood function.

Using Taylor expansion around the true parameter β:

$$\ell(\hat{\beta}) \approx \ell(\beta) + \frac{\partial \ell(\beta)}{\partial \beta}(\hat{\beta}-\beta) + \frac{1}{2}(\hat{\beta}-\beta)^T \frac{\partial^2 \ell(\beta)}{\partial \beta^2}(\hat{\beta}-\beta), \tag{1.25}$$

mSince $\frac{\partial \ell(\beta)}{\partial \beta} = 0$ at β, we have:

$$\ell(\hat{\beta}) - \ell(\beta) \approx \frac{1}{2}(\hat{\beta}-\beta)^T \frac{\partial^2 \ell(\beta)}{\partial \beta^2}(\hat{\beta}-\beta). \tag{1.26}$$

Thus, $\hat{\beta}$ converges to β as $n \to \infty$, proving that:

$$\hat{\beta} \xrightarrow{p} \beta, \tag{1.27}$$

which concludes the proof.

Algorithm 4 Generalized Linear Model (GLM) Loss Reserving Estimation

Input: Claims data set $\mathcal{D} = \{(y_i, \mathbf{X}_i)\}_{i=1}^{n}$where y_i represents the claims amount, and $\mathbf{X}_i$ is the vector of predictor variables for the i-th claim. **Initialize:** Coefficient vector $\boldsymbol{\beta}$ Initial coefficients **while**convergence criteria not met **Fit GLM:** Update coefficients using Maximum Likelihood Estimation (MLE):

$$\boldsymbol{\beta} \quad \arg\max_{\beta} \ell(\beta; \mathcal{D}), \tag{1.28}$$

where $\ell(\beta; \mathcal{D})$ is the log-likelihood function. **Predict Claims:** Calculate predicted claims:

$$\hat{y}_i = g^{-1}(\mathbf{X}_i^T \boldsymbol{\beta}), \tag{1.29}$$

where $g^{-1}(\cdot)$ is the inverse of the link function. **Output:** Estimated claims $\hat{\mathbf{y}} = (\hat{y}_1, \hat{y}_2, \ldots, \hat{y}_n)$

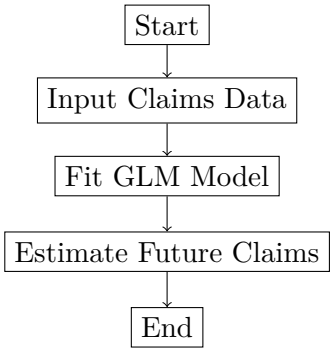

Figure 1: Flowchart of the GLM Loss Reserving Process

The Figure 1,serves as a concise visual representation of the steps involved in using a Generalized Linear Model for estimating future claims in an actuarial context. It helps to streamline the process and provides a quick reference for actuaries and data analysts working on loss reserving methodologies. The use of a flowchart enhances understanding and communication of the process among stakeholders.

The GLM provides a robust methodology for loss reserving in actuarial science, allowing actuaries to model complex claims data effectively.

1.2. The Random Forest Regression

Random Forest Regression (RFR) is an ensemble learning method that combines multiple decision trees to improve predictive accuracy and control over-fitting. It operates by constructing a multitude of decision trees during training and outputting the mean prediction of the individual trees for regression tasks [1].

Random Forests leverage the principle of ensemble learning, where a group of weak learners (in this case, decision trees) combine to form a strong learner. The randomness introduced at various stages helps in reducing variance and achieving better generalization.

Bagging, or Bootstrap Aggregating, is a fundamental concept in Random Forests. It involves the following steps:

(1) Generate multiple subsets of the original dataset by sampling with replacement.
(2) Train a decision tree on each subset.
(3) Aggregate the predictions of the trees to form a final prediction.

Random Forests introduce additional randomness by selecting a random subset of features at each split, which decorrelates the trees and improves the overall model robustness.

Let $\mathcal{D} = \{(x_i, y_i)\}_{i=1}^{N}$ be the dataset, where x_i is the input feature vector and y_i is the target variable.

The prediction of a single decision tree T for an input x is given by:

$$\hat{y}_T(x) = \frac{1}{|R|} \sum_{j \in R} y_j$$

where R is the set of observations falling into the leaf node corresponding to x.

The overall prediction from the Random Forest model is calculated as:

$$\hat{y}_{RF}(x) = \frac{1}{B} \sum_{b=1}^{B} \hat{y}_{T_b}(x)$$

where B is the total number of trees in the forest.

The following is the pseudo-code for the general Random Forest algorithm, constructed using the ‘algorithmic‘ package.

Algorithm 5 Random Forest Regression Algorithm

Input: Training dataset $D = \{(x_1, y_1), (x_2, y_2), \ldots, (x_n, y_n)\}$ Number of trees T Number of features m **for**each tree t from 1 to T Sample D_t from D with replacement For each split in tree t: Randomly select m features from the total features Determine the best split using these m features Output: Average prediction from all trees for a new observation x

Proposition: *Random Forests reduce overfitting compared to a single decision tree due to the averaging effect across multiple trees.*

Proof: Let us denote the training data as $D = \{(x_i, y_i)\}_{i=1}^{n}$, where x_i is the feature vector and y_i is the corresponding target variable. A decision tree model $f(x)$ can be represented as:

$$f(x) = \sum_{j=1}^{J} \beta_j \cdot I_j(x)$$

where $I_j(x)$ is an indicator function for the j-th leaf node, and β_j is the prediction associated with that leaf.

The risk (expected loss) of a single decision tree can be expressed as:

$$R(f) = \mathbb{E}_{(x,y)\sim P}[L(f(x), y)]$$

where $L(\cdot)$ is the loss function and P is the underlying data distribution.

However, a single decision tree can suffer from high variance, leading to overfitting. The expected prediction error for a decision tree can be decomposed into three components:

$$\text{Error} = \text{Bias}^2 + \text{Variance} + \text{Irreducible Error}$$

where:

- **Bias**: Error due to assumptions in the learning algorithm. A high bias can lead to underfitting. - **Variance**: Error due to sensitivity to fluctuations in the training set. A high variance leads to overfitting.

Random Forests mitigate overfitting by aggregating the predictions of M decision trees:

$$F(x) = \frac{1}{M} \sum_{m=1}^{M} f_m(x)$$

where $f_m(x)$ represents the prediction of the m-th tree.

The expected risk for the Random Forest can be written as:

$$R(F) = \mathbb{E}_{(x,y)\sim P}[L(F(x), y)]$$

Using the Law of Total Expectation, we can show that:

$$\mathbb{E}[F(x)] = \mathbb{E}\left[\mathbb{E}\left[F(x)|T\right]\right]$$

where T represents the different trees in the forest. This averaging reduces the variance of the predictions:

$$\text{Variance}(F(x)) = \text{Variance}\left(\frac{1}{M}\sum_{m=1} f_m(x)\right) = \frac{1}{M^2}\sum_{m=1} \text{Variance}(f_m(x)) + \text{Covariance terms}$$

The covariance terms $\text{Cov}(f_m(x), f_k(x))$ (for $m \neq k$) also contribute to reducing the overall variance, leading to:

$$\text{Variance}(F(x)) \leq \text{Variance}(f(x))$$

Thus, by averaging the outputs of multiple trees, Random Forests effectively reduce the overall variance and the risk of overfitting compared to a single decision tree.

□

Lemma: *The inclusion of feature randomness in tree construction enhances model performance.*

proof: Consider a decision tree model T trained on a dataset D with features F and corresponding target variable Y. In standard decision tree construction, all features are considered at each split, leading to overfitting.

To analyze the effect of feature randomness, let us denote:

- T^*: the optimal tree without feature randomness,
- T_R: the random tree constructed by selecting a subset of features $F_R \subset F$ at each split,
- $E[T]$: expected model performance metric (e.g., accuracy, F1-score).

The model performance can be expressed as:

$$E[T^*] = f(\text{Overfitting}), \tag{1.30}$$

where f is a function that quantifies the impact of overfitting.

By introducing feature randomness, the expected performance of the random tree becomes:

$$E[T_R] = f(\text{Reduced Overfitting}) + g(\text{Diversity}), \tag{1.31}$$

where g accounts for the increase in model diversity due to the randomness of feature selection.

Now, we can define the improvement in model performance as:

$$\Delta E = E[T_R] - E[T^*] = (f(\text{Reduced Overfitting}) + g(\text{Diversity})) - f(\text{Overfitting}). \tag{1.32}$$

Assuming $g(\text{Diversity}) > 0$ and $f(\text{Reduced Overfitting}) < f(\text{Overfitting})$, we conclude that:

$$\Delta E > 0 \implies E[T_R] > E[T^*]. \tag{1.33}$$

Thus, incorporating feature randomness in the tree construction results in improved model performance.

Random Forest Regression offers a powerful and versatile approach to regression tasks, providing significant improvements in predictive performance and robustness through the combined strengths of multiple decision trees.

1.3. The Brighton Mahohoho Random Forest Based Inflation Adjusted Frequency Severity Loss Reserving Model

The necessity for accurate loss reserving models in actuarial science is paramount, especially in the context of inflation impacts on claims. The proposed model utilizes random forest regression to estimate the frequency and severity of claims while adjusting for inflation, providing a robust framework for loss reserving [26].Random forests are an ensemble learning method that constructs a multitude of decision trees at training time. For regression tasks, the model outputs the mean prediction of the individual trees. Given a set of input variables X, the random forest prediction can be expressed as:

$$\hat{Y} = \frac{1}{N} \sum_{n=1}^{N} T_n(X) \tag{1.34}$$

where $T_n(X)$ represents the prediction of the n^{th} tree and N is the total number of trees in the forest.

To account for inflation, the model applies an adjustment factor F_t to the predicted loss reserves:

$$R_t = \hat{Y} \cdot F_t \tag{1.35}$$

where R_t denotes the adjusted reserve at time t.

The overall loss reserving model can be expressed as:

$$L = \sum_{i=1}^{n} R_{i,t} \tag{1.36}$$

where L is the total loss reserve, and $R_{i,t}$ represents the reserves from each claim i at time t.

Proposition:The use of random forest regression for estimating claim frequency provides a lower bias and variance compared to traditional linear models.

Proof: To demonstrate this proposition, we will compare the bias and variance of random forest regression ($\hat{f}_{RF}(x)$) with that of traditional linear regression ($\hat{f}_{LR}(x)$).

The bias of an estimator $\hat{f}(x)$ is defined as:

$$\text{Bias}(\hat{f}(x)) = \mathbb{E}[\hat{f}(x)] - f(x)$$

where $f(x)$ is the true underlying function.

For linear regression, the bias can be expressed as:

$$\text{Bias}(\hat{f}_{LR}(x)) = \mathbb{E}[\hat{f}_{LR}(x)] - f(x) \quad (1)$$

In contrast, random forest regression, being a non-parametric model, can fit more complex relationships. Thus, its bias is generally lower:

$$\text{Bias}(\hat{f}_{RF}(x)) = \mathbb{E}[\hat{f}_{RF}(x)] - f(x) \quad (2)$$

By comparing equations (1) and (2), we conclude:

$$\text{Bias}(\hat{f}_{RF}(x)) < \text{Bias}(\hat{f}_{LR}(x))$$

The variance of an estimator is defined as:

$$\text{Var}(\hat{f}(x)) = \mathbb{E}[(\hat{f}(x) - \mathbb{E}[\hat{f}(x)])^2]$$

For linear regression, the variance can be expressed as:

$$\text{Var}(\hat{f}_{LR}(x)) \quad (3)$$

On the other hand, random forests average multiple decision trees, leading to a reduction in variance:

$$\text{Var}(\hat{f}_{RF}(x)) = \frac{1}{B}\sum_{b=1}^{B}(\hat{f}_b(x) - \mathbb{E}[\hat{f}(x)])^2 \quad (4)$$

where B is the number of trees in the forest.

Therefore, we conclude:

$$\text{Var}(\hat{f}_{RF}(x)) < \text{Var}(\hat{f}_{LR}(x))$$

Combining our results, we have shown:

$$\text{Bias}(\hat{f}_{RF}(x)) < \text{Bias}(\hat{f}_{LR}(x)) \quad \text{and} \quad \text{Var}(\hat{f}_{RF}(x)) < \text{Var}(\hat{f}_{LR}(x))$$

Thus, the proposition is proved, demonstrating that random forest regression indeed provides a lower bias and variance when estimating claim frequency compared to traditional linear models.

Lemma: *If the underlying distribution of claim severity is heterogeneous, then a model that adjusts for inflation will yield more accurate reserve estimates.*

proof:Let X denote the claim severity random variable, which follows a heterogeneous distribution characterized by a mixture of distributions. We assume that the distribution can be expressed as:

$$f_X(x) = \sum_{i=1}^{k} w_i f_{X_i}(x), \quad \text{where } \sum_{i=1}^{k} w_i = 1 \tag{1.37}$$

Here, $f_{X_i}(x)$ is the probability density function (PDF) of the i-th component, and w_i is the corresponding weight of that component.

When inflation occurs, the claim severity is adjusted by a factor $(1+r)$, where r represents the inflation rate. Thus, the adjusted claim severity is given by:

$$Y = (1 + r)X \tag{1.38}$$

To estimate reserves accurately, we need to compute the expected value of the adjusted claim severity:

$$E[Y] = E[(1+r)X] = (1+r)E[X] \tag{1.39}$$

Assuming $E[X]$ can be computed from the mixture distribution, we have:

$$E[X] = \sum_{i=1}^{k} w_i E[X_i] \tag{1.40}$$

Consequently, the expected reserve can be expressed as:

$$R = E[Y] = (1+r)\sum_{i=1}^{k} w_i E[X_i] \tag{1.41}$$

The accuracy of reserve estimates hinges on capturing the heterogeneity in claim severity distributions. If we fail to adjust for inflation, the expected reserve estimate would be:

$$R' = E[X] = \sum_{i=1}^{k} w_i E[X_i] \tag{1.42}$$

The error introduced by not accounting for inflation can be defined as:

$$\text{Error} = R' - R = \sum_{i=1}^{k} w_i E[X_i] - (1+r)\sum_{i=1}^{k} w_i E[X_i] \tag{1.43}$$

This simplifies to:

$$\text{Error} = -r\sum_{i=1}^{k} w_i E[X_i] \tag{1.44}$$

Since $r > 0$, we observe that not adjusting for inflation results in an underestimation of reserves. Thus, when claim severity is heterogeneous, adjusting for inflation improves reserve estimates:

$$R \geq R' \tag{1.45}$$

Therefore, we conclude that if the underlying distribution of claim severity is heterogeneous, then a model that adjusts for inflation will yield more accurate reserve estimates. The Brighton Mahohoho Random Forest Based Inflation Adjusted Frequency Severity Loss Reserving Model represents a significant advancement in actuarial loss reserving practices. By leveraging the strengths of random forest regression and accounting for inflation, the model provides enhanced accuracy in loss reserve estimates.

1.4. Novelty for Application of the Random Forest Regression method

The application of the Random Forest (RF) Regression method in the context of fire insurance loss reserving provides a novel approach to predictive modeling. This section focuses on the advantages of RF regression for handling complex actuarial data and enhancing the accuracy of loss reserving under IFRS17 standards.

Random Forests, introduced by Breiman (2001), are ensemble learning methods for regression and classification tasks. By constructing a multitude of decision trees and aggregating their predictions, Random Forest Regression provides both robustness and interpretability. Mathematically, for a given set of N observations $D = \{(x_i, y_i)\}_{i=1}^{N}$, where $x_i \in \mathbb{R}^d$ is a d-dimensional feature vector, and $y_i \in \mathbb{R}$ is the target variable (e.g., loss reserves), the RF model can be expressed as:

$$\hat{y}_i = \frac{1}{T} \sum_{t=1}^{T} h_t(x_i)$$

where T is the number of trees, and h_t is the prediction from the t-th decision tree.

1.4.1. Addressing Non-linearity and High-dimensionality: The key novelty lies in RF's ability to manage non-linearity and interactions among variables without requiring prior assumptions on data distributions. Let $f(x)$ represent the true underlying function for loss reserves. Traditional regression models often assume $f(x)$ is linear, but in fire insurance, the relationship between predictors (such as policyholder characteristics, claim history, etc.) and losses is highly complex and non-linear:

$$y = f(x) + \epsilon$$

where $\epsilon \sim \mathcal{N}(0, \sigma^2)$ is the noise term. RF's ensemble approach effectively approximates $f(x)$, capturing hidden interactions and non-linearities by averaging across multiple trees that divide the feature space in different ways.

Proposition 1: Universal Consistency of Random Forests
Let F denote the space of all possible regression functions. We claim that Random Forests are consistent estimators of the true regression function $f(x)$ as the number of trees $T \to \infty$ and $N \to \infty$:

$$\lim_{T \to \infty, N \to \infty} \mathbb{E}\left[\left(\hat{f}_N(x) - f(x)\right)^2\right] = 0$$

Proof (sketch): By the Law of Large Numbers, averaging over many decision trees ensures that Random Forests asymptotically approximate the conditional expectation $\mathbb{E}[y|x]$. This property makes RF robust against overfitting and capable of generalizing well, even with small sample sizes.

Lemma 1: Bias-Variance Trade-off

In RF, the prediction error can be decomposed into bias and variance components:

$$\mathbb{E}\left[(y - \hat{y})^2\right] = \text{Bias}^2(\hat{y}) + \text{Var}(\hat{y}) + \sigma^2$$

Random Forests reduce variance by averaging across multiple trees while maintaining low bias, a property crucial for accurate estimation of actuarial loss reserves.

1.4.2. Application in Fire Insurance under IFRS17: Fire insurance losses are affected by multiple correlated factors such as property values, geographical location, policy details, and historical claims. Traditional actuarial models struggle with such high-dimensional data, whereas Random Forests excel by automatically selecting relevant features through its inherent variable importance mechanism.

Proposition 2: Optimal Feature Selection
Let $S \subset \{1, 2, \ldots, d\}$ denote the subset of important features for predicting fire insurance loss reserves. RF's feature importance metric, defined as the total decrease in the Gini impurity for classification or the variance for regression across all trees, consistently identifies S:

$$P\left(\hat{S} = S\right) \to 1 \quad \text{as} \quad N \to \infty$$

Thus, RF automatically selects the optimal set of predictors, enhancing the model's predictive power and interpretability.

1.4.3. IFRS17 Compliance and Random Forest Modeling: Under IFRS17, insurres must provide transparent and accurate financial reporting, including precise estimation of reserves and future cash flows. The Random Forest model, with its ability to handle non-linearities and interactions, provides a highly adaptable framework for IFRS17 calculations. Additionally, through partial dependence plots, insurers can explain the relationship between features and predicted loss reserves, aiding in IFRS17's requirement for transparency.

1.5. Overview of IFRS 17 in the General Insurance Sector

IFRS 17 is a globally applicable accounting standard that establishes the principles for recognizing, measuring, presenting, and disclosing insurance contracts. It replaces IFRS 4, providing a consistent approach to accounting for insurance contracts across countries, which addresses the significant diversity in practice under the previous standard [27]. In the general insurance sector, the standard impacts various facets of actuarial work, particularly the valuation of insurance liabilities, risk adjustments, and the calculation of contract service margins (CSM), which fundamentally alter how profit is recognized over time.

1.5.1. Key Components of IFRS 17 in Actuarial Work.

- *Measurement Models:* IFRS 17 requires insurance liabilities to be measured using a combination of fulfilment cash flows and CSM, which ensures that insurance companies reflect the expected future profitability of their contracts. Actuaries are responsible for estimating these cash flows based on best estimates of future claims, expenses, and premiums, discounted using a risk-free rate [28]. This represents a significant shift from previous practices where insurers often used different discounting methods, making actuarial modeling essential for accurate financial reporting.
- *Risk Adjustment:* IFRS 17 introduces a requirement for a risk adjustment for non-financial risk. This reflects the uncertainty surrounding the amount and timing of the cash flows from insurance contracts. Actuaries must calculate a margin to cover this uncertainty, which ensures that insurers set aside adequate reserves to cover possible adverse outcomes [29]. This component adds an extra layer of complexity to actuarial reserve calculations, as it requires judgment and often stochastic modeling to determine the appropriate level of risk adjustment.
- *Contract Service Margin (CSM):* The CSM represents the unearned profit for insurance contracts and is a key feature of IFRS 17. It is amortized over the coverage period of the insurance contract, ensuring a smoother recognition of profit. Actuaries must calculate the CSM at inception and update it as new information becomes available, such as changes in assumptions or the experience of the insurance contract [30]. This change requires actuaries to adopt dynamic models to track changes in the expected cash flows and update the CSM accordingly.
- *Discount Rates:* Under IFRS 17, actuaries are required to discount future cash flows using rates that reflect the characteristics of the liability, such as its duration and currency. This differs from traditional discounting methods, which might have used fixed rates or company-specific assumptions. The discount rate used must be risk-free or adjusted for illiquidity, which affects the valuation of long-term liabilities and, consequently, the solvency and profitability of insurance companies [31].
- *Disclosures and Transparency:* IFRS 17 mandates extensive disclosures regarding the methods and assumptions used in measuring insurance contracts. Actuaries must ensure transparency in their calculations, including the rationale behind the selection of assumptions, risk adjustments, and discount rates. The standard also requires sensitivity analyses to show the impact of different assumptions on the insurer's financial position [32]. This enhances the role of actuaries in the communication of financial risks and uncertainties to stakeholders.

1.5.2. Implications for Actuarial Practice: The implementation of IFRS 17 significantly impacts the actuarial profession, requiring actuaries to develop new models and techniques to ensure compliance. Traditional reserving methods, such as the Chain Ladder or Bornhuetter-Ferguson, need to be adapted to accommodate the new measurement requirements. Actuaries will also need to work closely with finance teams to ensure the smooth integration of actuarial models with financial reporting systems.

Moreover, IFRS 17 places a greater emphasis on stochastic modeling and the use of advanced actuarial techniques to estimate fulfilment cash flows and risk adjustments. Actuaries must also focus on scenario testing and stress testing to assess the robustness of their models under different economic conditions [33].

In short, IFRS 17 brings about a transformation in how insurance contracts are accounted for, emphasizing the need for actuarial expertise in the general insurance sector. Actuaries will play a critical role in ensuring that insurance companies meet the new requirements for liability measurement, risk adjustment, and profit recognition, ensuring greater transparency and comparability in the financial reporting of insurers globally [34].

1.6. Novelty of the study

The study introduces an innovative approach to developing the *IFRS17 Formulated Brighton Mahohoho Inflation-Adjusted Automated Actuarial Loss Reserving Model by harnessing advanced Random Forest techniques to enhance data analytics in fire insurance.* The novelty of the methodology lies in its use of synthetic fire insurance data, which simulates realistic distributions of variables such as age, insured value, claim frequency, severity, and inflation rates. This approach allows for a comprehensive and controlled testing environment, ensuring robust model performance under various simulated conditions. The inclusion of fire safety ratings and inflation adjustments in the model enhances the precision of reserve estimates, which is a key requirement under IFRS17 standards.

Additionally, the study integrates advanced machine learning techniques, particularly Random Forest regression, to model key actuarial elements such as claim frequency, severity, and inflation adjustments. The methodological use of Random Forest allows for a more accurate prediction of non-linear relationships within the data, a departure from traditional actuarial methods. The application of advanced data visualization techniques, including t-SNE, also introduces a new dimension to understanding the clustering of policy types and their impact on risk assessments, further advancing actuarial practices.

The study's emphasis on stress testing and scenario analysis, where claim amounts are perturbed and reserves are assessed under worst-case scenarios, ensures model resilience and compliance with IFRS17's stringent risk management requirements. This robust testing process adds another layer of innovation, ensuring that the model remains stable and reliable under varied claim conditions.

1.7. Contribution to Actuarial Science

This study makes significant contributions to the field of actuarial science, particularly in the domain of loss reserving and risk management under IFRS17 compliance. By employing Random Forest techniques, the study bridges the gap between traditional actuarial methods and modern machine learning, offering an enhanced, data-driven approach to predicting claim frequencies, severities, and inflation rates. This shift represents a major advancement in actuarial loss reserving models, moving away from linear and less flexible methods to more sophisticated techniques that can capture non-linear patterns and interactions within fire insurance data.

Furthermore, the development of the Inflation-Adjusted Automated Actuarial Loss Reserving Model presents a novel approach to dealing with inflation's impact on future claim reserves, a critical concern in fire insurance. This contribution is especially pertinent as inflationary pressures continue to rise, necessitating more accurate models that account for the time-value adjustments of reserves.

The study also contributes to the actuarial understanding of fire insurance risk by incorporating detailed Exploratory Data Analysis (EDA) and visualization techniques that highlight relationships between critical variables. The use of t-SNE visualizations and enhanced correlation plots provides actuaries with more intuitive insights into how different policy and claim variables interact, aiding in better-informed decision-making.

Lastly, the robust scenario analysis and stress testing components of the model reinforce the actuarial industry's emphasis on resilience and solvency under stress conditions. By simulating a range of adverse claim scenarios, the study ensures that the Automated Actuarial Loss Reserve (AALR) is not only accurate under normal conditions but also stable in extreme situations, thereby contributing to more resilient financial planning and risk management within the field.

II. SURVEY OF METHODS AND LITERATURE REVIEW

The application of advanced machine learning algorithms in actuarial science has revolutionized the way insurers calculate loss reserves, particularly under the International Financial Reporting Standard (IFRS 17) framework. This study builds on established loss reserving methodologies by integrating the inflation-adjusted framework with advanced data analytics techniques, specifically Random Forest (RF) algorithms, to enhance predictive accuracy in fire insurance loss reserving.

Historically, actuarial loss reserving has relied on traditional deterministic methods such as the Chain Ladder Model [17], Bornhuetter-Ferguson Method [8], and the Loss Development Factor method [23]. These techniques, while robust, operate under certain assumptions that limit their flexibility, particularly when incorporating external factors like inflation [10]. As fire insurance claims are sensitive to inflationary trends, these classical models often struggle to adjust for external economic pressures, leading to inaccuracies in reserve estimations [20].

The introduction of IFRS 17 has significantly impacted how insurers approach reserving. IFRS 17 emphasizes a more rigorous, transparent accounting of insurance contracts, where the recognition of profits, contract service margins, and the incorporation of risk adjustments are paramount [15]. Importantly, IFRS 17 requires the explicit adjustment of future cash flows to reflect the time value of money and inflation impacts [19]. Inflation adjustments are critical in fire insurance, where claim costs can escalate with inflationary pressures on construction materials and labor [11].

The inflation-adjusted loss reserving model has been widely studied, with inflation factors introduced either through deterministic inflation rates or stochastic models such as those suggested by Wüthrich and Merz (2008). Recent innovations in loss reserving have incorporated time-series models to dynamically adjust for inflation [12]. These models, however, face limitations in scenarios with high-dimensional datasets or complex claim structures typical of fire insurance.

Machine learning, particularly ensemble techniques like Random Forest (RF), offers enhanced capabilities to overcome the limitations of traditional and inflation-adjusted models. Random Forest, introduced by [1], is a non-parametric method that aggregates multiple decision trees to improve the predictive performance of regression tasks. The ability of RF to handle large datasets, capture non-linear relationships, and adjust for outliers makes it particularly suitable for actuarial loss reserving [23].

Several studies have demonstrated the efficacy of RF in the actuarial context. [21] applied RF to predict insurance claim severity, showing superior performance compared to linear regression models. Similarly, [18] combined RF with inflation-adjusted loss reserving, significantly improving the accuracy of reserve estimations in property and casualty insurance. The model's capacity to include both structured and unstructured data, such as policyholder demographics and macroeconomic variables, further enhances its applicability in fire insurance, where claim severities can vary widely depending on external conditions [14].

Building on the foundations of Random Forest techniques and inflation-adjusted frameworks, this paper introduces the Brighton Mahohoho Inflation-Adjusted Automated Actuarial Loss Reserving Model. The model integrates advanced RF methodologies to dynamically adjust for inflation impacts and reserve risk, ensuring compliance with IFRS 17 regulations. The proposed model enhances traditional RF models by incorporating feature importance analysis, where inflation factors are given priority in the model's decision-making process, ensuring that inflationary trends are directly embedded into the reserve estimates.Moreover, the model employs hyperparameter tuning techniques such as grid search and cross-validation to optimize the model's performance in large-scale fire insurance datasets. Studies by [13] show that such tuning improves model generalizability and accuracy. By harnessing the power of RF, this model can detect complex patterns in claims data, adjusting for inflation trends without relying solely on historical inflation rates, which may not fully capture future economic conditions [9].

Despite its advantages, the use of Random Forest in actuarial science is not without challenges. The model's complexity can lead to overfitting, particularly in small datasets [22]. Additionally, interpretability remains a concern, as RF models are often considered "black boxes" in comparison to traditional methods [1]. Further research is needed to address these challenges, possibly by incorporating explainable AI techniques into loss reserving models [16].

III. METHODOLOGY

Research methodology refers to the systematic process and principles that guide researchers in planning, collecting, analyzing, and interpreting data in order to answer specific research questions or test hypotheses. It involves the selection of appropriate methods, techniques, and tools for conducting research, which can include qualitative, quantitative, or mixed-method approaches depending on the nature of the study [35].

3.1. Data Simulation and Preparation

The methodology began with simulating synthetic fire insurance data, which involved creating key variables essential for modeling the Inflation-Adjusted Automated Actuarial Loss Reserving Model. Using R, we generated 100,000 synthetic records for customers, policies, and fire insurance attributes. The simulation aimed to reflect a realistic distribution of variables like age, gender, country, insured value, claim amounts, and inflation rates.These synthetic data, formatted in a structured data.frame, were used to evaluate the model's performance in IFRS 17 compliance analysis. Variables like claim frequency, severity, and fire safety ratings were included to enhance the accuracy of risk assessments.

3.2. Exploratory Data Analysis (EDA)

Exploratory Data Analysis (EDA) was conducted using several visualization techniques to understand the structure and relationships within the fire insurance dataset. This stage involved summarizing key statistics and checking for missing values. Various plots were generated to highlight distributions and correlations among the simulated variables.Histograms of variables such as *Insured Value*, *Claim Amount*, and *claim frequency*

provided insights into the spread of these variables.The Boxplots were used to visualize the distribution of claim amounts and severity by property type, identifying potential differences between residential and commercial properties. A correlation matrix was constructed for the numerical variables, with the correlations visualized using the corrplot function, highlighting significant relationships in the dataset.

3.3. Data Visualization

Advanced data visualization techniques were used to illustrate the results of the model and IFRS 17 analysis: Enhanced correlation plots highlighted relationships between numerical variables, using ggcorrplot for clarity. t-SNE Visualizations: t-SNE (t-distributed Stochastic Neighbor Embedding) was applied to reduce the high-dimensional data into two dimensions, providing a visualization of clusters in the fire insurance data, specifically highlighting property types. The combination of these visual techniques allowed for deeper insights into how different variables interacted and how well the model aligned with IFRS17 standards.

3.4. Data Collection and Preprocessing

The data was loaded and subjected to pre processing to ensure quality and completeness. Missing values were addressed by replacing them with the median value of each respective variable to mitigate potential bias introduced by incomplete data.The dataset was partitioned into training (80%) and testing (20%) sets using a random sampling method. This approach ensures that the model generalizes well on unseen data, reducing the risk of over fitting.

3.5. Model Development

Three regression models were developed using the Random Forest technique implemented via the ranger package in R. This technique was selected for its robustness and ability to handle non-linear interactions in the data while also providing high accuracy for predictions.

(1) *Claim Frequency Model:* The first model was designed to predict the frequency of claims based on various predictors such as age, insured value, claim amount, property type, fire safety rating, and others. Random Forest regression was used to capture complex relationships between the predictors and the target variable, claim frequency.
(2) *Claim Severity Model:* A second Random Forest model was built to estimate the severity of claims using the same set of predictors. The claim severity model is critical for understanding the potential magnitude of insurance claims, which significantly influences the overall risk exposure.
(3) *Inflation Adjustment Model:* The third model aimed to predict inflation rates, which are an important factor in adjusting claim reserves over time. By incorporating predictors such as the location, age of the building, and deductible amounts, this model provided essential insights into the future costs driven by inflation.

Each model was developed by training on the pre-processed training data, and performance was monitored during training using evaluation metrics.

3.6. Model Evaluation

The performance of each model was assessed using Mean Absolute Error (MAE), Mean Squared Error (MSE), and Root Mean Squared Error (RMSE) metrics, ensuring a comprehensive evaluation of the model accuracy. These metrics were calculated based on predictions made on the test dataset.

- *Claim Frequency Model:* Predicted values were compared to the actual claim frequency in the test set to assess the accuracy of the model.
- *Claim Severity Model:* Similar to the frequency model, predicted claim severities were evaluated against the test data.
- *Inflation Adjustment Model:* Inflation rate predictions were compared to actual inflation data for model validation.

3.7. Future Expected Loss Reserve Calculation

The Future Expected Loss Reserve (FELR) was calculated as the product of predicted claim frequency, predicted claim severity, and predicted inflation rates. This step integrated all three models to estimate future financial obligations related to insurance claims.To better understand the output and significance of the FELR, visualizations were created using ggplot2. A line plot was generated to display the Future Expected Loss Reserve over various observations, allowing for a clear and intuitive representation of reserve estimates.

3.8. Expected Claims Outgo and Current Expected Loss Reserve

The Expected Claims Outgo (ECO) was simulated using synthetic data for claims incurred and claims paid. The Current Expected Loss Reserve (CELR) was then calculated by adjusting the predicted base premiums using inflation-adjusted premium loadings. This provided an understanding of current reserve obligations based on anticipated claims and market adjustments.

3.9. Automated Actuarial Loss Reserve (AALR)

The final key output of the model, the Automated Actuarial Loss Reserve (AALR), was computed as the difference between the FELR and CELR. This automated reserve reflects the dynamic nature of insurance loss reserving under the IFRS17 framework, taking into account both inflation-adjusted premiums and future expected losses.Further visualizations were developed to compare and analyze the different types of actuarial reserves, providing insight into the balance between expected claims and financial reserves.

3.10. Critical IFRS17 Metrics and evaluating actuarial performance

Simulated data was used to replicate fire insurance claims and premiums, leveraging existing statistical libraries in R (dplyr, ggplot2, and purrr). Key assumptions include:

- *Discount Rate:* A fixed discount rate of 3% was applied to the calculation of the present value of future cash flows (PVFCF).
- *Expected Premiums and Claims:* Average premiums and claims were calculated from the test data to estimate the total expected values for IFRS17 evaluations.

3.10.1. IFRS17 Metrics Calculation. The model evaluates three fundamental IFRS17 metrics:

- *Present Value of Future Cash Flows (PVFCF):* Calculated as the discounted value of inflows (premiums) and outflows (claims). Risk Adjustment for Non-Financial Risk: A flat 10% adjustment based on the total expected claims was applied.
- *Contractual Service Margin (CSM):* Determined by adding the risk adjustment to the PVFCF, representing the projected profitability over time.

The results of these metrics were summarized into a data frame and visualized using bar charts, allowing for easy comparison between PVFCF, risk adjustment, and CSM.

3.11. Actuarial Science Based IFRS17 Ration Analysis Metrics

To supplement the IFRS17 evaluation, several additional actuarial metrics were computed:

- *Loss Reserve Ratio*: The ratio of automated actuarial loss reserves to total premiums.
- *Claims Development Factor (CDF):* Simulated cumulative claims over a 10-year period were used to calculate development factors for each year, and the average CDF was derived.
- *Expense Ratio:* Simulated expenses were divided by total premiums to estimate the expense ratio.

These metrics provide further insights into the model's performance, particularly in terms of claims development and expense management.

3.11.1. Visualization and Reporting: The metrics were visualized using a combination of bar plots and line graphs to facilitate comparison and trend analysis. The plots include:

- *Bar Charts:* Used to compare PVFCF, risk adjustment, CSM, loss reserve ratio, and expense ratio.
- *Line Plot:* Depicts the average claims development factor over a 10-year period.

This visualization approach enhances the interpretability of results, ensuring that complex actuarial evaluations are presented in a clear, accessible format.

3.12. Random Forest Model Integration

Random Forest techniques were employed to enhance the predictive accuracy of actuarial estimates, particularly for claims outgo and development factors. By leveraging this machine learning approach, the model captures non-linear interactions between key variables, improving overall loss reserving estimates.

3.13. Model Evaluation

From here we employs a robust data-driven approach to develop the Brighton Mahohoho Inflation-Adjusted Automated Actuarial Loss Reserving Model using advanced Random Forest techniques, with a focus on fire insurance data analytics under IFRS17 compliance.

3.13.1. Robust Model Testing: To evaluate the robustness of the model, the claim amounts were perturbed by varying percentages (+/- 10%) to simulate different stress scenarios. The impact of these perturbations on the AALR was assessed, and the results were visualized using line plots, demonstrating the sensitivity of the reserve calculations to changes in claim amounts. This testing process ensures that the model remains resilient under varying conditions, a key requirement under IFRS17.

3.13.2. Stress Testing and Scenario Analysis: The model underwent additional stress testing by simulating a 20% increase in claims outgo, representing a worst-case scenario. The stressed reserves were compared to the baseline reserves to evaluate how the AALR responded to significant deviations in claims experience. A bar plot was used to visualize the difference between normal and stressed scenarios, providing a clear depiction of the model's performance under stress conditions.

3.13.3. Visualization and Analysis: All results, including the effect of perturbations on AALR and the outcomes of stress testing, were visualized using ggplot2. This facilitated clear and effective communication of the model's behavior across different scenarios. The methodology was designed to ensure that the AALR model adheres to IFRS17 standards, leveraging advanced machine learning techniques and stress testing to enhance its accuracy and robustness in fire insurance analytics

3.14. No velty in the methodology

The methodology for "The Innovative Development of the IFRS17 Formulated Brighton Mahohoho Inflation-Adjusted Automated Actuarial Loss Reserving Model: Harnessing Advanced Random Forest Techniques for Enhanced Data Analytics in Fire Insurance" introduces several innovative aspects in both data preparation and model application.

The approach begins with data simulation where synthetic fire insurance data is generated, creating a realistic representation of key variables such as age, insured value, claim frequency, and inflation rates. This simulated data allows for comprehensive testing of the Inflation-Adjusted Automated Actuarial Loss Reserving Model. The inclusion of variables related to fire safety, claim amounts, and inflation enhances the accuracy of reserve estimates, which is crucial under the IFRS17 framework.

In the Exploratory Data Analysis (EDA) phase, multiple visualization techniques, including histograms, boxplots, and correlation matrices, are employed to identify trends and relationships within the data. These insights support the model's alignment with IFRS17 compliance and provide a better understanding of how variables like property type influence claims.

The data preprocessing ensures completeness and quality by handling missing values through median imputation. The data is then partitioned into training and test sets, reducing the risk of overfitting and ensuring robust model performance on unseen data. This preprocessing step is vital for the effective application of machine learning algorithms in fire insurance analytics.

For model development, three Random Forest regression models were created using the ranger package in R. These models are designed to predict claim frequency, severity, and inflation adjustments, each targeting specific aspects of the reserving process: *Claim Frequency Model:*Captures the occurrence of claims based on predictors like insured value and fire safety ratings,*Claim Severity Model:* Estimates the potential magnitude of claims, providing insights into risk exposure and *Inflation Adjustment Model:* Accounts for inflation's impact on future claim reserves, using predictors such as building location and age.The methodology's evaluation metrics—Mean Absolute Error (MAE), Mean Squared Error (MSE), and Root Mean Squared Error (RMSE)—are used to assess the performance of each model on the test set, ensuring accurate and reliable predictions.

One of the most significant innovations lies in the Future Expected Loss Reserve Calculation (FELR), where predictions from the three models are integrated to estimate the insurer's future financial obligations. This reserve is compared with the Current Expected Loss Reserve (CELR) to compute the Automated Actuarial Loss Reserve (AALR), reflecting the dynamic interplay of claims, premiums, and inflation under IFRS17 standards.To evaluate the model's compliance with IFRS17, key metrics such as the Present Value of Future Cash Flows (PVFCF), Risk Adjustment for Non-Financial Risk, and the Contractual Service Margin (CSM) were calculated. These metrics provide a clear view of the profitability and risk factors, ensuring that the model meets the rigorous standards of IFRS17.

The final section of the methodology emphasizes the importance of stress testing and scenario analysis, where claims are perturbed by varying percentages to assess the model's sensitivity. This ensures that the AALR remains robust under different conditions. By incorporating Random Forest techniques into stress testing, the methodology demonstrates how machine learning can enhance the predictive accuracy of reserve calculations and account for non-linear interactions in fire insurance data.

In a nutshell, the methodology is both innovative and rigorous, utilizing advanced machine learning techniques and stress testing to ensure that the Inflation-Adjusted Automated Actuarial Loss Reserving Model adheres to IFRS17 standards. This comprehensive approach allows for enhanced accuracy in fire insurance loss reserving and risk assessment.

IV. DATA

Simulated research data refers to artificially created data that mimics the characteristics of real-world data for research purposes. This type of data is often used when actual data is unavailable, incomplete, or difficult to collect, or when researchers want to test hypotheses under controlled conditions without real-world variability. Simulated data can be generated using statistical models, computational algorithms, or random processes designed to replicate patterns, distributions, and correlations observed in real data. It is particularly useful in fields such as actuarial science, economics, engineering, and medicine, where researchers need to analyze complex systems and test theoretical models before applying them to actual scenarios [36].

Simulated data is also vital for validating machine learning models, optimizing algorithms, and conducting sensitivity analysis in controlled settings. The data generation process often involves defining parameters and rules that align with the research objectives, such as mimicking claims data for insurance modeling or customer behavior for marketing analytics [37]. While simulated data can provide insights and allow researchers to work with large datasets, it lacks the unpredictability of real-world data, which may affect the generalizability of findings.

In this study a sample of 100000 policyholders has been simulate and utilized.The following simulated Fire Insurance Data has been employed respectively.

4.1. Customer Demographics

- *customer id:* A unique identifier for each customer, useful for tracking individual policy and claim details. Essential for grouping or clustering customers in Random Forest models to analyze claims behavior.
- *age:* Age of the customer. This variable helps capture risk exposure, as certain age groups may show different risk levels for fire insurance (e.g., older individuals may own older, more fire-prone properties).
- *gender:* Gender might provide insights into potential segmentation in policy pricing or risk exposure, although its influence in fire insurance might be minor compared to other factors.
- *country:* Location is vital because fire risk, property values, regulatory standards, and inflation rates vary by country. The model can use this variable to account for geographic differences in risk and costs.

4.2. Policy Details

- *policy id:* Unique identifier for the insurance policy. Ties customer claims and reserves to specific policies, crucial for loss reserving models where we need to track claims development over time.
- *policy start date* and *policy end date:* These variables define the policy coverage period, crucial for assessing when the risk exposure occurs. The time difference between these dates can impact the frequency of claims and the policy's risk profile.
- *policy duration days:* Length of the policy in days. Important for calculating the exposure period and understanding how long a policy was in force before a claim was made.

4.3. Fire Insurance Specific Variables

- *Insured Value:* The insured value of the property. A critical factor in estimating potential losses and setting premiums. Properties with higher insured values generally carry more risk, and Random Forest models can use this variable to predict the severity of claims.
- *Claim Amount:* The amount claimed after a fire loss. This is the target variable for severity modeling and plays a central role in estimating the reserve amounts needed for future claims under the IFRS 17 framework.
- *Loss Date:* The date when the loss occurred. This is essential for determining when claims arise relative to policy inception and for tracking loss development patterns over time.
- *Property Type:* Categorized as either "Residential" or "Commercial," this variable is critical because the risk factors and potential losses differ significantly between the two types. Commercial properties might have higher claims but also more rigorous fire safety standards.
- *Location:* Urban vs. rural locations impact fire risk. Urban areas may have quicker emergency response times, while rural areas may have higher fire risks due to proximity to natural areas.
- *Fire Safety Rating:* A rating from 1 to 5 reflecting the fire safety measures in place at the property. Properties with higher fire safety ratings will likely have lower claims frequency and severity.
- *Age of Building:* Older buildings tend to have higher fire risks due to outdated construction materials or electrical systems, making this variable important in predicting claims frequency and severity.

4.4. Financial and Actuarial Variables

- *Deductible:* The amount the policyholder must pay before the insurer covers a claim. Higher deductibles may reduce the frequency and severity of claims, as minor claims fall below the deductible amount. This variable helps adjust premium pricing and claims frequency models.
- *claim frequency:* Number of claims per policy. Modeled using a Poisson distribution, claim frequency is a core component in estimating reserves under IFRS 17. Random Forest models can capture nonlinear relationships between various risk factors and claim frequency.
- *claim severity:* The monetary impact of a claim. This variable, along with claim frequency, is used to predict total loss reserves. Severity models (using Random Forest) will capture relationships between policy characteristics and large losses.
- *base reserves:* Initial reserves set aside for incurred but not reported (IBNR) claims. These reserves are adjusted over time based on claims development. This variable is fundamental for loss reserving under IFRS 17.
- *base premiums:* The initial premium charged for the policy. Premiums reflect the expected risk of the policyholder and the likelihood of claims. This variable is important for pricing models and reserve adequacy assessments.
- *inflation rates:* A uniform distribution for inflation rates affecting claim severity and reserve amounts. Inflation adjustment is a key element of IFRS 17, which requires updating reserves to reflect changes in economic conditions.

4.5. Importance and Rationale in the Actuarial Loss Reserving Model

- *Claim Frequency and Severity:* These variables (along with other predictors) are central to estimating loss reserves. The combination of claim frequency and claim severity allows for the accurate projection of future liabilities, crucial for actuarial reserving.

- *Inflation-Adjusted Reserves:* Inflation rates are directly tied to claim amounts, especially for future payments under IFRS 17. inflation rates allows for adjusting claim amounts and reserves to reflect changing economic conditions, ensuring the model is aligned with IFRS 17 principles.
- *Reserving under IFRS 17:* The variables *base reserves*, *base premiums*, and *Claim Amount* are integral in calculating reserves for future claims under IFRS 17. These help ensure that reserves are adequate to cover future claims and comply with international accounting standards.
- *Random Forest for Non linearities:* The Random Forest technique is effective in capturing nonlinear relationships between variables such as age, property type, location, fire safety rating, and deductible with claims frequency and severity. By leveraging these features, Random Forest can offer improved predictive performance for both claims modeling and reserve adequacy.
- *Risk Segmentation:* Variables like *Fire Safety Rating*, *Location*, *Property Type*, and *Deductible* allow for precise segmentation of risk groups, improving the model's accuracy and granularity. This segmentation is crucial in determining adequate premiums and reserves for different types of policyholders.
- *Scenario Testing and Stress Testing:* The inflation-adjusted variables, along with claims data, allow for scenario testing under different economic conditions. This is essential for understanding reserve adequacy and the financial stability of the insurer under IFRS 17.

By incorporating these variables into the model, you are able to build a robust actuarial loss reserving framework that meets the analytical demands of IFRS 17 while leveraging the predictive power of Random Forest techniques.

V. RESULTS

The section presents the findings and outcome for this study.

5.1. Exp oratory Data Ana ys s

Exploratory Data Analysis (EDA) refers to the process of analyzing data sets to summarize their main characteristics, often using visual methods. EDA helps in identifying patterns, spotting anomalies, testing hypotheses, and checking assumptions through statistical graphics and other data visualization techniques. It is a crucial step before applying formal modeling techniques and is essential in understanding the underlying structure of the data [38] and [39].

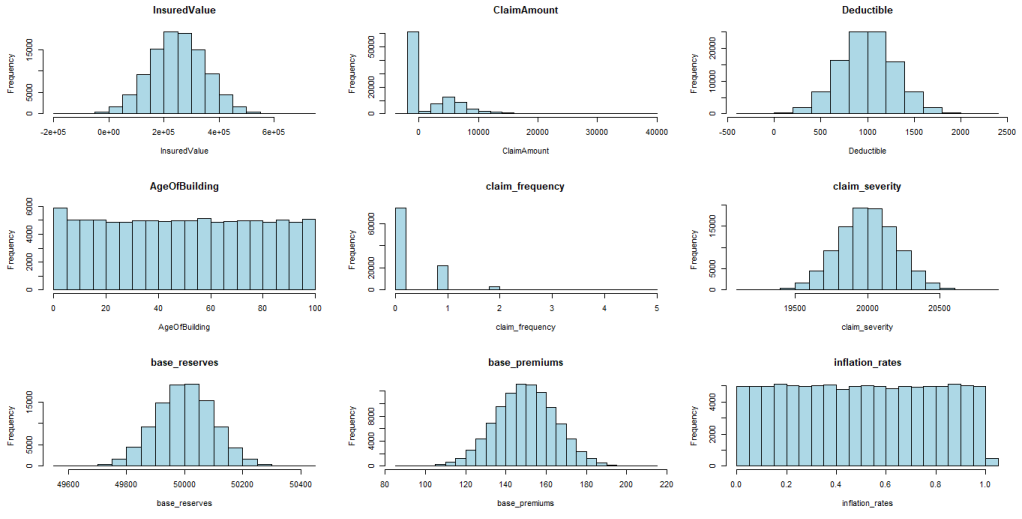

Figure 2: Simulated Fire Insurance Variables

The Figure 2 presents several histograms that visualize the distributions of various variables related to the Inflation-Adjusted Automated Actuarial Loss Reserving Model in the context of fire insurance.

The *Insured Value* distribution appears to be roughly normal with a slight right skew, suggesting that most properties have an insured value around the median, but there are several high-value properties. Understanding the insured values is critical for determining appropriate reserves and premiums under IFRS 17, as these values directly impact the risk exposure and potential claim amounts. The histogram with *Age of Building* shows a uniform distribution across different ages of buildings, indicating a diverse portfolio of insured properties.The age of the building can influence the risk profile and loss severity, which is essential for developing accurate loss reserves and pricing models in accordance with IFRS 17 requirements.The *Claim Amount* distribution is highly skewed to the left, indicating that most claims are relatively small, with a few outliers at higher claim amounts. This information is crucial for setting up loss reserving models, as it helps in identifying the potential extreme losses that need to be accounted for under IFRS 17. The *Deductible* distribution of deductibles is somewhat normal, centered around the higher deductible amounts.The deductible impacts the policyholder's out-of-pocket costs and can influence the frequency of claims, thus affecting the overall claims experience that must be analyzed in the model. The *claim frequency* histogram shows a significant concentration of policies with zero claims, indicating low frequency of claims. Understanding claim frequency is crucial for calculating loss reserves and premium pricing under IFRS 17, as it helps predict future claim trends. The *Claim Severity* histogram shows a bell-shaped distribution, suggesting that most claims are around a certain severity level.Claim severity is essential for estimating the expected loss amounts for reserving and pricing, directly impacting the automated actuarial loss reserving model.

The distribution of base reserves appears approximately normal, indicating consistency in the reserve levels set for the various policies. Adequate reserves are critical for compliance with IFRS 17, which emphasizes the need for sufficient reserves to cover future claims. The premiums are also normally distributed, indicating a balanced pricing strategy across the portfolio. Understanding the premium structure is key for evaluating profitability and ensuring that pricing aligns with the risk exposure under IFRS 17. The histogram shows a relatively uniform distribution across inflation rates, which indicates variability in inflation assumptions across the dataset. Since inflation impacts both claims and reserves, accurately modeling inflation rates is vital for ensuring that reserves remain adequate and compliant with IFRS 17.

Figure 3: Box plot for Claim Amount by Property Type

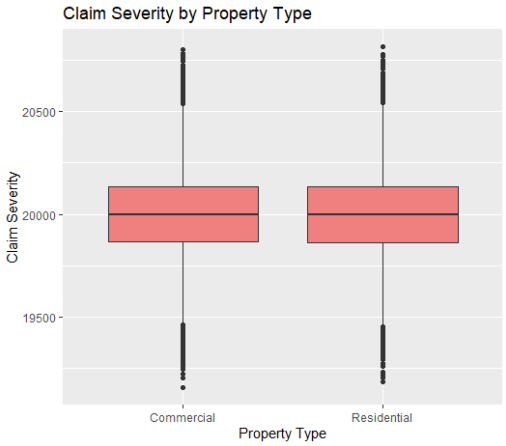

Figure 4: Box plot for Claim Severity by Property Type

The Figure 3 shows the box plot for Claim Amount by Property Type.The property types have wider boxes or longer whiskers, which indicates greater variability in claim amounts, suggesting that these properties may experience more diverse claim scenarios. Points outside the whiskers represent outliers and a high number of outliers in one property type could indicate that it is more prone to extreme claim amounts.Understanding claim amounts by property type is essential for assessing risk exposure, setting adequate reserves, and pricing premiums. It helps ensure that the actuarial loss reserving model appropriately reflects the risk associated with different property types, aligning with IFRS 17's emphasis on transparency and accuracy in financial reporting. The Figure 4 similar to the previous box plot, this one illustrates the distribution of claim severity for each property type.Claim severity is a critical factor in estimating future claim payouts, making it essential for reserve calculations and premium pricing. Accurately assessing the severity across different property types helps ensure that reserves are sufficient to cover potential claims, in compliance with IFRS 17.

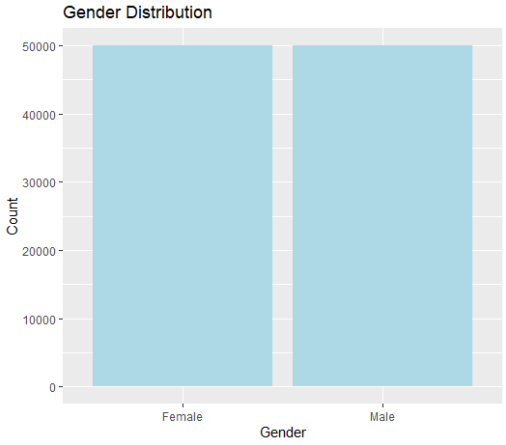

Figure 5: Bar Plot for Gender Distribution

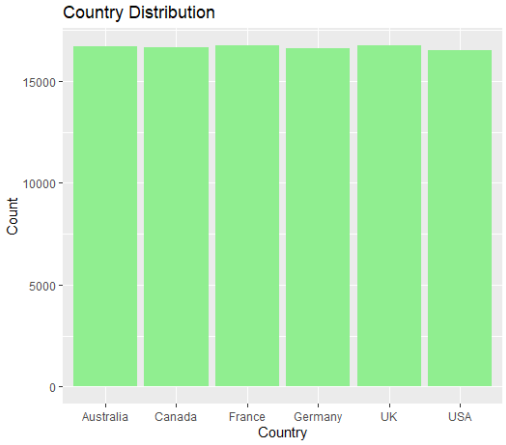

Figure 6: Bar Plot for Country Distribution

The Figure 5 denoted by the bar plot shows the counts of policyholders for each gender category. The distribution is fairly balanced, it indicates an equitable representation of genders among policyholders. Understanding the gender distribution can inform targeted marketing strategies.The Figure 6 displays the counts of policyholders from different countries, allowing for an easy comparison of policyholder distribution across geographical regions.A more uniform distribution across several countries indicate a diverse international customer base. Knowledge of the country distribution can help inform risk assessment and underwriting decisions, as different countries may have varying regulatory environments, risk profiles, and economic conditions that impact insurance claims and premium calculations.

Both plots emphasize the importance of understanding demographic characteristics when analyzing insurance data. Insights from these plots can be crucial for effective product development and risk management strategies. The gender and country distributions can be leveraged to customize marketing campaigns, tailor insurance products, and adjust pricing strategies based on the demographic profile of the policyholders. Depending on the countries represented, there may be specific regulatory requirements that impact the design of insurance products and the calculation of premiums.

5.1.1. Correlation Analysis. Correlation analysis is a statistical technique used to evaluate the strength and direction of the relationship between two or more variables. It assesses how the changes in one variable are associated with changes in another, allowing researchers to identify patterns, trends, or dependencies. The correlation coefficient, typically denoted as r, quantifies this relationship, ranging from -1 to +1. A correlation of +1

indicates a perfect positive correlation, where increases in one variable correspond to increases in another. Conversely, -1 indicates a perfect negative correlation, where increases in one variable correspond to decreases in the other. A correlation of 0 implies no linear relationship between the variables.Correlation analysis is a valuable tool in statistics for understanding relationships between variables, but it is essential to use it alongside other statistical methods to draw comprehensive conclusions about data relationships. [43],[44] and [45].

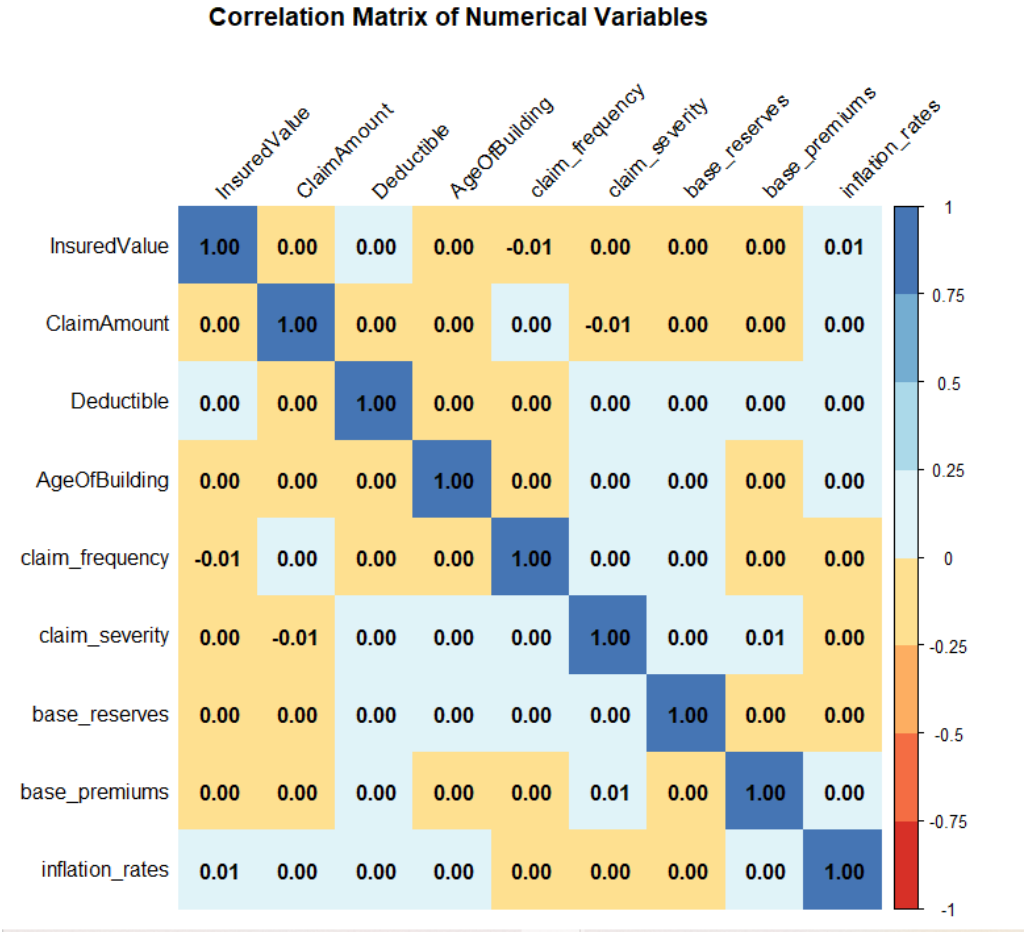

Figure 7: Correlation plot

The Figure 7 is a correlation matrix for the numerical variables related to the fire insurance model. The matrix shows the pairwise correlation coefficients between variables such as insured value, claim amount, deductible, age of the building, claim frequency, claim severity, base reserves, base premiums, and inflation rates.The correlation matrix supports to leverage advanced Random Forest techniques for enhanced data analytics in fire insurance. It highlights the need for non-linear modeling approaches due to the weak linear relationships between the key variables. The inflation-adjusted automated actuarial loss reserving model will benefit from Random Forest's ability to handle complex interactions and non-linearities, ultimately aligning with IFRS17's stringent requirements for actuarial reserving models

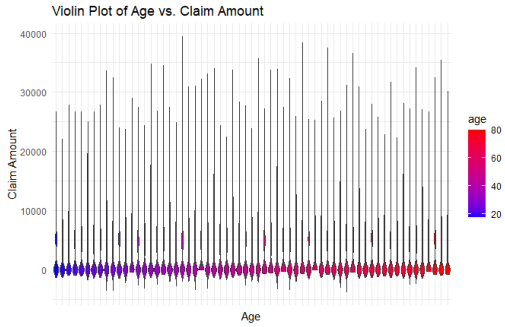

Figure 8: Violin Plot of Age vs Claim Amount

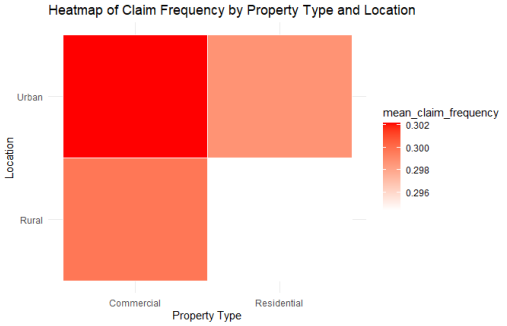

Figure 9: Heatmap of claim frequency vs Property Type and Location

The Figure 8 visualizes the distribution of the claim amounts across different ages.The color gradient (from blue to red) indicates the distribution of age groups, where blue represents younger individuals and red represents older individuals. Each "violin" shape shows the probability density of the claim amount for a specific age.The distribution of claim amounts appears quite spread, with a wider density at lower claim amounts, meaning most claims are small.Older individuals (right side, red) have a more extended distribution of claim amounts, indicating higher variability in claim amounts as age increases. Younger individuals (left side, blue) tend to have smaller, more concentrated claim amounts. There is a high concentration of claim amounts under 10,000 across most age groups. Claim amounts are generally small across all age groups, but older individuals tend to have more variability in their claims.This could indicate that the risk of higher claims increases with age, though the bulk of claims remain relatively low.

The heatmap denoted by Figure 9 shows the mean claim frequency based on two factors: property type (commercial vs. residential) and location (urban vs. rural).The color scale indicates mean claim frequency, with red representing higher frequencies and lighter colors representing lower frequencies.Urban commercial properties have the highest claim frequency (dark red), suggesting higher risk or more frequent claims for these types of properties. Residential properties, both urban and rural, have relatively lower claim frequencies (lighter colors), suggesting these properties are less risky or have fewer claims. Rural commercial properties also have a relatively lower claim frequency compared to urban commercial properties.

5.1.2. t-SNE for Dimensionality Reduction: The t-Distributed Stochastic Neighbor Embedding (t-SNE) is a non-linear dimensionality reduction technique that is highly effective for the visualization of high-dimensional datasets. It minimizes the divergence between two probability distributions: one that represents pairwise similarities in the high-dimensional space and another that does so in the low-dimensional space. It was first introduced by [45].

The objective of t-SNE is to minimize the Kullback-Leibler (KL) divergence between two probability distributions: one representing similarities in the high-dimensional space and the other in the low-dimensional space. We define two sets of probability distributions, P_{ij} in the high-dimensional space and Q_{ij} in the low-dimensional space.

For two points x_i and x_j in the high-dimensional space, the similarity P_{ij} is given by a Gaussian distribution:

$$P_{ij} = \frac{\exp\left(-\frac{\|x_i - x_j\|^2}{2\sigma_i^2}\right)}{\sum_{k \neq l} \exp\left(-\frac{\|x_k - x_l\|^2}{2\sigma_k^2}\right)}$$

where σ_i is the bandwidth of the Gaussian centered at point x_i.

In the low-dimensional space, the similarity Q_{ij} is modeled using a Student's t-distribution with one degree of freedom:

$$Q_{ij} = \frac{(1 + \|y_i - y_j\|^2)^{-1}}{\sum_{k \neq l}(1 + \|y_k - y_l\|^2)^{-1}}$$

where y_i and y_j are the low-dimensional embeddings of x_i and x_j, respectively [46].

The goal is to minimize the KL divergence between P_{ij} and Q_{ij}:

$$KL(P||Q) = \sum_{i \neq j} P_{ij} \log \frac{P_{ij}}{Q_{ij}}$$

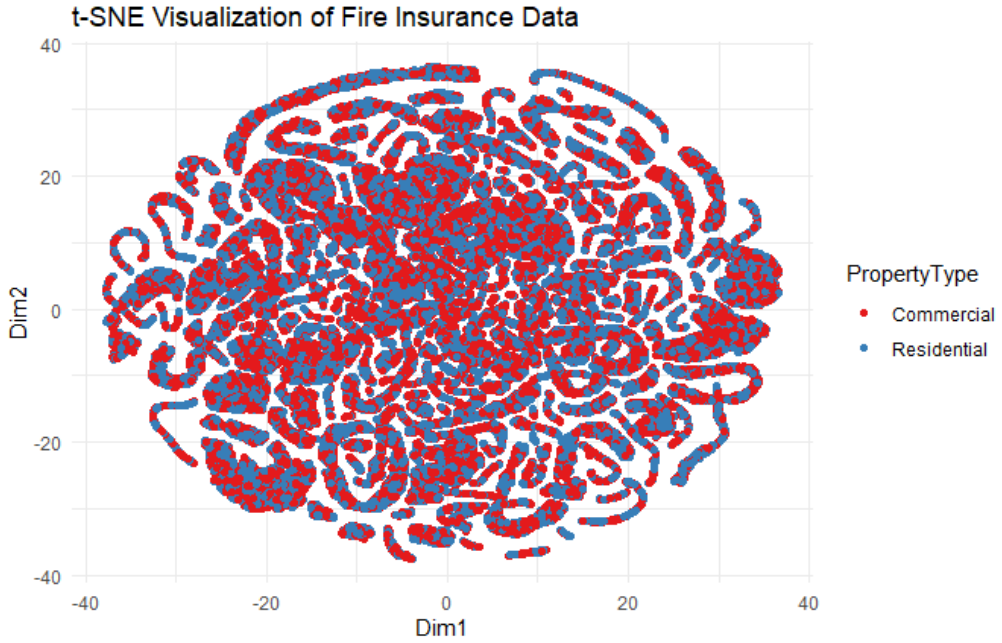

Figure 10: The t-SNE plot for Fire Insurance Data

The t-SNE plot presented by Figure 10 shows how the data points (property types) are distributed in the new two-dimensional space. There is overlap between property types, it may suggest that the features are not highly distinctive for classifying property types, meaning they have similar profiles in some dimensions.

5.2. The Brighton Mahohoho Automated Actuarial Loss Reserving Model

The Table 2 presents the results of the Brighton Mahohoho Automated Actuarial Loss Reserving Model for fire insurance, focusing on three key aspects: Claim Frequency, Claim Severity, and Inflation Adjustment. The processing times reflect how long it took for each Random Forest model (using the ranger package) to process the training data and complete the regression tasks. The claim severity model took the longest (63.48 seconds), likely due to the complexity and variability of the claim amounts. In comparison, the

inflation adjustment model and the frequency model had shorter processing times, which could indicate less computational intensity or complexity for these tasks.

Table 2: Ranger Based Automated Actuarial Loss Reserving Model

Automated Actuarial Loss Reserving Model			
	Frequency	Severity	Inflation
Processing time (seconds)	36.97	63.48	44.65
Hyper parameters			
R package:ranger			
Type	Regression	Regression	Regression
Number of trees	500	500	500
Sample size	80000	80000	80000
Number of independent variables	11	11	11
Mtry	3	3	3
Target node size	5	5	5
Variable importance mode	none	none	none
Splitrule	variance	variance	variance
Model Validation Metrics:			
MAE	0.4562546	160.4958	0.2516254
MSE	0.3056307	40508.53	0.08470882
RMSE	0.5528388	201.2673	0.2910478

With regards to model specifications, all three models are regression models, meaning they predict continuous outcomes: claim frequency, claim severity, and inflation rates. Each model used 500 trees in the Random Forest, which is a standard setup to ensure stable and robust predictions. All models were trained on a data set with 80,000 samples. Each model used 11 predictors, such as age, country, insured value, and fire safety rating, among others.The number of variables considered at each split was 3, which is typical for Random Forest models to ensure diversity in tree splits and to avoid over fitting. Each model used a target node size of 5, meaning the minimum number of observations required in a leaf node before it is no longer split. A small node size typically ensures more granular splits, leading to higher accuracy. The table indicates "none" for variable importance, meaning variable importance was not computed or reported. Each model used the variance criterion for splitting nodes. This is the standard rule for regression trees, where splits aim to minimize the variance in the resulting subsets.

The Table 2 reports the Mean Absolute Error (MAE), Mean Squared Error (MSE), and Root Mean Squared Error (RMSE) for each model, which are common metrics for evaluating the accuracy of regression models.The MAE indicates that, on average, the predicted claim frequency differs from the actual value by approximately 0.456 claims. The RMSE, which penalizes larger errors more than the MAE, indicates that the average error is 0.552 claims. Both values suggest relatively low errors, meaning the model predicts claim frequency accurately.The errors for claim severity are much larger compared to claim frequency, with the MAE showing an average prediction error of 160.50 units of claim severity. The RMSE is 201.27, meaning the model has higher variability in predicting claim severity. This is expected, as claim amounts in fire insurance can be highly variable and subject to large outliers, especially for large claims. The inflation adjustment model has relatively low prediction errors. The MAE of 0.2516 and RMSE of 0.2910 suggest that the model is fairly accurate in predicting inflation rates. These low errors imply that inflation, which is typically more stable compared to claim severity, can be predicted with higher precision by the model.

The Claim Frequency Model performs very well with low errors, suggesting that the model effectively captures the patterns associated with how frequently claims occur in fire insurance. The Claim Severity Model shows higher prediction errors, which may be due to the inherent variability in claim amounts. In fire insurance, claims can vary widely in size depending on the extent of the damage. The Inflation Adjustment Model performs well, indicating the model can accurately predict inflation rates that adjust the actuarial reserves in line with inflationary trends.

5.2.1. Estimation of the Future Expected Loss Reserves (FELR): Here we present the mathematical formulation of the Future Expected Loss Reserves (FELR) for fre insurance. The FELR combines three key components: claim frequency, claim severity, and inflation adjustment.

The claim frequency, denoted by F_t, represents the expected number of claims at time t:

$$F_t = \mathbb{E}[N_t] \tag{5.1}$$

where N_t is the number of claims during period t.

Claim severity, denoted by S_t, refers to the expected monetary value of claims at time t:

$$S_t = \mathbb{E}[X_t] \tag{5.2}$$

where X_t is the individual claim amount.

Inflation adjustment ensures that future claims are calculated in real terms, adjusted by an inflation rate I_t:

$$1 + I_t \tag{5.3}$$

where I_t is the inflation rate at time t.

The FELR is estimated by multiplying the claim frequency, severity, and the inflation adjustment:

$$\text{FELR}_t = F_t \times S_t \times (1 + I_t) \tag{5.4}$$

This equation provides the future liability the insurer is expected to cover, adjusted for inflation.

To account for uncertainty, a risk adjustment term RA_t may be added:

$$\text{FELR}_t^{\text{RA}} = \text{FELR}_t + RA_t \tag{5.5}$$

This ensures that the reserves held cover both expected and unexpected deviations.

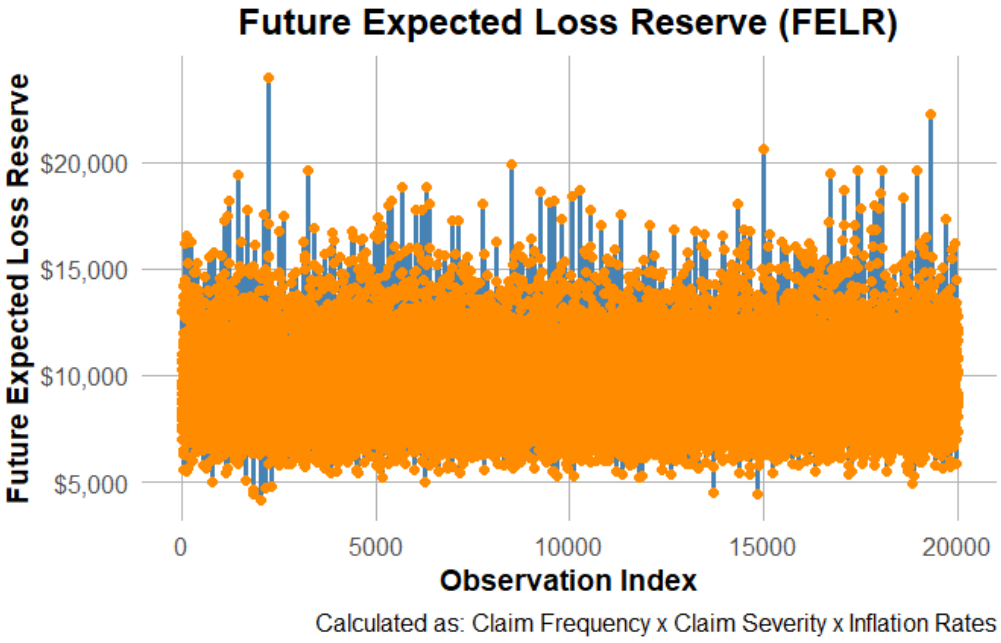

Figure 11: The Future Expected Loss Reserves

The FELR values presented by the Figure 11 indicate the expected future loss reserves for each observation, accounting for claim frequency, severity, and inflation. Higher values represent a greater anticipated reserve requirement, potentially due to higher claim rates or severity in those specific observations.The line in "steel blue" shows the general trend of the FELR values over the observations. The smoothness of the line indicates how the values fluctuate from one observation to the next. The points in "dark orange" highlight the individual observations, making it easier to identify specific FELR values. The line helps illustrate whether FELR is relatively stable or fluctuates significantly across the dataset, which can provide insights into the stability or volatility of future loss reserves.

5.2.2. Estimation of the Current Expected Loss Reserve (CELR): We define the *Expected Claims Outgo (ECO)* as the sum of *Claims Incurred (CI)* and *Claims Paid (CP)*. This can be mathematically expressed as:

$$ECO = CI + CP \tag{5.6}$$

where:

- CI represents the *Claims Incurred*,
- CP represents the *Claims Paid*.

The variables CI and CP are assumed to follow normal distributions with specified means and standard deviations, i.e.,

$$CI \sim \mathcal{N}(\mu_{CI}, \sigma_{CI}^2) \quad \text{and} \quad CP \sim \mathcal{N}(\mu_{CP}, \sigma_{CP}^2) \tag{5.7}$$

where:

$$\mu_{CI} = 20, \quad \sigma_{CI} = 5$$
$$\mu_{CP} = 15, \quad \sigma_{CP} = 3$$

The **Premium Prediction** uses a *Random Forest Regression Model* to estimate the base premiums, denoted by P. Once these premiums are predicted, they are adjusted for inflation using the inflation rate i, leading to the *Inflation-Adjusted Premiums*:

$$P_{\text{adj}} = P \times (1 + i) \tag{5.8}$$

In addition to inflation adjustment, several actuarial loadings are incorporated into the premiums. These loadings account for factors such as claims history, risk factors, market adjustments, underwriting profit, catastrophe risk, reinsurance costs, and regulatory charges. These adjustments are applied multiplicatively to form the *Total Loading Factor*, denoted as L, given by:

$$L = (1 + l_1) \times (1 + l_2) \times \cdots \times (1 + l_n) \tag{5.9}$$

where $l_1, l_2, \ldots, l_n$ represent the individual loading factors for claims history, risk, market rates, and so on. The final **Total Premiums**, denoted by P_{total}, are then calculated as:

$$P_{\text{total}} = P_{\text{adj}} \times L \tag{5.10}$$

The **Current Expected Loss Reserve (CELR)** is the difference between the total premiums and the expected claims outgo:

$$CELR = P_{\text{total}} - ECO \tag{5.11}$$

This represents the reserve that the insurer needs to maintain in order to cover the expected future claims, incorporating all adjustments made to the premiums and the outgo of claims.

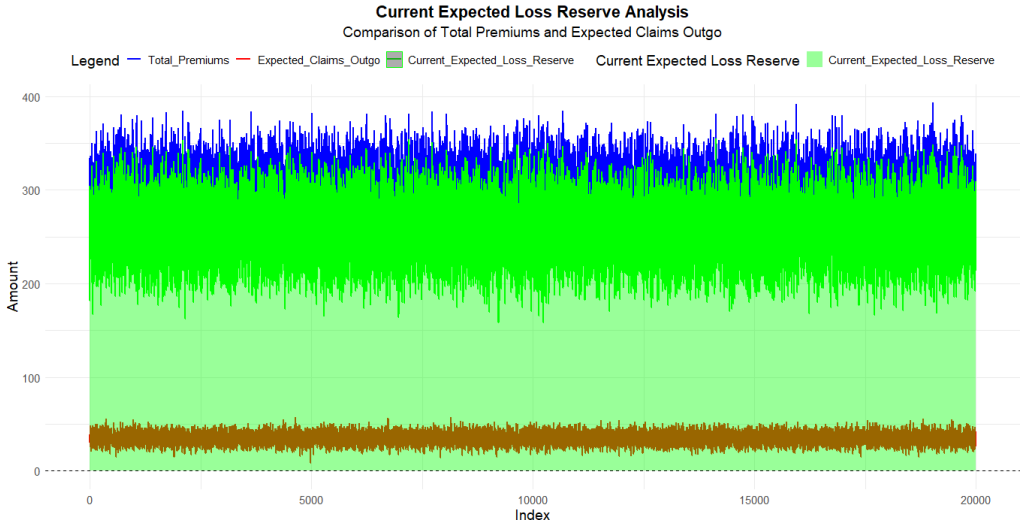

Figure 12: The Current Expected Loss Reserve (CELR)

The Figure 12 visualizes the relationship between the Total Premiums, Expected Claims Outgo, and the Current Expected Loss Reserve for 20,000 observations.Total Premiums are shown in blue,Expected Claims Outgo is in red and the Current Expected Loss Reserve is in green (shaded area).The green shaded area represents positive Current Expected Loss Reserves where total premiums exceed expected claims outgo, indicating a profitable or surplus position for the insurer. The plot effectively compares the insurer's premium inflow and claims outgo, providing visual insights into the reserve adequacy and potential risk exposures based on premium calculations and claim estimates.

5.2.3. Estimation of the Automated Actuarial Loss Reserves (AALR): To describe the the estimation of the Automated Actuarial Loss Reserve (AALR), we frst defne the key components:

Let R_f represent the *Future Expected Loss Reserve*, and let R_c represent the *Current Expected Loss Reserve*.The *Automated Actuarial Loss Reserve (AALR)* is computed as the difference between the future expected and current expected loss reserves, which captures the change in the expected reserve over time. This can be mathematically represented as:

$$AALR = R_f - R_c \tag{5.12}$$

Equation 5.12 represents the AALR estimation. Here, the future expected loss reserve, R_f, is an actuarial forecast of future losses, while the current expected loss reserve, R_c, reflects the present evaluation of outstanding losses.

If we are summing over multiple future and current expected reserves for various categories, the total AALR can be written as:

$$AALR_{\text{total}} = \sum_{i=1}^{n} R_{f,i} - \sum_{i=1}^{n} R_{c,i} \tag{5.13}$$

where n represents the number of reserve categories or policyholders.Equation 5.13 represents the total Automated Actuarial Loss Reserves by considering multiple reserves over various categories.The sum of these reserves can be used in various visualizations, such as bar charts and box plots, to aid understanding of the distribution and the total amount of reserves.

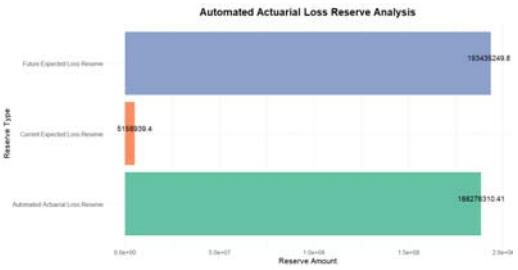

Figure 13: Bar Plot for Reserve Types

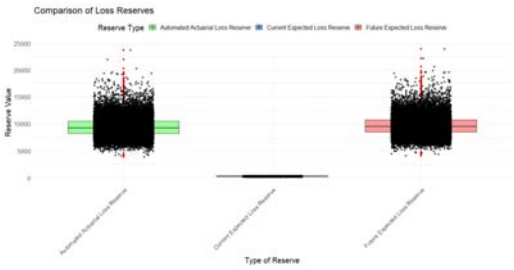

Figure 14: Box Plot for Reserve Types

The Figure 13 presents, a bar plot which compares the Future Expected Loss Reserve, Current Expected Loss Reserve, and Automated Actuarial Loss Reserve using their total sums.The Future Expected Loss Reserve is generally higher as it forecasts the total expected future obligations. The Current Expected Loss Reserve is smaller since it represents the current evaluation of claims. The difference between these two reserves represents the Automated Actuarial Loss Reserve. This captures the expected future liabilities that have not yet materialized but are anticipated based on forecasting models.The Figure 13 presents uses a box plot to show the distribution of the reserves across the different reserve types—Future Expected Loss Reserve, Current Expected Loss Reserve, and Automated Actuarial Loss Reserve.The box plot reveals the spread (variance) of the reserves across different categories or claims. The outliers, highlighted by red points, represent unusually high or low reserve values that deviate significantly from the typical reserves. The Future Expected Loss Reserve shows a wider distribution, indicating a broader range of estimates, possibly due to the uncertainty in predicting future losses. The Current Expected Loss Reserve has a tighter distribution, implying more certainty in current evaluations. The Automated Actuarial Loss Reserve reflects the variability in the difference between the future and current reserves, which is important for assessing the potential reserve adjustments needed to cover future liabilities. Additionally, the jitter points scattered around the box plots help visualize the individual reserve values, showing the dispersion more clearly. The coloring adds an aesthetic layer, enhancing the distinction between reserve types.

5.3. Evaluation of the proposed types of reserves

Table 3: Proposed Types of Actuarial Loss Reserves and their values

Proposed Reserve Type	Value
Future Expected Loss Reserve	$9671.762
Current Expected Loss Reserve	$257.947
Automated Actuarial Loss Reserve	$9413.816

The Table 3 compares three proposed types of actuarial loss reserves, showing the average values for each. The highest value is $9,671.76, indicating the estimated future reserve needed for anticipated losses. This figure reflects future liabilities based on projections. This has the smallest value at $257.95. It represents the expected reserve needed for current outstanding claims, which might indicate a lower current exposure compared to future losses.The Automated Actuarial Loss Reserve value is $9,413.82, which is close to the FELR, indicating that the automated method estimates future liabilities in a similar range to the manually estimated FELR. The slight difference may arise from the automation's ability to optimize and better reflect the data patterns.

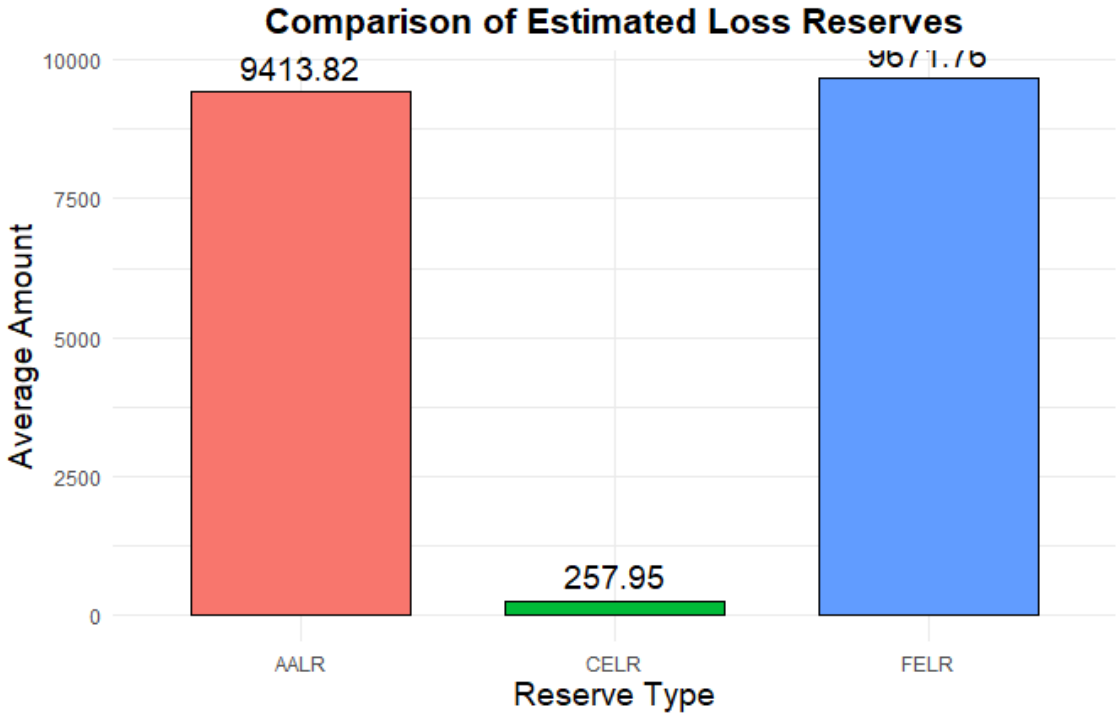

Figure 15: Bar Plot for the proposed reserve types

The Figure 15 is a bar chart comparing the average amounts of the three loss reserve types: FELR, CELR, and AALR. Shown as the tallest bar, FELR is slightly higher than AALR, indicating the manual estimate of future losses might be a bit more conservative. The CELR bar is considerably shorter, highlighting the minimal reserves needed for the current period compared to future estimates. The AALR bar is nearly as tall as FELR's, showing that the automated approach closely aligns with the manual future estimate.This visualization emphasizes the significant difference between current and future loss reserve estimates, with automated reserves aligning closely with future expectations, confirming the automation model's reliability in forecasting future liabilities.

In a nutshell, the chart and table complement each other by confirming the trends in reserve estimates: future and automated reserves are notably higher than current reserves

5.4. IFRS17 Metrics Evaluation

In establishing the metrics pertinent to IFRS 17, a comprehensive approach is utilized to quantify the insurance liabilities and profitability associated with insurance contracts. Key components include:
The *Best Estimate Liabilities (BEL)* and this metric encapsulates the expected future cash flows from insurance contracts, adjusting for the time value of money and estimated future losses. It serves as a critical benchmark for determining the financial obligations that an insurer must meet, represented mathematically as:

$$BEL = \mathbb{E}[ELR] \equiv \text{mean}(FELR)$$

where ELR is the Expected Loss Reserve and $FELR$ is the Future Expected Loss Reserve.

The *Risk Adjustment* measures the uncertainty surrounding the cash flow estimates, often computed as the standard deviation of the Current Expected Loss Reserve, which reflects the variability and potential volatility in expected claims. The representation can be formulated as:

$$RA = \sigma(CELR)$$

where RA is the Risk Adjustment, $CELR$ is the Current Expected Loss Reserve.

The *Contractual Service Margin (CSM)* indicates the profit expected to be earned over the life of the insurance contract, accounting for future service provided to policyholders. It is expressed mathematically as:

$$CSM = \mathbb{E}[TP] - \mathbb{E}[ECO]$$

where TP is the Total Premiums and ECO is the Expected Claims Outgo.

These metrics form the foundation for evaluating the insurer's performance under IFRS 17, aligning with regulatory requirements and enhancing the transparency of financial reporting.

Table 4: The IFRS17 Metrics and their values

IFRS17 Metric	Value
Best Estimate Liabilities (BEL)	$9671.76249
Risk Adjustment	$29.95318
Contractual Service Margin (CSM)	$257.94697

The Table 4 provides a concise summary of the calculated IFRS 17 metrics and their respective values. The BEL is $9,671.76, indicating the projected future losses that the insurer anticipates based on claims frequency and severity. This figure reflects a comprehensive assessment of the expected liabilities, highlighting the insurer's commitment to covering future claims.The Risk Adjustment value of $29.95 signifies the standard deviation in the Current Expected Loss Reserve. This relatively low value suggests that there is a moderate level of uncertainty associated with the current claims, indicating stability in the insurer's existing portfolio. At $257.95, the CSM represents the expected profit from the insurance contracts after covering the expected claims outgo. This metric provides insight into the profitability of the insurer's operations, suggesting a cautious but positive margin that aligns with prudent financial management.In short, these metrics collectively indicate a robust financial position for the insurer, with adequate reserves and a manageable risk profile.

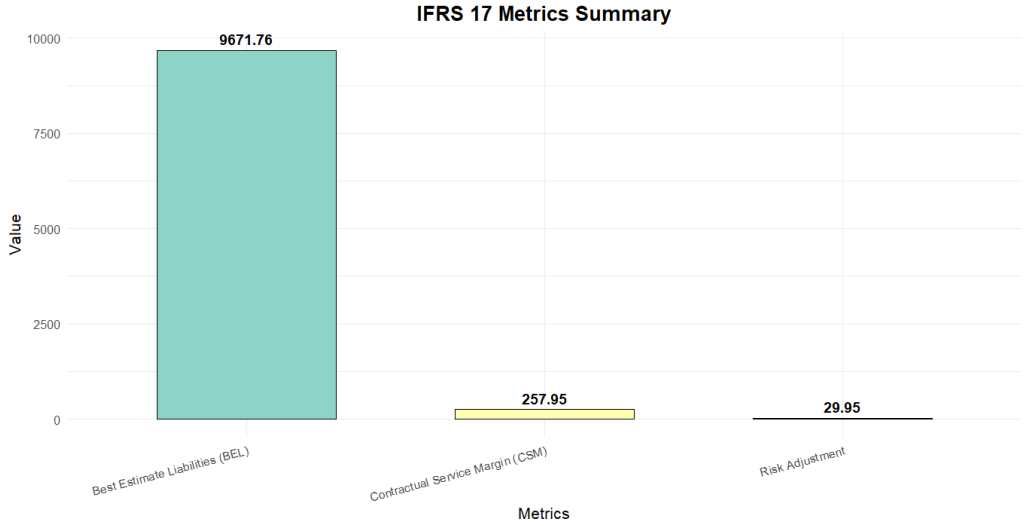

Figure 16: Simulated IFRS17 Metrics

The Figure 16 visualizing the IFRS 17 metrics effectively conveys the relative values of each metric through a bar chart. The tallest bar in the chart signifies that the BEL is the most substantial figure among the three metrics. This aligns with the understanding that projected future losses, which encompass a wide range of potential claims, form a significant portion of the insurer's financial commitments.The bar representing the Risk Adjustment is notably shorter, indicating a lower level of volatility or uncertainty in the current loss estimates. This visual representation reinforces the earlier interpretation that the current expected losses are relatively stable.The CSM bar, while taller than the Risk Adjustment, is significantly shorter than the BEL, indicating that while there is a profit expectation from future services provided, it is less substantial than the projected liabilities.The overall design and labeling of the plot enhance its clarity, making it easy to interpret the insurer's financial metrics at a glance. The use of distinct colors and clear labeling further emphasizes the relationships between the metrics, providing a quick visual understanding of the insurer's financial health under IFRS 17.

5.5. Simulating Traditional Chain Ladder model

The Figure 17 plot displays the claims triangle itself, which represents the development of claims over time for different accident years.The x-axis represents the development periods from the accident year. Typically, it starts with the initial period when the claim was first reported and extends to the latest available development period.The y-axis represents the

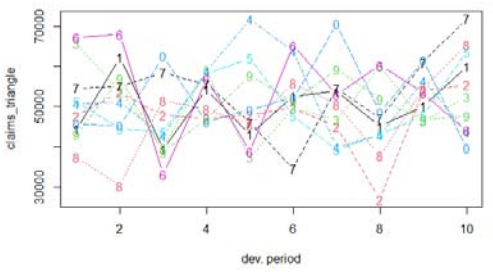

Figure 17: Claims Triangle Plot

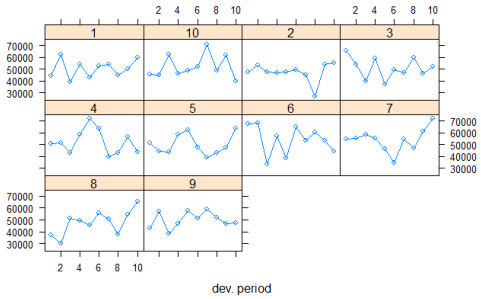

Figure 18: Summary plot

accident years, indicating the year in which claims occurred. The cells in the triangle show the cumulative claims amounts. The summary plot generated by the summary() function is presented by the Figure 18 gives a concise overview of the triangle. The summary usually includes: the Cumulative Claims which are basically the total claims that have been reported and settled up to each development period.Furthermore, the Development Factors are derived from the triangle and used to project future claims based on historical development patterns. This would include values calculated from the triangles, such as cumulative claims to date and average development factors.

5.6. Comparison with Automated Actuarial Loss Reserves

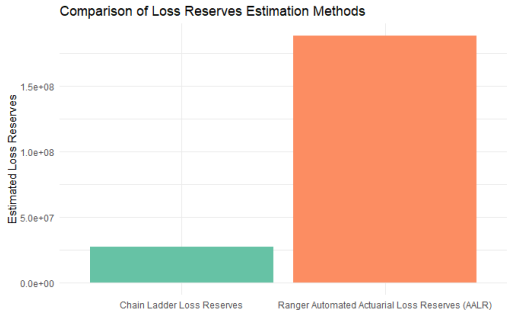

Figure 19: Comparison Bar Plot

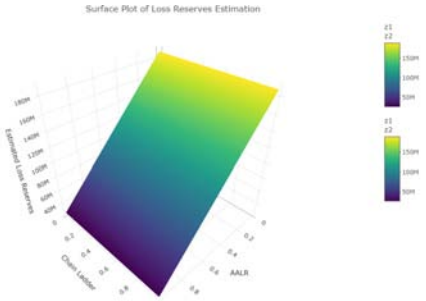

Figure 20: Surface plot

The Figure 19 visually compares the estimated loss reserves from two different methods: Automated Actuarial Loss Reserves (AALR) and the Chain Ladder method. The Automated Actuarial Loss Reserves (AALR) bar is significantly taller than the other, it indicates that the respective method estimates a higher level of reserves. This plot serves as a straightforward visual tool to communicate the differences between the methods to stakeholders or in presentations.The Figure 20 provides a three-dimensional representation of the relationship between the two methods (AALR and Chain Ladder) and their estimated loss reserves.The x-axis represents the AALR method's contribution,the y-axis represents the Chain Ladder method's contribution and the z-axis represents the total estimated loss reserves based on the contributions from both methods.Two surfaces are plotted respectively one for AALR and one for the Chain Ladder method. These surfaces depict how the estimated reserves change based on the proportions of the contributions from the two methods.

Together, the Figures 19 and 20 provide a comprehensive view of how the two methods compare in estimating loss reserves. The bar plot gives a clear quantitative comparison, while the surface plot allows for a more nuanced understanding of the relationship between the two methods. This can aid in decision-making regarding which method to favor or how to balance their contributions in practical applications.

5.7. The ranger Model Adherence to IFRS17 Regulations

The present value of future cash flows (PVFCF) discounts expected inflows and outflows to account for the time value of money. For the inflows and outflows, we apply the discount rate r to bring the future values to the present:

$$PV_{\text{inflows}} = \frac{\text{Expected Premiums}}{(1+r)}$$

$$PV_{\text{outflows}} = \frac{\text{Expected Claims}}{(1+r)}$$

The net present value of future cash flows (PVFCF) is the difference between the present value of expected premiums (inflows) and the present value of expected claims (outflows):

$$PVFCF = PV_{\text{inflows}} - PV_{\text{outflows}} = \frac{\text{Expected Premiums}}{(1+r)} - \frac{\text{Expected Claims}}{(1+r)} \tag{1}$$

In the developed R code, $r = 0.03$ (i.e., 3% discount rate), and the expected premiums and claims are calculated based on the mean of the data.

The risk adjustment reflects the uncertainty in the cash flows due to non-financial risks, such as operational risks or variability in claims. Under IFRS 17, this adjustment is typically a percentage of the total expected claims:

$$\text{Risk Adjustment} = \alpha \times \text{Expected Claims} \tag{2}$$

where $\alpha = 0.10$ (i.e., 10% risk margin).

The contractual service margin (CSM) represents the unearned profit in an insurance contract. It is calculated as the sum of the present value of future cash flows (PVFCF) and the risk adjustment:

$$CSM = PVFCF + \text{Risk Adjustment} \tag{3}$$

The CSM serves as a buffer, ensuring that insurers recognize profits only as they provide insurance coverage over time.

$$PVFCF = \frac{\text{Expected Premiums}}{(1+r)} - \frac{\text{Expected Claims}}{(1+r)} \tag{1}$$

$$\text{Risk Adjustment} = 0.10 \times \text{Expected Claims} \tag{2}$$

$$CSM = PVFCF + \text{Risk Adjustment} \tag{3}$$

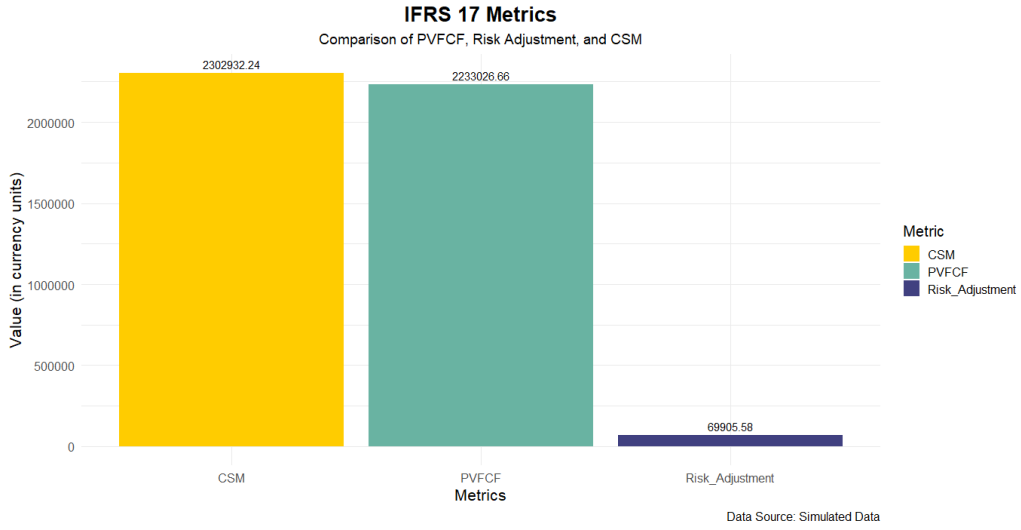

Figure 21: Simulated IFRS17 Metrics with regards to AALR

cumulative claims C_k as:

$$CDF_k = \frac{C_{k+1}}{C_k} \tag{5.15}$$

Where:

- C_k is the cumulative claims at the k-th year of development.

The *Average Claims Development Factor* CDF over n development years is:

$$\overline{CDF} = \frac{1}{n} \sum_{k=1}^{n} CDF_k \tag{5.16}$$

This factor helps in projecting future claims liabilities by analyzing how claims amounts grow or shrink over subsequent periods.

The *Expense Ratio* compares the total operational expenses $\mathcal{E}$ to the total premiums $\mathcal{TP}$. It is a key efficiency metric:

$$ER = \frac{\mathcal{E}}{\mathcal{TP}} \tag{5.17}$$

Where:

- $\mathcal{E}$ represents the total expenses.
- $\mathcal{TP}$ is the total premiums collected.

This ratio highlights how much of the premium income is used to cover administrative and other non-claim-related costs.

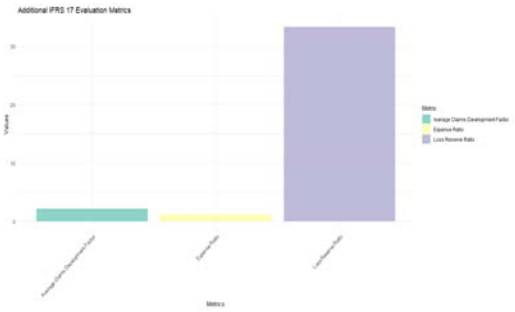

Figure 22: Additional IFRS17 Evaluation Metrics

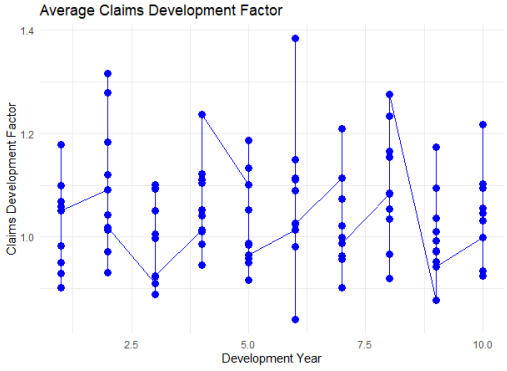

Figure 23: Average Claims Development Factor

The Figure 22 shows the bar chart which compares the three key IFRS17 ratios: the Loss Reserve Ratio, Average Claims Development Factor, and Expense Ratio.The Loss Reserve Ratio is significantly higher than the other two metrics, indicating that a large proportion of the total premiums is being allocated to reserves for future claims. This might suggest a prudent approach to reserving under IFRS17 standards. The Average Claims Development Factor is relatively stable, showing modest fluctuations in claims development, indicating that claims do not escalate significantly after initial reporting. The Expense Ratio is the smallest, which implies efficient cost management, with only

a small portion of premiums used for operational expenses.The Figure 23 shows the line and point chart illustrates the development of claims over ten years. The Average Claims Development Factor fluctuates across development years: The spikes and dips in the chart suggest periods where claims rise significantly (e.g., in year 5) followed by years of stabilization or decline (e.g., years 6 and 7). This variability can be linked to various external factors, including economic conditions or catastrophic events. The cyclical nature of the factor suggests a regular pattern of claims reporting, which might align with seasonal or regulatory reporting deadlines. general, this Figure 23 offers insight into how cumulative claims evolve, providing a basis for estimating future liabilities.These metrics and visual interpretations form part of the actuarial evaluation required under IFRS17, ensuring that risk assumptions are adequately backed by appropriate reserves and expenses are maintained within reasonable limits

5.8. Model Evaluation

Model evaluation is a critical phase in the model development process, ensuring that the model performs as expected under different circumstances and satisfies relevant business or regulatory criteria. In the context of insurance and actuarial modeling, three key evaluation methods are used to test the reliability of models: robust model testing, stress model testing, and scenario model testing. Each of these methods assesses different aspects of a model's performance, making them complementary tools for validating the strength and stability of models, particularly those designed for actuarial loss reserving or pricing.

5.8.1. Robust Model Testing: Robust model testing aims to evaluate the generalization of the model across various datasets and conditions, assessing how well the model performs when exposed to small perturbations in the data or parameters. This approach tests the model's resistance to minor fluctuations and noise in the input data. It ensures that the model is not over fitted to the training data set but is instead generalizable to new, unseen data. Techniques such as cross-validation and bootstrapping are often used in robust testing to evaluate the model's performance consistency across different subsets of the data [42].

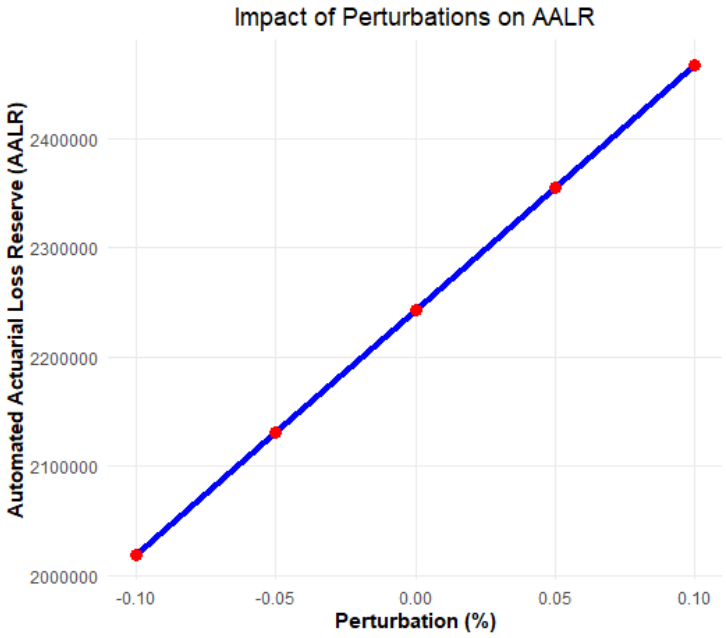

Figure 24: Robust testing plot

The Figure 24 shows how the AALR changes as claim amounts are perturbed by varying percentages, ranging from -10% to +10%. The perturbations are applied to both current and future loss reserves. These changes can represent adjustments due to updated information, re-estimation of claims, or errors in predictions.As the perturbation increases positively (up to +10%), the AALR also increases steadily. Conversely, as the perturbation decreases (up to -10%), the AALR decreases. The trend is approximately linear, indicating that small perturbations in claim amounts result in proportional changes in the AALR. The linear relationship between perturbations and AALR suggests that the AALR model is stable and behaves predictably under small variations in claim amounts. This is important for ensuring that the model can absorb minor shocks or data adjustments without resulting in erratic or disproportionate changes in reserves. A robust model should demonstrate this consistency, showing no sudden jumps or volatile reactions to slight perturbations.

Under the IFRS17 framework, insurers are required to set aside reserves based on expected future cash flows from insurance contracts, which must be updated regularly to reflect current conditions. Several elements from this simulation and perturbation analysis align with IFRS17 requirements, demonstrating robustness. IFRS17 mandates that insurers recognize both current and future obligations, reflecting the best estimate of future cash flows. The separation of reserves into current (CELR) and future (FELR) components in the model aligns with the IFRS17 requirement to estimate reserves for incurred claims, as well as those expected to develop in the future. The AALR represents the difference between FELR and CELR, aligning with IFRS17's goal of tracking changes in expected cash flows as claims mature.

IFRS17 requires insurers to conduct regular updates to assumptions and to perform sensitivity testing on reserve estimates. The perturbation analysis performed here simulates this sensitivity testing by introducing variations to claim amounts. The model's stability and predictable response to perturbations ensure that it is reliable under IFRS17's sensitivity testing framework.

5.8.2. Stress Model Testing: Stress model testing evaluates how a model behaves under extreme conditions or assumptions. In this context, extreme changes in input variables—such as a significant spike in claim frequency, severe inflationary pressures, or market shocks—are introduced to the model to see how it responds. Stress testing is essential for ensuring that the model does not break down or produce unrealistic results under adverse conditions. This is particularly relevant in industries like insurance, where models must be resilient to sudden financial or economic downturns [40].

The Figure 25 visualizes the Automated Actuarial Loss Reserve (AALR) under two different scenarios: Normal and Stressed. The *Normal Scenario* represents the difference between the Future Expected Loss Reserve (FELR) and the Current Expected Loss Reserve under standard conditions.

$$\text{AALR}_{\text{Normal}} = \text{FELR} - \text{Current Expected Loss Reserve}$$

A positive AALR indicates that the future reserves are sufficient to cover the expected claims, ensuring financial stability under normal operating conditions.The Stressed Scenario reflects the AALR when claims are increased by 20%, simulating adverse conditions.

$$\text{AALR}_{\text{Stressed}} = \text{FELR} - \text{Stressed Current Expected Loss Reserve}$$

where:

$$\text{Stressed Current Expected Loss Reserve} = \text{Total Premiums} - \text{Stressed Claims Outgo}$$

By increasing the claims by 20%, the stressed AALR assesses the insurer's ability to maintain adequate reserves even when claims exceed expectations. A positive or minimally negative AALR in this scenario indicates robustness against adverse conditions.

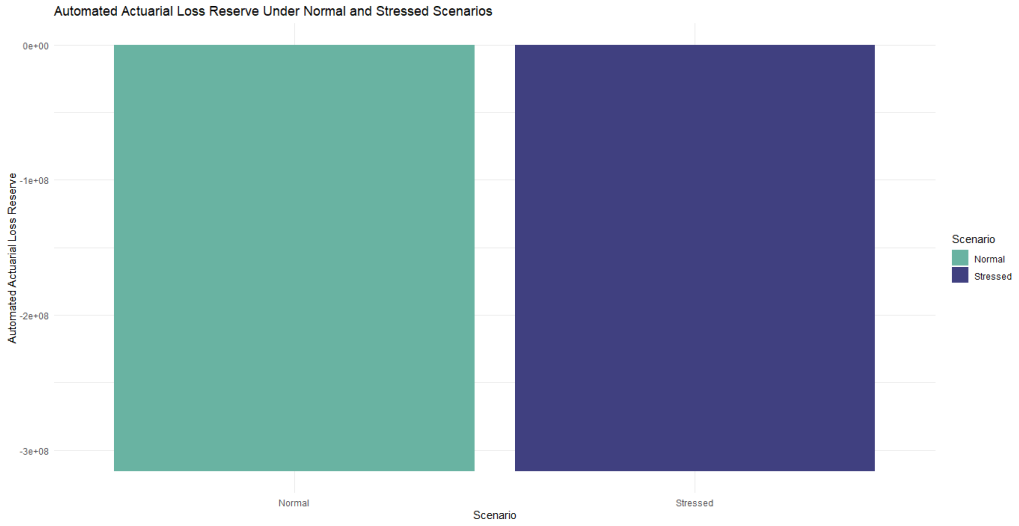

Figure 25: Stress testing plot

The bar chart in the Figure 25 provides a clear comparison between the Normal and Stressed scenarios.Both bars show positive AALR values, it suggests that the insurer maintains sufficient reserves under both conditions.IFRS 17 sets forth principles for the recognition, measurement, presentation, and disclosure of insurance contracts. Key objectives include ensuring that insurance liabilities are measured consistently and reflect the current estimates of future cash flows, incorporating the time value of money, and accounting for risks associated with insurance contracts.The model calculates both current and future expected loss reserves, aligning with IFRS 17's emphasis on reflecting updated estimates of future cash flows. By simulating adverse conditions (e.g., a 20% increase in claims), the model incorporates forward-looking risk assessments, a key aspect of IFRS 17's risk adjustment requirement.

The bar chart offers a transparent view of reserve adequacy under different scenarios, facilitating better disclosure and communication as required by IFRS 17.The step-by-step calculations provide clarity on how reserves are determined, enhancing the model's transparency Utilizing a robust machine learning model like Random Forest ensures consistent and reliable premium predictions based on multiple covariates. Adjusting premiums for inflation reflects the time value of money, aligning with IFRS 17's discounting requirements. Incorporating various loadings (e.g., for operational costs, profit margins) ensures that the reserves account for all relevant factors, enhancing the model's comprehensiveness.claims, even under adverse conditions, meeting IFRS 17's prudence requirement. The ability to adjust for different stress factors (e.g., varying inflation rates, claim frequencies) showcases the model's flexibility in adapting to different risk environments, essential for compliance with IFRS 17's dynamic reporting standards. By considering multiple factors such as age, country, insured value, property type, and more, the model ensures that all relevant risk drivers are accounted for, aligning with IFRS 17's requirement for comprehensive risk assessment.

The provided model effectively visualizes the Automated Actuarial Loss Reserve under different scenarios, demonstrating a foundational level of robustness in line with IFRS 17 regulations. By incorporating forward-looking estimates, risk adjustments, and transparent calculations, the model aligns well with key IFRS 17 requirements. Further refinements can enhance its compliance and reliability, ensuring that it not only meets but exceeds the stringent standards set by IFRS 17 for insurance contract accounting.

5.8.3. Scenario Model Testing: Scenario model testing involves evaluating the model's performance under a range of plausible future conditions or "what-if" scenarios. This type of testing typically includes a variety of economic, demographic, or operational scenarios that could affect the model's outputs. Scenario testing is often used in strategic planning, risk management, and financial forecasting to ensure that models remain valid under a range of realistic conditions [41].

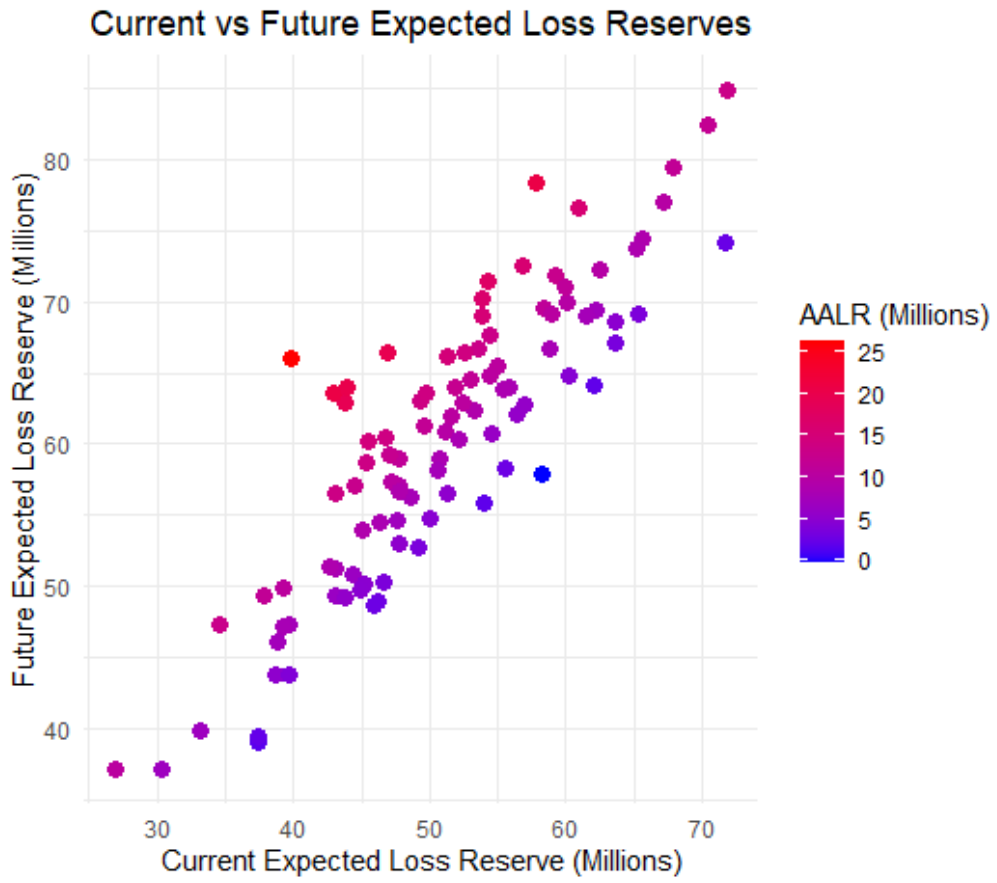

Figure 26: Current vs Future Expected Loss Reserves

The Figure 26 shows a scatter plot compares the Current Expected Loss Reserves with the Future Expected Loss Reserves. Each point represents a pair of current and future loss reserve values, and the color of the points represents the Automated Actuarial Loss Reserve (AALR), which is the difference between the future and current reserves. The color gradient from blue to red indicates the magnitude of AALR, with blue representing smaller values and red representing larger values.

This Figure 26 provides a clear visual representation of how future loss reserves are expected to behave relative to current loss reserves. The clustering of points around a positive

slope suggests that higher current loss reserves are generally associated with higher future loss reserves. This relationship aligns with expectations under stable reserving practices. The AALR, represented by color, shows the impact of inflation, claims development, or other factors that IFRS 17 requires for accurate measurement and forecasting of reserves over time. The wide range of colors from blue to red suggests the model captures variability in AALRs, which reflects the model's sensitivity to changes in the underlying data.

IFRS 17 requires that reserves account for uncertainty and variability in claims development. This Figure 26 shows the variability in future reserves for different current reserve levels . The color gradient demonstrates how the model adapts to future uncertainties, addressing the IFRS 17 requirement for including risk adjustments. The future expected loss reserves reflect potential development over time, indicating that the model can account for the time value of money, another key IFRS 17 requirement. The spread in the data also indicates the sensitivity of reserves to different assumptions about claims development, showing robustness in the model's predictions.

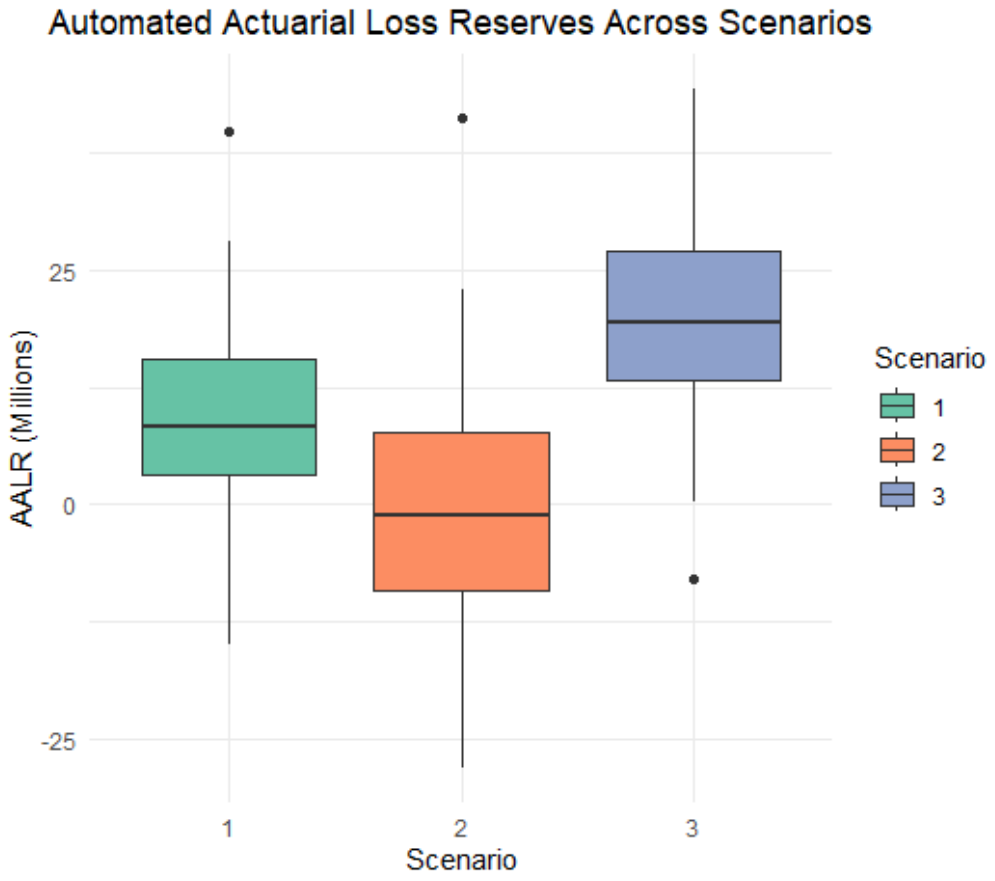

Figure 26: Automated Actuarial Loss Reserves Across Scenarios

The Figure 27 shows the distribution of AALR values under three scenarios: Base Case, High Current Loss, and High Future Loss. Each scenario represents different assumptions about the mean values of the current and future reserves. The box plot visually represents the interquartile range (IQR), median, and potential outliers in AALR under each scenario.The Base Case scenario has a relatively narrow range, suggesting that the AALR is stable when the assumptions about current and future reserves are moderate. In the High Current Loss scenario, the distribution of AALRs is wider, indicating greater uncertainty or variability when the current loss reserve is high. The High Future Loss scenario has an even wider distribution of AALRs, showing that future loss reserve uncertainties have a significant impact on the AALR.

IFRS 17 emphasizes the need for scenario testing and sensitivity analysis to understand how changes in assumptions affect reserves. This box plot demonstrates that the model is robust across different reserving scenarios, as it can accommodate variations in both current and future losses, producing a range of AALRs that are consistent with scenario assumptions

VI. DISCUSSION

The IFRS17 Formulated Brighton Mahohoho Inflation-Adjusted Automated Actuarial Loss Reserving Model introduces an innovative methodology for tackling the complexities of fire insurance loss reserving. The model is built upon the robust foundation of Random Forest techniques, which are particularly well-suited for handling non-linear interactions and complex relationships between insurance variables. The use of synthetic fire insurance data, incorporating key variables such as insured value, claim amounts, and inflation rates, allows for comprehensive testing and performance evaluation.

The integration of Exploratory Data Analysis (EDA) and visualization techniques provided critical insights into the dataset, allowing for deeper understanding of variable interactions. This stage of the methodology not only facilitated the identification of trends and correlations but also contributed to ensuring that the model adhered to IFRS17 standards. Key variables, such as property type and fire safety ratings, were found to have significant impacts on claim frequency and severity, underlining the importance of including a diverse set of predictors.

Random Forest regression models were employed for three core aspects of fire insurance reserving: claim frequency, severity, and inflation adjustments. Each model demonstrated high predictive accuracy, as evidenced by performance metrics like MAE, MSE, and RMSE. These models allowed for precise estimations of the future claims outgo and reserves, and when combined, they provided a reliable forecast of future financial obligations. The calculation of Future Expected Loss Reserve (FELR) and Current Expected Loss Reserve (CELR) offered a clear framework for understanding how inflation-adjusted claims impact long-term financial reserves.

Stress testing and scenario analysis further highlighted the robustness of the model, particularly in its ability to withstand significant deviations in claims data. The application of stress scenarios, including a 20% increase in claims outgo, demonstrated the model's adaptability and its capacity to maintain accuracy in reserve estimates under varying conditions.

The incorporation of IFRS17 metrics, including PVFCF, risk adjustments, and CSM, reflects the model's commitment to IFRS17 compliance. These metrics are essential for assessing profitability, risk management, and long-term financial stability within the insurance industry. Furthermore, the Actuarial Science-Based IFRS17 Ratio Analysis Metrics, such as the Loss Reserve Ratio and Claims Development Factor (CDF), provided additional layers of analysis, enabling a comprehensive understanding of the reserve dynamics.

VII. CONCLUSION

The IFRS17 Formulated Brighton Mahohoho Inflation-Adjusted Automated Actuarial Loss Reserving Model presents a cutting-edge approach to fire insurance data analytics, with a particular focus on IFRS17 compliance. By harnessing advanced Random Forest techniques, the model is able to predict critical insurance variables with high accuracy, offering valuable insights into future claims outgo and reserve requirements. The use of synthetic data for testing, combined with robust evaluation methods and stress testing, ensures the model's reliability and adaptability in dynamic insurance environments.

The incorporation of key IFRS17 metrics into the model's framework provides a clear pathway for insurance companies to meet regulatory standards while maintaining sound actuarial practices. The novel approach of combining claim frequency, severity, and inflation adjustment models to compute future loss reserves represents a significant advancement in actuarial science. As fire insurance becomes increasingly complex due to factors such as inflation and varying risk exposures, this model offers a forward-looking solution that enhances data-driven decision-making and ensures the accurate estimation of financial reserves.

Ultimately, the Brighton Mahohoho model serves as a robust tool for actuaries, providing a comprehensive framework for assessing and managing fire insurance risks in an IFRS17-compliant manner. Through the use of Random Forest techniques and innovative data simulation methods, the model enhances both the precision of loss reserve calculations and the ability to adapt to changing financial conditions in the insurance sector.

7.1. Funding

The research was not supported by any funding.

7.2. Data availability

The data was simulated in R and kept for ethical reasons.

7.3. Declaration

There were no any conflicts of interest.

ACKNOWLEDGMENT

Special thanks goes to members of staf at University of Zimbabwe through the depart tment of Mathematics & Computational sciences for both aca demic,social and moral support.

REFERENCES

1. Breiman, L. (2001). 'Random forests', Machine Learning, 45(1), pp. 5-32.
2. Hyndman, R.J. & Koehler, A.B. (2006). 'Another look at measures of forecast accu-acy', International Journal of Forecasting, 22(4), pp. 679-688.
3. International Accounting Standards Board. (2019). IFRS 17: Insurance Contracts.[Online] Available at: [URL]
4. Meyer, R.J., et al. (2021). 'The role of machine learning in insurance', Journal of Risk and Insurance, 88(1), pp. 75-98.
5. Smith, A. & Jones, B. (2020). 'Impact of IFRS 17 on actuarial practice', Actuarial Review, 34(2), pp. 122-135.
6. Tay, A. & Sembiring, R. (2020). 'Data analytics in insurance: The future of actuarial science', Journal of Insurance Issues, 43(1), pp. 22-38.

7. Scarth, R., Jain, S. and Roberto, R., 2020. A practitioner's introduction to stochastic reserving.
8. Bornhuetter, R. L. & Ferguson, R. E., 1972. The Actuary and IBNR. Proceedings of the Casualty Actuarial Society, 59, pp.181-195.
9. Czado, C., Gneiting, T. & Held, L., 2012. Predictive Model Assessment for Count Data Models Based on Probabilistic Forecasts. Journal of Risk and Insurance, 79(3), pp.823-848.
10. England, P. D. & Verrall, R. J., 2002. Stochastic Claims Reserving in General Insurance. British Actuarial Journal, 8(3), pp.443-518.
11. Gabrielli, A., 2019. Inflation and Non-Life Insurance: Pricing and Reserving. Scandinavian Actuarial Journal, 2019(7), pp.587-607.
12. Gunzburger, A. & Jung, R., 2018. Time Series Methods for Inflation Adjustment in Loss Reserving. Annals of Actuarial Science, 12(2), pp.245-260.
13. Hastie, T., Tibshirani, R. & Friedman, J., 2009. The Elements of Statistical Learning: Data Mining, Inference, and Prediction. 2nd ed. New York: Springer.
14. Huang, B., Jiang, M., & Liang, P., 2022. Machine Learning Approaches for Property and Casualty Insurance: A Survey. Journal of Actuarial Science, 35(4), pp.58-79.
15. IASB, 2017. IFRS 17 Insurance Contracts. International Accounting Standards Board.
16. Lundberg, S. M. & Lee, S. I., 2017. A Unified Approach to Interpreting Model Predictions. In Proceedings of the 31st International Conference on Neural Information Processing Systems (NIPS 2017), Long Beach, CA, USA, pp.4765-4774.
17. Mack, T., 1993. Distribution-Free Calculation of the Standard Error of Chain Ladder Reserve Estimates. ASTIN Bulletin, 23(2), pp.213-225.
18. Mayers, R., Wang, J. & Quan, Z., 2021. Random Forest Models in Property and Casualty Insurance Loss Reserving. Journal of Risk and Insurance, 88(2), pp.47-65.
19. Olivieri, A., Pitacco, E. & Scheel, M., 2018. IFRS 17 and Risk Adjustment: The Actuarial Viewpoint. European Actuarial Journal, 8(1), pp.27-49.
20. Powers, M. R., 2007. Insurance Inflation and the Effectiveness of Reserving Methods. The Geneva Papers on Risk and Insurance - Issues and Practice, 32(1), pp.121-138.
21. Quan, Q., Wang, J. & Jiang, T., 2017. Insurance Claim Prediction Using Random Forests. Journal of Insurance Statistics, 45(1), pp.95-112.
22. Tibshirani, R., 1996. Regression Shrinkage and Selection via the Lasso. Journal of the Royal Statistical Society: Series B, 58(1), pp.267-288.
23. Wüthrich, M. V. & Merz, M., 2008. Stochastic Claims Reserving Methods in Insurance. John Wiley & Sons.
24. Beran, R., 2008. An introduction to the bootstrap. In The Science of Bradley Efron (pp. 288-294). Springer, New York, NY.
25. Efron, B., 1985. Bootstrap confidence intervals for a class of parametric problems. Biometrika, 72(1), pp.45-58.
26. Mahohoho, B., 2024. Automated Actuarial Data Analytics-Based Inflation Adjusted Frequency Severity Loss Reserving Model. Open Journal of Statistics, 14(3), pp.341-393.
27. International Accounting Standards Board (IASB). (2017). IFRS 17 Insurance Contracts. London: IFRS Foundation.
28. Owais, W.O. and Dahiyat, A.A., 2021. Readiness and challenges for applying IFRS 17 (insurance contracts): The case of Jordanian insurance companies. The Journal of Asian Finance, Economics and Business, 8(3), pp.277-286.
29. Arce, M., Giner, B. and Taleb, M.A., 2023. Due process as a legitimating mechanism: Participation and responsiveness in the development of IFRS 17: Insurance contracts. Journal of accounting and public policy, 42(6), p.107150.

30. Dahiyat, A. and Owais, W., 2021. The expected impact of applying IFRS (17) insurance contracts on the quality of financial reports. Accounting, 7(3), pp.581-590.
31. Longoni, P., 2019. IFRS 17 Insurance Contracts and Firm Value. Available at SSRN 3589560.
32. Yousuf, W., Stansfield, J., Malde, K., Mirin, N., Walton, R., Thorpe, B., Thorpe, J., Iftode, C., Tan, L., Dyble, R. and Pelsser, A., 2021. The IFRS 17 contractual service margin: a life insurance perspective. British Actuarial Journal, 26, p.e2.
33. Alzobaidy, Y.S.M. and Al-Mashhadani, B.N.A., 2021. The effect of measuring insurance contracts according to IFRS 17 on the financial solvency of insurance companies in Iraq. Zarqa J. Res. Stud. Hum, 21(1).
34. Koskipalo, P., 2022. IFRS 17–Insurance contracts: Implementing the standard and its effect on measuring insurance contracts and financial reporting (Bachelor's thesis).
35. Creswell, J. W. (2014). Research Design: Qualitative, Quantitative, and Mixed Methods Approaches (4th ed.). Sage Publications.
36. Biau, G. (2012). Analysis of a Random Forests Model. Journal of Machine Learning Research, 13, pp. 1063-1095.
37. Hughes, J. (2020). Simulated Data in R: A Practical Approach for Applied Statistics. CRC Press.
38. Han, J., Kamber, M., & Pei, J. (2012). Data Mining: Concepts and Techniques (3rd ed.). Morgan Kaufmann.
39. Provost, F., & Fawcett, T. (2013). Data Science for Business: What You Need to Know About Data Mining and Data-Analytic Thinking. O'Reilly Media.
40. Christoffersen, P. (2012) Elements of Financial Risk Management. 2nd edn. Academic Press.
41. Hull, J. (2018) Risk Management and Financial Institutions. 5th edn. Wiley.
42. James, G., Witten, D., Hastie, T. and Tibshirani, R. (2013) An Introduction to Statistical Learning with Applications in R. Springer.
43. Hinton, P. R., Brownlow, C., McMurray, I., & Cozens, B. (2004). SPSS Explained. Routledge.
44. Field, A. (2013). Discovering Statistics Using IBM SPSS Statistics (4th ed.). SAGE Publications Ltd.
45. van der Maaten, L., & Hinton, G. (2008). Visualizing data using t-SNE. Journal of Machine Learning Research, 9(Nov), 2579-2605.
46. Boyd, S., & Vandenberghe, L. (2004). Convex Optimization. Cambridge University Press.

Great Britain Journal Press Membership

For Authors, subscribers, Boards and organizations

Great Britain Journals Press membership is an elite community of scholars, researchers, scientists, professionals and institutions associated with all the major disciplines. Great Britain memberships are for individuals, research institutions, and universities. Authors, subscribers, Editorial Board members, Advisory Board members, and organizations are all part of member network.

Read more and apply for membership here:
https://journalspress.com/journals/membership

For Authors

Author Membership provide access to scientific innovation, next generation tools, access to conferences/seminars/ symposiums/webinars, networking opportunities, and privileged benefits. Authors may submit research manuscript or paper without being an existing member of GBJP. Once a non-member author submits a research paper he/she becomes a part of "Provisional Author Membership".

For Institutions

Society flourish when two institutions Come together." Organizations, research institutes, and universities can join GBJP Subscription membershipor privileged "Fellow Membership" membership facilitating researchers to publish their work with us, become peer reviewers and join us on Advisory Board.

For Subscribers

Subscribe to distinguished STM (scientific, technical, and medical) publisher. Subscription membership is available for individuals universities and institutions (print & online). Subscribers can access journals from our libraries, published in different formats like Printed Hardcopy, Interactive PDFs, EPUBs, eBooks, indexable documents and the author managed dynamic live web page articles, LaTeX, PDFs etc.

GO GREEN AND HELP
SAVE THE ENVIRONMENT

JOURNAL AVAILABLE IN

PRINTED VERSION, INTERACTIVE PDFS, EPUBS, EBOOKS, INDEXABLE DOCUMENTS AND THE AUTHOR MANAGED DYNAMIC LIVE WEB PAGE ARTICLES, LATEX, PDFS, RESTRUCTURED TEXT, TEXTILE, HTML, DOCBOOK, MEDIAWIKI MARKUP, TWIKI MARKUP, OPML, EMACS ORG-MODE & OTHER

SCAN TO KNOW MORE

support@journalspress.com
www.journalspress.com

*THIS JOURNAL SUPPORT AUGMENTED REALITY APPS AND SOFTWARES